DOI:10.14753/SE.2024.2997

SEMMELWEIS EGYETEM

DOKTORI ISKOLA

Ph.D. értekezések

2997.

BOUSSOUSSOU MELINDA

Szív- és érrendszeri betegségek élettana és klinikuma
című program

Programvezető: Dr. Merkely Béla, egyetemi tanár

Témavezető: Dr. Maurovich-Horvat Pál, egyetemi tanár

Dr. Szilveszter Bálint, adjunktus

DOI:10.14753/SE.2024.2997

The role of coronary CT angiography in advanced pericoronary adipose tissue analysis and planning of atrial fibrillation ablation procedure

Ph.D. thesis

Melinda Boussoussou M.D.

Doctoral School of Theoretical and Translational Medicine

Supervisors: Prof. Dr. Pál Maurovich-Horvat M.D. D.Sc.

Dr. Bálint Szilveszter M.D. Ph.D

Official reviewers: Dr. Viktor Kolozsvári Rudolf M.D. Ph.D.

Dr. Zsigmond Máté Jenei M.D. Ph.D.

Head of the Complex Examination Committee:

Prof. Dr. István Karádi M.D. D.Sc

Members of the Complex Examination Committee:

Prof. Dr. Henriette Farkas M.D. D.Sc

Dr. Hassan Charaf Ph.D.

Budapest
2023

DOI:10.14753/SE.2024.2997

Table of Contents

DOI:10.14753/SE.2024.2997

DOI:10.14753/SE.2024.2997

DOI:10.14753/SE.2024.2997

LIST OF ABBREVIATIONS

AF: atrial fibrillation

AI: ablation index

AMI: acute myocardial infarction

BMI: body mass index

CAD: coronary artery disease

CAC score: coronary artery calcium score

CAD-RADS: Coronary Artery Disease-Reporting and Data System

CCTA: coronary CT angiography

CI: confidence interval

CNR: contrast to noise ratio

CV: cardiovascular

CL: cycle length

DLP: dose length product

EAT: epicardial adipose tissue

GE: General Electric

HRP: high-risk plaque

HU: Hounsfield unit

ICC: intraclass correlation coefficient

IMP: impedancekVp: kilovoltage peak

LA: left atrium

LA-VP: left atrium - pulmonary vein

LAWT: left atrial wall thickness

LIPV: left inferior pulmonary vein

LSPV: left superior pulmonary vein

MACE: major adverse cardiovascular event

mAs: milliampere-second

mSv: millisievert

NCP: non-calcified plaque

PA: postero-anterior

PACS: Picture Archiving and Communication System

PAT: pericardial adipose tissues

PCAT: pericoronary adipose tissue

PV: pulmonary vein

PVI: pulmonary vein isolation

RCA: right coronary artery

RIPV: right inferior pulmonary vein

RSPV: right superior pulmonary vein

SD: standard deviation

SIS: segment involvement score

SNR: signal-to-noise ratio

SSS: segment stenosis score

TIA: transient ischemic attack

OR: odds ratio

DOI:10.14753/SE.2024.2997

1 INTRODUCTION

Coronary computed tomography angiography (CCTA) plays a significant role in the field of cardiology by providing detailed imaging of the coronary arteries their surrounding structures and helping in the diagnosis, risk stratification and management of several cardiac interventions (1-4).

CCTA has emerged as a valuable non-invasive imaging technique for the evaluation of CAD which is among the leading causes of morbidity and mortality worldwide (5-9). Due to its high spatial and temporal resolution, CCTA allows for the accurate visualization of the coronary arteries, providing a comprehensive assessment of their luminal diameter and the presence of stenosis caused by atherosclerotic plaque. The ability to detect and quantify the degree of stenosis aids in determining the severity of CAD and assists in making appropriate treatment decisions (8). Beyond detecting stenosis, CCTA can assess plaque characteristics associated with increased cardiovascular risk. It can differentiate between different types of plaques, such as calcified, non-calcified, or vulnerable. Non-calcified and vulnerable plaques are prone to rupture, which leads to acute coronary events (8). CCTA also provides a comprehensive evaluation of the overall coronary atherosclerotic burden by visualizing multiple coronary segments and identifying the presence of diffuse atherosclerotic disease (10). Furthermore, it allows for evaluating pericoronary structures, such as pericoroany adipose tissue (PCAT). PCAT has been recently introduced in the scientific literature as a factor that can contribute to the development of major adverse cardiovascular events (3). PCAT analysis can help identify high-risk plaques as research results demonstrated that low PCAT attenuation on CCTA indicates denser or more inflamed fat associated with vulnerable plaques that are more likely to cause plaque rupture and subsequent myocardial infarction (11).

Considering PCAT next to the traditional risk factors such as age, gender, smoking, hypertension and dyslipidemia the predictive accuracy of risk models can potentially be enhanced as traditional risk factors tend to under or overestimate the risk of CAD (12) therefore incorporating CCTA findings into risk models would allow more personalized and improved patient management strategies.

Despite the promising results regarding PCAT, it is considered a new approach in CAD evaluation therefore, more CCTA studies are warranted to better understand its role.

Besides the essential role of CCTA in identifying CAD, it also has a valuable part in treating atrial fibrillation (AF), considered the most common sustained cardiac arrhythmia worldwide (13). AF is characterized by rapid and irregular electrical activity in the atria mainly around pulmonary veins (13). A catheter-based pulmonary vein isolation (PVI) became the cornerstone of AF treatment (14). Durable pulmonary vein (PV) isolation poses a challenge therefore several technological advancement was made to achieve better results, one of them is the recently introduced CLOSE protocol (15). It employs a contact-force-guided technique, utilizing contiguous and optimized radiofrequency lesions for enclosing pulmonary veins (15-17). CCTA plays an important role in the preoperative planning of pulmonary vein isolation. By visualizing the pulmonary veins and their anatomical relationship with the left atrium, CCTA helps identify the number, size, and orientation of the pulmonary veins, as well as the presence of variant pulmonary venous anatomy (18-20). This information aids in determining the optimal approach for the procedure and assists in reducing the risk of complications. Furthermore, it could also help to validate new ablation techniques through the CCTA-derived information gained from the left atrium and its surrounding structures (21, 22). As atrial fibrillation is considered a major public health burden (13) and the field of electrophysiology constantly evolves (16) the need to use CCTA is getting more prominent.

This dissertation aims to assess the role of CCTA in advanced PCAT analysis and the preprocedural planning of AF ablation.

1.1 Epicardial and pericardial adipose tissue of the heart

Epicardial adipose tissue (EAT) and pericardial adipose tissues (PAT) differ in anatomical location and developmental origin. In terms of development and blood supply, the EAT originates from the splanchnopleural mesoderm and is fed by the coronary arteries, contrarily the PAT develops from the thoracic mesenchyme and receives its blood supply from the internal mammary artery instead of the coronary arteries (23). While the EAT is located between the outer wall of the myocardium and the visceral wall of the pericardium, the PAT is found between the visceral and parietal plates of the pericardium. Based on ultrasonography analysis, the EAT appears as an echogenic area between the myocardium and the visceral pericardium. The PAT is the echogenic space anterior to the epicardial adipose tissue and underlies the parietal pericardium (24). They also differ from a biochemical point of view. In vivo studies demonstrated that PAT has a significant paracrine function and can significantly affect the myocardium due to its proximity to it. While the endocrine functions of EAT have not been fully understood yet, it is proven to impact the coronary network (25, 26). There are also clinical differences between the two adipose tissue types. Based on several studies, EAT can affect metabolic syndrome, liver enzyme levels, fasting blood glucose, insulin resistance, subclinical atherosclerosis, and cardiac morphology (27-29), while PAT is associated with cardiovascular diseases (30). It has been demonstrated that PAT volume is significantly linked with the severity and extent of coronary atherosclerosis and it might play a role as a determinant in plaque vulnerability (31).

1.2 Anatomy and histology of the pericoronary adipose tissue

Due to its anatomical proximity to blood vessels, PCAT, part of the EAT, has been a significant focus of research into cardiovascular disease. In the absence of a consistent definition and a clear anatomical boundary, pericoronary adipose tissue has received heterogeneous definitions in the scientific literature. Traditionally, it is defined as any extension of the adipose tissue that denotes the pericoronary fat compartment around the vessel (32). Antonopoulos et al. described PCAT as the distance of the diameter of the vessel from the outer vessel wall. This definition is based on several histological and gene expression investigations demonstrating the close relationship between the vascular wall and adipose tissue through bidirectional paracrine interactions. Like adipose tissue, PCAT

comprises several cells, namely adipocytes, preadipocytes, and mesenchymal stem cells, located in the extracellular matrix interspersed with microvessels (3). PCAT is continuous with the adventitia layer of the wall of large vessels, whereas, in small vessels, it is integrated into the wall. Predominantly white adipose tissue is found in the resistance vessels, but there is a mixture of brown and white adipose tissue around the large vessels (33). Adipose tissue was initially known for its mechanical, metabolic (energy source, glucose homeostasis), and thermal functions. However, in recent years, it has been proved that adipose tissue, including PCAT, is also responsible for the secretion of bioactive substances known as adipocytokines. The exact source of these molecules varies, with cytokines produced mainly by inflammatory cells and adipokines (e.g., adiponectin) by adipocytes. All adipocytokines play crucial roles in regulating vascular physiology, including vascular redox status, muscle tone, and endothelial function (34). In addition, a bidirectional relationship between the vascular wall and PCAT has recently been revealed. Locally generated inflammatory mediators and free radicals from the vessel directly affect the function of adjacent adipocytes (35, 36). In its physiological state, PCAT exerts anti-inflammatory, anti-contractile, and anti-oxidant effects on the vascular wall. For example, vascular tone regulation depends on the continued presence of PCAT-derived relaxing factors, which induce vasodilatation through endothelium-dependent and independent mechanisms. Adiponectin and omentin exert their anti-inflammatory and anti-oxidant effects through inhibition of the NF-KB (nuclear factor kappa beta) pathway and enhancement of NADPH (nicotinamide adenine dinucleotide phosphate) oxidase, thereby restoring endothelial nitric oxide synthase function (37, 38).

1.3 Pathophysiology of the pericoronary adipose tissue

PCAT inflammation was first studied in mouse models. Balloon or wire-induced vascular injury effectively induced inflammation and increased adiponectin production (39). In a similar experiment in pigs, a drug-eluting stent induced vasoconstriction and, thus PCAT inflammation, which was confirmed by 18F-fluorodeoxyglucose positron emission tomography (18F-FDG PET) (40). Due to the bidirectional interaction, pro-inflammatory cytokines from the vascular wall induce lipolysis in adipocytes, inhibit adipogenesis, and develop perivascular edema. Adipocyte maturation is slowed, and the proportion of preadipocytes increases, with a decrease in lipid content. This phenomenon is known as

local cachexia, where a gradient of adipocytes develops around the vessel wall, with a higher water/lipid ratio in the immediate area of the inflamed vessel (41). The bidirectional interaction during PCAT inflammation is shown in Figure 1.

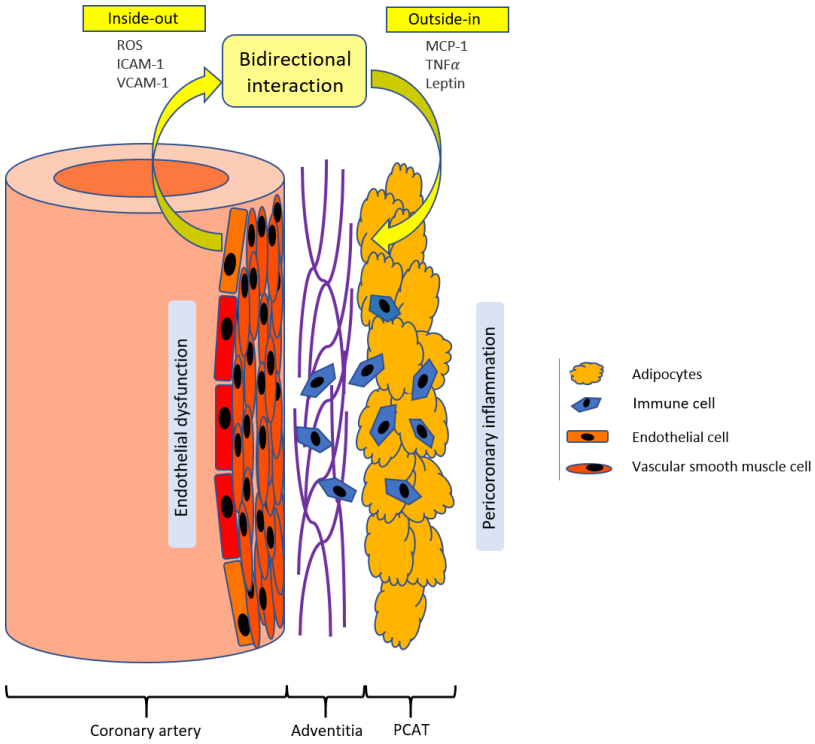

Figure 1. Atherosclerosis in coronary arteries: inside-out vs. outside-in signaling. (Own work.)

Endothelial dysfunction triggers endothelial cell-mediated vascular inflammation via ROS production and VCAM-1, ICAM-1 expression inducing atherosclerotic lesion formation (inside-out signaling). In comparison, PCAT mediates proinflammatory adipocytokines such as MCP-1, TNFα, and leptin by immune cells and adipocytes which also promote the development of atherosclerosis (3).

Abbreviations: ICAM-1: intracellular adhesion molecule-1, PCAT: pericoronary adipose tissue, ROS: reactive oxygen species, VCAM-1: vascular cell adhesion molecule-1

1.4 The theoretical background of cardiac CT imaging

CT imaging is based on the absorption of X-rays. During the scan, the patient's body is scanned axially. Hence, the rays are perpendicular to the patient's longitudinal axis, resulting in slice images (42). The radiation source and the detector are positioned opposite each other in the gantry, and the table on which the patient lies moves longitudinally through the gantry. CT scanners are equipped with multiple detector arrays. Therefore, several slices can be imaged simultaneously (multi-slice CT or MSCT) (43). The attenuation coefficients (i.e., the density), expressed in Hounsfield units (HU), can be calculated from the slices of the patient scanned from several directions. The Hounsfield scale ranges from -1000 to 3000, where 0 HU is the attenuation coefficient of the water. High-density materials are metal, bone, or contrast material, and air, liquid, and fat represent lower densities. The same HU differences can be used to evaluate plaque composition or fat attenuation. These different densities can be represented on a greyscale, with the low-density areas being darker and the high-density areas lighter (44). X-rays are generated in the X-ray tube. The acceleration of electrons in the tube is created by the tube voltage (kVp) and the anode current (mA). The anode current and tube voltage determines the number of X-rays produced and their energy levels. The more direct photons that reach the detector panel, the better the image quality obtained. Hence, increasing the tube voltage and current improves the signal-to-noise ratio (SNR) and contrast-to-noise ratio (CNR), although it increases the patient's radiation exposure. Image quality can also be improved with pixel spacing. Smaller pixel spacing leads to higher spatial resolution, allowing for more accurate detection and characterization of small structures such as coronary arteries and plaques. In addition, it increases the signal-to-noise ratio and decreases the possible amount of motion artifacts. (45)

1.5 The role of CT-derived coronary artery calcium score in coronary artery disease risk stratification.

In most cardiac CT scans, a native, non-contrast image is acquired before administering the contrast material for planning the contrast-enhanced scan. On the other hand, it allows for the quantification of calcium burden by examining the attenuation of the vessel wall (46). One of the best-studied methods for determining coronary calcification is the

Agatston coronary artery calcium score (CAC Score). The CAC Score can be quickly and simply measured using semi-automated software to quantify the volume and relative density of high attenuation pixels, which correlates well with coronary calcification and reflects the patients' total plaque burden (47). The threshold for calcific lesions is set at 130 HU with an area ≥1 mm^2 (48). CAC is known to increase with age in both sexes, (49, 50), both absolute and relative CAC increases have been associated with coronary artery disease severity, independent of traditional cardiovascular risk factors (47, 51). Hence, the additional use of CAC score can improve risk stratification as traditional risk factors often under or overestimate CAD risk (12). In asymptomatic elderly patients, CAC is a valuable tool for reclassifying risk groups beyond the Framingham risk score (52). As a result, risk estimation methods such as the Multi-Ethnic Study of Atherosclerosis (MESA) have been developed, including information obtained from CAC (53). Both acute (54) or stable chest pain patients (55) who have zero CAC present rarely with obstructive CAD and have an excellent prognosis. However, even among this patient population, there is a noticeable prevalence and progression of non-calcified plaque (NCP) (56). As a result of inflammation, NCPs are commonly considered a more vulnerable phenotype than calcified plaques and a stronger predictor of major adverse cardiovascular events (MACE) (57). Although, CAC score is better than traditional risk scores in identifying patients at CAD risk, it is only used for risk stratification in asymptomatic patients and in case of symptoms CCTA is recommended.

1.6 The role of CT-derived segment stenosis score and segment involvement score in coronary artery disease risk stratification

After the native scan, CCTA involves the injection of contrast material intravenously, with the possibility of taking images at different times depending on the structure to be examined. The information obtained can be used to study the anatomy of coronary arteries, atherosclerosis, stenosis, and cardiac function (23-25). Coronary stenosis can be well assessed on CCTA scans and are characterized by stenosis grading comparable to invasive angiography. Based on the American CT Society's recommendation (SCCT), we classify stenosis into five groups according to severity (58). In ascending order: minimal (1-24%), mild (25-49%), moderate 50-69%, severe (70-99%) stenosis, and occlusion (100%) Based on the information about stenosis severity, a segment stenosis score was

created as a measure of overall coronary artery plaque extent. Moreover, a segment involvement score was defined as a measure of overall coronary artery plaque distribution. Based on Lin et al., these scores were proved to be independent predictors of all-cause mortality (59).

1.7 The role of CT-derived coronary plaque characterization.

According to the composition, three types of plaques can be distinguished. 1.) Non-calcified plaque is lipid-rich and therefore has a lower density than contrast material. 2.) Calcified plaque: high density compared to contrast material and well detectable. 3.) Partially calcified plaque: calcification, necrotic core, and a fatty component can be found in it (60, 61). Based on CCTA scans, certain plaques are more prone to rupture and could lead to an adverse event (62, 63). Spotty calcification is defined when a plaque's density exceeds 130 HU, and the calcified area is less than 3 mm (64). Positive remodelling is characterized when the atheroma grows outwards, resulting in compensatory dilatation of the vessel wall. In this case, obstructive lumen narrowing is often not observed. The process is quantitatively characterized by the remodelling index, defined as the ratio of the area of the vascular lumen measured proximal to the plaque to the total vascular area, including plaque and lumen. The remodelling index should be at least 1.1 for positive remodelling (65, 66). Low attenuation plaques are defined as having a density of less than 30 HU, with low attenuation due to the cholesterol-rich lipid core (61). A qualitative marker, the napkin-ring sign, is present when a plaque has annular characteristics comprised of a low-attenuation necrotic core adjacent to a lipid-rich lumen and a surrounding higher-density fibrotic cap (63, 67).

Non-calcified low attenuation plaque burden on CCTA was proved to be the strongest predictor of nonfatal or fatal AMI among cardiovascular risk scores, CAC score, or coronary artery stenosis severity based on the results of the SCOT-HEART Trial (Scottish Computed Tomography of the HEART).

1.8 The role of CT-derived PCAT analysis in coronary artery disease risk stratification.

CCTA allows volumetric and qualitative PCAT characterization in addition to coronary anatomy imaging. PCAT is characterized by a HU value between -190 and -30. Using a radiotranscriptomic approach, artificial intelligence, and adipose tissue biopsies from approximately 2,000 individuals, a quantitative biomarker was created that reflects changes in PCAT composition that may be induced by inflamed/pathological coronary arteries (3). The rationale behind PCAT measurement is that inflammation-induced modifications result in changes in adipocyte size and a decrease in lipid content, shifting CT attenuation towards less negative HU values (towards -30 HU) called PCAT markers (PCAT attenuation and PCAT gradient). A representative image of CCTA-derive PCAT around the right coronary artery (RCA) is shown in Figure 2. Mean PCAT attenuation is defined as the average HU value within the radial distance of the vessel. PCAT gradient represents the relative change in PCAT HU values perpendicular to the vessel wall. PCAT attenuation was created to define adipocyte and lipid content, whereas PCAT gradient was developed to provide additional information about local stimuli (3). Previous studies found a correlation between PCAT attenuation and patients with or without coronary plaques. PCAT attenuation was also associated with 18F-sodium fluoride uptake on positron emission tomography CT (27, 28). PCAT may be a novel and predictive biomarker that can provide a better risk estimate than conventional cardiovascular risk factors. However, CCTA-derived PCAT measurements can be affected by image quality, reconstruction techniques, CT scan protocols and, most importantly, heart rate. Furthermore, based on the scientific literature, differences between PCAT markers and patient groups are indistinct. Figure 2 displays PCAT segmented by the AutoPlaque software.

DOI:10.14753/SE.2024.2997

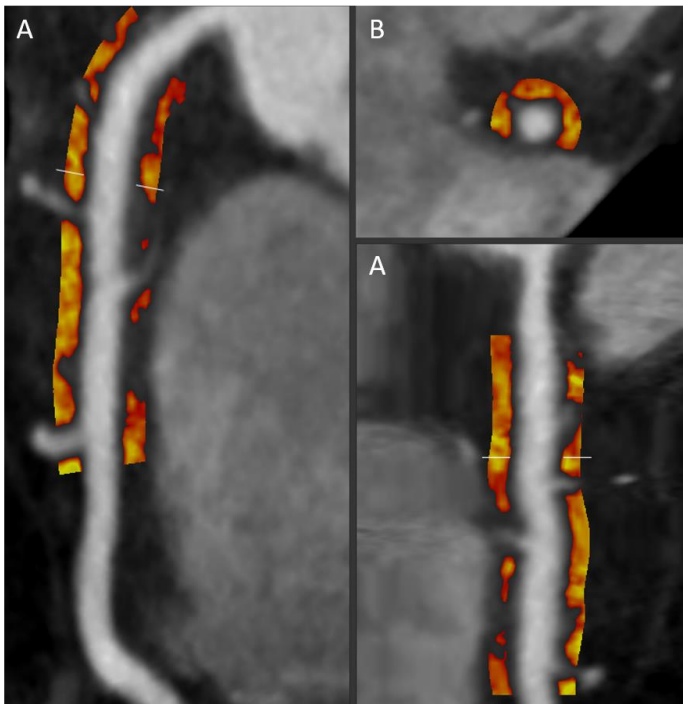

Figure 2. PCAT, segmented by the AutoPlaque software. (Own work.)

The two **A** panels show the sagital views of the RCA and panel **B** shows the axial view of the RCA. The orange area around the RCA represents the PCAT.

Abbreviations: RCA: right coronary artery, PCAT: pericoronary adipose tissue

1.9 Electrophysiological characterization of the left atrium

Atrial cell depolarization in healthy individuals is facilitated by a large, rapidly activating and deactivating inward Na+ current and the slower L-type Ca^{2+} current. Repolarization is also fast due to the activation of voltage-gated K^{+} channels. Although there is notable regional heterogeneity within and between the atria, which reflects systematic differences in intra-atrial ion channel density, action potential duration and refractory period are shorter in the atria, particularly in the left atrium, when compared to the ventricular myocardium (68). Consequently, the atrial myocardium is more vulnerable to developing complex patterns of conduction at very rapid rates, even before factoring in the proarrhythmic effects of atrial remodelling (69).

1.10 Triggers of atrial fibrillation

Atrial fibrillation substantially burdens public health systems worldwide with increasing prevalence and incidence. In addition, it increases the risk of stroke and heart failure, leading to the deterioration of life quality (70-72). Haïssaguerre and colleagues' studies identified the muscular sleeves within the pulmonary vein (PV) ostia as the source of ectopic beats that trigger atrial fibrillation (AF) in many patients with paroxysmal AF (13). The unique cellular electrophysiology, (73) gross anatomy, and fiber geometry of the myocardial sleeves in PVs appear to make them prone to rapid focal firing or re-entrant activation, making electrical isolation of the PVs from the rest of the atrium (called "PV isolation") a crucial step in catheter ablation of AF (74). Other triggers for AF have also been identified (75), including crista terminalis, ligament of Marshall, the superior vena cava, coronary sinus, left atrial appendage, and left atrial posterior free wall, possibly due to the presence of myocardial sleeves or regional atrial fibrosis in these areas. Other types of supraventricular arrhythmias, such as atrioventricular nodal re-entrant tachycardia, atrioventricular re-entrant tachycardia, and typical counterclockwise right atrial flutter, may also occasionally act as triggers for AF. The triggers that lead to AF are frequently caused or sustained by "upstream" factors such as atrial stretch, ischaemia, and autonomic imbalance. This may clarify why AF is more prevalent in patients with comorbidities that make them vulnerable to these factors, such as myocardial infarction, mitral regurgitation, and vagal stimulation (69).

1.11 Pulmonary vein isolation and the CLOSE protocol

Haïssaguerre et al. groundbreaking discovery about the origin of AF presented a new potential target for treatment. Catheter ablation is proved to be a potent therapy for treating symptomatic, drug-refractory, recurrent AF patients and has undergone significant evolution over the past twenty years, starting from segmental ostial pulmonary vein ablation and advancing to the use of 3D electroanatomical mapping to guide ablation and eventually to wide-area circumferential ablation with verification of conduction block. Durable PV isolation remains a challenge; however, recent technological advancement might help achieve better results (76).

One of the latest catheter ablation strategies is the CLOSE protocol, a contact-force-guided approach using optimized and contiguous radiofrequency lesions for the enclosure

of pulmonary veins (15-17). This is achieved by using fixed interlesion distance and ablation indexes (AI) at the anterior and posterior walls. AI is a tool used in CLOSE protocol in order to optimize the amount of energy delivery during PVI to safely create contiguous and transmural lesions around the PVs. Using this method can reduce the risk of incomplete ablation or excessive energy delivery (16). Recent studies analyzing the efficacy and safety of the CLOSE protocol showed excellent procedural outcomes (77). The contiguous and durable lesion set is a key element toward a higher chance of acute procedural success and long-term arrhythmia-free survival (78). Figure 3 demonstrates an ablation procedure using an electro-anatomical mapping system.

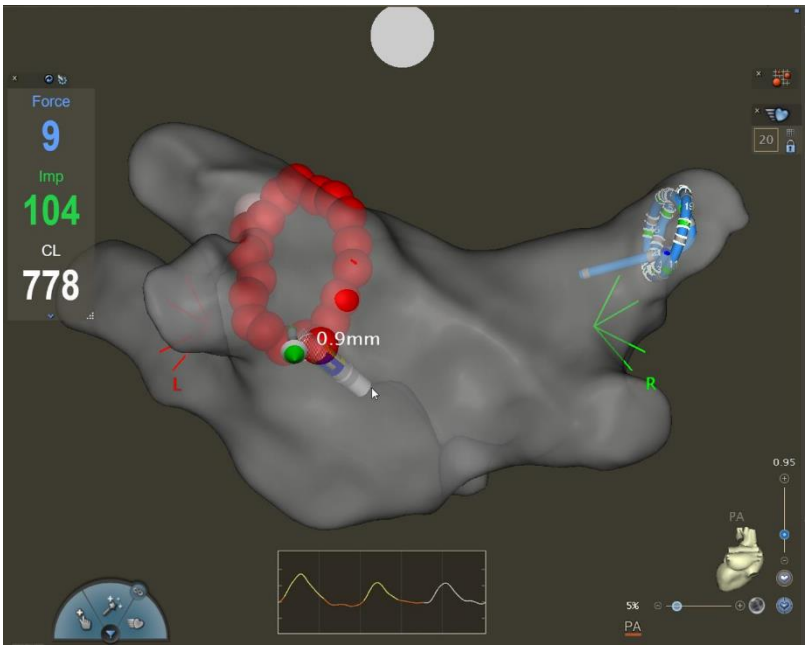

Figure 3. 3D map of the left atrium during ablation procedure.

3D map of the left atrium in postero-anterior view using CARTO 3, Biosense Webster software. The white circle displays the postero-anterior orientation. The ablation procedure started at the LSPV. The red ablation tags represent the regions where ablations were carried out around the pulmonary veins. The blue Lasso^{TM} catheter is in the RSPV, in order to blind the operator to the absence or presence of the first-pass isolation. (Own work.)

Abbreviation: 3D: three-dimensional, CL: cycle length IMP: impedance, LSPV: left superior pulmonary vein, PA: postero-anterior, RSPV: right superior pulmonary vein

1.12 First-pass isolation

In several PVI studies, a better ablation outcome was associated with the presence of first-pass isolation. (79, 80) The presence or absence of the first-pass isolation of a given PVI can be considered an indicator of the acute procedural success of the procedure. The elimination of PV potentials distal from the ablation line is well-defined as an "entrance block", and it is commonly accepted as a PVI endpoint. Whereas, exit block refers to the inability to stimulate the left atrium at a high output from the mapping catheter located distally from the ablated area during sinus rhythm. (81) First-pass isolation is achieved if both exit and entrance blocks are present. The aim of this technique is to improve the effectiveness of PVI and reduce the risk of complications by minimizing the number of times the catheter is manipulated within the left atrium. (82)

1.13 The role of coronary CTA in radiofrequency catheter ablation

Undoubtedly, CCTA has an essential role in AF ablation, as it guides the optimal patient selection and helps in procedural planning. The information gained from CCTA helps the imaging of the PVs by merging the CCTA images for the mapping system used during PVI. In addition, left atrial appendage thrombus can also be ruled out. (19, 83, 84).
Another role of CCTA has been recently introduced. Based on several research results, CCTA-assessed left atrial wall thickness (LAWT) and PV anatomy may alter the efficacy of radiofrequency catheter ablation. It has been hypothesized that larger local atrial wall thickness might lead to the reconnection of PVs after ablation; hence, a more aggressive ablation strategy may be needed to create appropriate LA lesions (21, 22, 78). Although, it is essential to note that less advanced ablation strategies were used in those studies; therefore, those results might not apply to the most recent ablation techniques.

2 OBJECTIVES

2.1 Pericoronary adipose tissue analysis

a.) To evaluate the link between CAD markers (presence of non calcified plaque, presence of obstructive stenosis, segment stenosis score (SSS), segment involvement score (SIS), presence of high-risk plaque) and PCAT markers (PCAT attenuation and gradient) in patients with a low cardiovascular risk (calcium scores =0)

While PCAT markers were analyzed in several studies in CAD patient populations, in terms of coronary plaques, serum levels of atherosclerotic relevant inflammatory and anti-inflammatory mediators (Supplementary Table 1 (85)), there are no studies in the scientific literature about the association of low cardiovascular risk patients and their PCAT marker values. We hypothesized that as zero calcium score patients represent a low risk for adverse cardiovascular events, PCAT values would be universally low with low variability.

b.) To evaluate to what degree patient and imaging parameters can influence PCAT markers

Most prior studies regarding PCAT markers did not consider correction factors applied for possible confounding. Few studies included only a couple of factors, even though in the models, the number of variables was inconsequent and varied to a large extent. In our study, we sought to include and consolidate factors that possibly influence PCAT markers, such as several patient and imaging characteristics besides plaque metrics. We hypothesized that patient and image acquisition parameters have an influence on PCAT attenuation and gradient values.

c.) To assess whether potential associations between PCAT markers and NCP persisted after correcting for patient and image acquisition parameters

A great number of studies have been published regarding the association of vulnerable plaque characteristics and PCAT markers, but none of them included patient and imaging characteristics as correction factors in their analysis. Therefore, our aim was to evaluate the association of noncalcified lesions and PCAT values with the inclusion of patient and image acquisition parameters.

d.) To validate our findings in a patient cohort with zero calcium scores but analyzed with a different CT scanner and on a group of individuals with moderate to severe stenosis on CCTA

We presented results from two additional cohorts. One consisting of individuals with a calcium score of 0 but imaged on a different CT scanner, and more importantly, one where we included individuals with moderate to severe stenosis (CAD-RADS 3 or 4a or 4b), to

assess whether the cofounders still significantly influenced results and whether the univariable associations disappear in these cohorts.

2.2 Left atrial wall thickness and pulmonary vein analysis

a.) To determine the relationship between the acute procedural success of CLOSE protocol and LAWT

We conducted LAWT measurements based on the CCTA scans of the patients that were carried out before each ablation procedure. Subsequently, we assessed the presence of first-pass isolation using the modified CLOSE protocol for the ablation procedures. In light of LAWT, the presence of first-pass isolation can be considered a marker of the PVIs' acute procedural success, thus the modified CLOSE protocol.

We hypothesized that using the novel modified CLOSE protocol, appropriate isolation of the PVs is feasible regardless of patients' LAWT. The effect of LAWT on successful first-pass isolation has not yet been evaluated. Hence our study aim was to define the relationship between CCTA-derived LAWT measurements and the acute procedural success of the modified CLOSE protocol assessed by first-pass isolation.

b.) To evaluate the potential role of PV anatomy in the rate of first-pass isolation

Furthermore, the possible role of PV anatomy in the first-pass isolation rate was also examined for the first time. We hypothesized that PV anatomy could affect catheter navigation, hence the success rate of first-pass isolation; therefore, we analyzed every patient's PV anatomy based on their CCTA scans.

DOI:10.14753/SE.2024.2997

3 METHODS

3.1 Pericoronary adipose tissue analysis

3.1.1 Patient population

In our retrospective, observational, single-centre study, 4120 consecutive patients had CCTA examinations between April 2016 and August 2019 for stable chest pain evaluation. Of this patient population, the effect of clinical characteristics, calcium score values, and image acquisition parameters were examined in a previous analysis (86). In this present sub-analysis, only patients with a calcium score of zero were included (Zero calcium score group, n=1652) as an indicator of a low cardiovascular risk patient population. The inclusion criteria of the study were the following: 1) proper image quality of the patients for PCAT analysis and 2) the absence of calcium on non-contrast CT images. Exclusion criteria were 1) images not available from the PACS system, 2) poor image quality, 3) tube voltage other than 100 or 120 kVp 4) prior CAD of the patients. Our study protocol was approved by the institutional review board. Because our study was retrospective, written informed consent was waived. All procedures used in this study were in accordance with the Health Insurance Portability and Accountability Act, local and federal regulations, and the Declaration of Helsinki.

3.1.2 Validation groups

We retrospectively identified two additional validation groups, 330-330 patients in each group, to validate our finding (20-20 % of the Zero calcium score group). The Zero calcium-score group (n=330) with a different scanner (CardioGraphe, GE Healthcare) was the first validation group with the same inclusion and exclusion criteria as the primary group. The moderate to severe CAD group (n=330) represented the second validation group comprised of individuals scanned on the same scanner as the primary study group (Brilliance iCT 256, Philips Healthcare).

The study design is displayed in Figure 4.

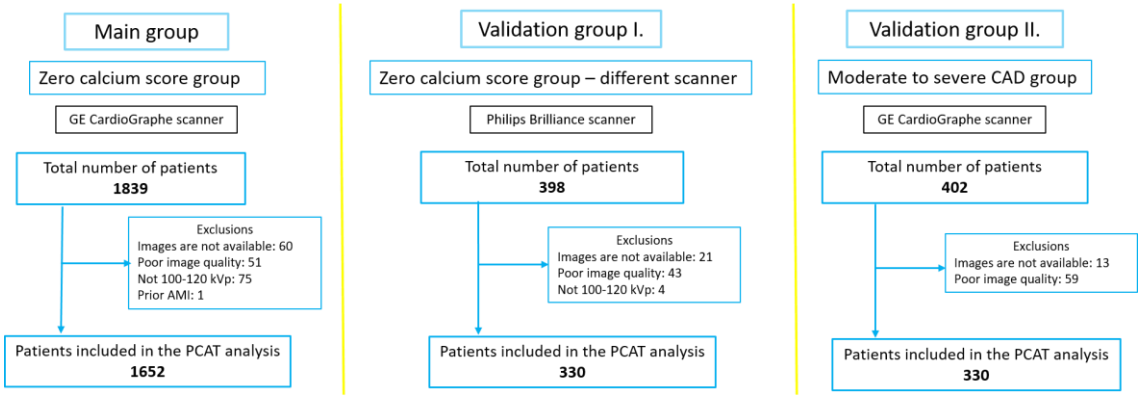

Figure 4. Study design. (Own work.)

Study design of the Main group and the two Validation groups.

Abbreviations: AMI: acute myocardial infarction, CAD: coronary artery disease, kVp: kilovoltage peak, PCAT: pericoronary adipose tissue

3.1.3 Sensitivity analysis

To assess whether our results regarding the link between patient and image acquisition parameters and PCAT markers are valid in patients without any CAD, we conducted a sensitivity analysis in patients from our primary study group: Zero calcium score group (Philips Brilliance scanner) with zero calcium score and no NCP.

3.1.4 Coronary CTA acquisition

Imaging was performed with a 256-slice scanner (Brilliance iCT 256, Philips Healthcare) on individuals that were in the Zero calcium score group and the Moderate to severe CAD validation group. In contrast, the Zero calcium score group -different scanner validation group consisted of patients with images done by a dedicated 560 -slice cardiac CT scanner (CardioGraphe, GE Healthcare). Both scanners used prospective ECG-triggering in axial acquisition mode.

Image acquisition for the CardioGraphe was 280x0.5 mm detector collimation and 240-330 ms rotation time, while for the Philips scanner, 128x0.625 mm detector collimation and 270-ms gantry rotation time (depending on patient BMI). Oral or intravenous beta–blocker was given to patients with a heart rate of above 65 beats/minute. Systolic triggering (35-45 % of the R-R interval) was set when a given patient's heart rate was ≥75 beats/minute, whereas in the case of ≤75 beats/minute, mid-diastolic triggering was

chosen (73-83% of the R-R interval). In both scanners, tube current of 200-300 mAs and tube voltage of 100-120 kV were applied depending on the BMIs of the patients.

For CCTA datasets obtained using CardioGraphe, 0.5 mm section thickness with continuous sections that were reconstructed to a 512x512 matrix with a differing field of views optimized cardiac evaluation was applied, whereas using Philips scanner 0.8-mm section thickness and 0.4-mm spacing between the slices were used. A four-phasic contrast protocol was set for both scanners with intravenous 80-100 ml iodinated contrast agent (Iomeron 400, Bracco Imaging Ltd.) at 4,5-5,5 ml/s flow rate through an 18-gauge catheter from antecubital vein access (87).

3.1.5 Coronary CTA plaque characterization

Segment stenosis was defined by summing the stenosis score of each segment and classified as the following: (0) none (0%); (1) minimal (1–24%); (2) mild (25–49%); (3) moderate (50–69%), (4) severe (70–99%) or (5) occluded (100%). Obstructive stenosis was defined as equal to or more than 50% of the diameter stenosis (88). Segment involvement score was estimated by the summation of all segments with plaque. In the case of no plaque, the score was zero in the given segment, while a score of one was determined when a plaque or plaques were present in the given segment (88). Both scores were continuous variables and were included in the statistical models. High-risk plaque features were determined as positive remodelling, low-attenuation plaque, spotty calcification, and napkin-ring sign based on previously described definitions (89). The high-risk plaque was defined when two of the abovementioned features were present (57).

3.1.6 Image quality analysis

Contrast-to-noise ratio (CNR) and signal-to-noise ratio (SNR) were calculated by manually placing a circular region of interest in the pericoronary adipose tissue (PCAT) around the proximal right coronary artery (regions of interest area ~ $3mm^2$), in the aorta (regions of interest area ~ $10mm^2$) and in the right coronary artery (regions of interest area ~ $3mm^2$) to attain mean CT numbers in Hounsfield Units (HU).

Motion artifacts and inhomogeneous regions were carefully avoided. As our interest was the location of the PCAT, CNR and SNR were calculated based on the CT attenuation of the aortic root at the level of the ostium of the RCA. The definition of the CNR is CNR=

(RCA HU-PCAT HU)/Aorta standard deviation, while SNR= RCA HU/Aorta standard deviation (90). The measurements were blinded to all PCAT and clinical data.

Pixel spacing is expressed in units of distance in millimeters and refers to the physical distance between adjacent pixels in an image. In cubic millimeters, this refers to the physical distance between adjacent voxels in a 3D image, where voxels are the 3D equivalent of pixels in a 2D image. It was calculated by multiplying the pixel spacing in the x, y and z dimensions of the CCTA images.

3.1.7 Pericoronary adipose tissue analysis

The proximal segment of the RCA was the location where PCAT analysis was carried out using the AutoPlaque software (version 2.0, Cedars-Sinai Medical Center) (Figure 5.) (41, 91). Based on several research results as a standardized model, PCAT analysis was carried out in the 40 mm proximal RCA segment, excluding the first 10 mm segment from the ostium (3, 11, 92). Voxels between -190 HU and -30 HU are defined as adipose tissue (Figure 5.) Therefore, all PCAT markers were assessed after removing all voxels with values above or below this range (3). PCAT attenuation was determined as the average HU attenuation within a radial distance from the outer coronary artery wall equal to the average diameter of the vessel (3). Uniformly, PCAT attenuation was calculated using a 3 mm radial distance from the vessel wall for every patient, as the average radius of the right coronary artery was 3.4±0.3 mm in the Zero calcium score group (3, 93, 94). PCAT gradient was calculated as the percentage change in PCAT attenuation when comparing HU values within the 3 mm radius to non-PCAT HU values at a 20 mm distance from the outer vessel wall (100%*(PCAT attenuation - non-PCAT attenuation)/|PCAT attenuation|) (3).

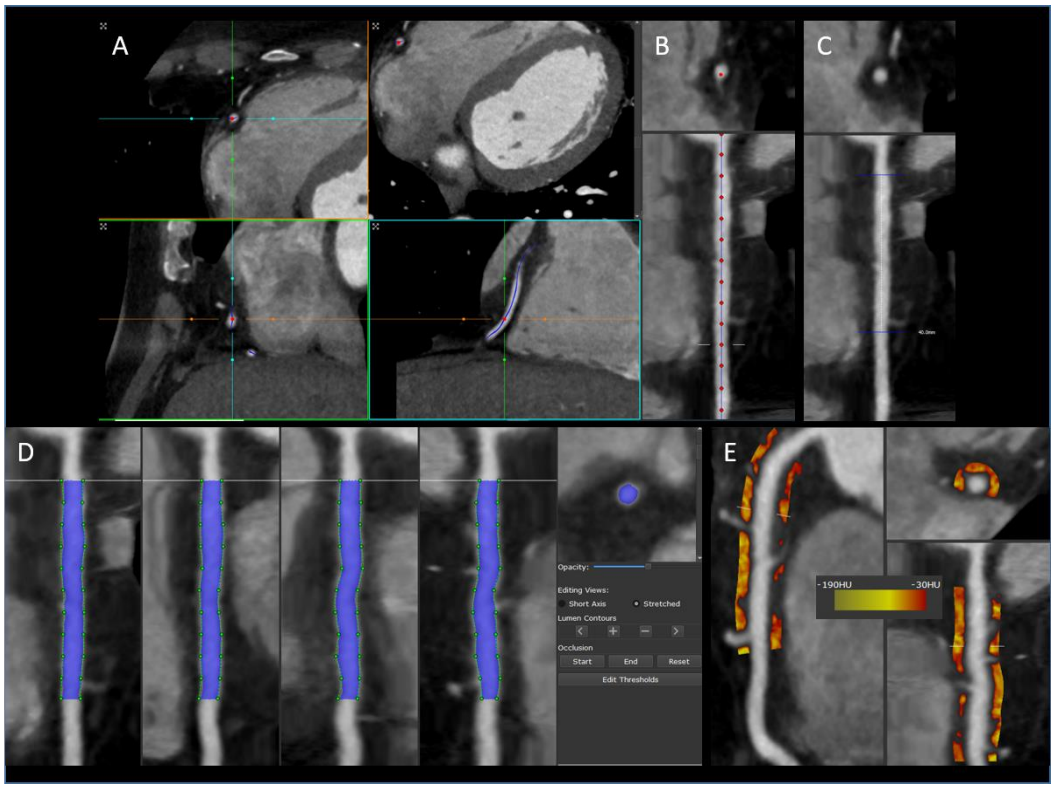

Figure 5. PCAT analysis by the AutoPlaque software step by step. (Own work.)

Panel **A** shows the first step of PCAT analysis. The RCA segment is chosen by marking the proximal (RCA ostium) and the distal part of the RCA. Panel **B** displays the step when the RCA centreline is corrected point by point if necessary. Panel **C** shows the standardized model with a 40 mm segment marked 10 mm distal from the RCA ostium. This 40 mm segment is depicted in panel **D** where the blue areas represent the RCA's lumen in four different angles in a sagittal view and one in an axial view. After the necessary corrections, the AutoPlaque software calculates the PCAT around the given 40 mm segment (Panel **E**). The shades of orange represent the HU unit values within the range of -190 HU to - 30 HU in the two sagittal planes as well as in the axial plane.

Abbreviation: RCA: right coronary artery, PCAT: pericoronary adipose tissue

3.1.8 Article search for pericoronary adipose tissue manuscripts

Systematic research was performed for original research articles to present an overview of the effect size of PCAT markers reported in the scientific literature until December 2021. The article search was completed in several electronic databases (Medline, Web of Science, PubMed, Embase, Scopus, The Cochrane Library, and ProQuest). The free text

words and MeSH terms that were used are the following: pericoronary adipose tissue, volumetric perivascular characterization index, fat attenuation index, and coronary CT angiography. The result of the article search is shown in Supplementary Table 1 (85).

3.1.9 Cardiovascular outcome analysis

In every study group, the patients were followed up using the Hungarian Myocardial Infarction Registry to screen if they experienced an acute myocardial infarction after the CCTA examination (95, 96).

3.1.10 Statistical analysis

Analyses were calculated in the R environment (v4.0.2). Categorical parameters are presented as frequency (percentages), while continuous variables are represented as mean (standard deviation). A linear regression model was used to analyze clinical, imaging, and CAD predictors of PCAT markers. Multivariable models were built comprising all predictors into the regression model. Survival analysis was not done due to the limited number of events. A $p < 0.05$ was considered significant.

3.2 Left atrial wall thickness and pulmonary vein analysis

3.2.1 Patient population

In our prospective, observational single-centre cohort study, 186 consecutive patients were screened who had symptomatic drug-refractory AF and received radiofrequency catheter ablation from January 2019 to September 2020. Exclusion criteria were the following: 1) prior catheter ablation procedure, 2) no pre-procedural CCTA was done, and 3) poor CCTA image quality. Overall, 94 patients' scans were analyzed who met all inclusion and exclusion criteria. Every patient had understood and agreed to the pre-procedural CCTA imaging and the subsequent PVI and gave written consent to retrieve and analyze their data. The study protocol was in accordance with the Helsinki Declaration and approved by the institutional review board.

3.2.2 Imaging of the left atrium and pulmonary veins with coronary CTA

In the study population, every patient had contrast-enhanced prospective ECG-triggered CCTA (256-slice scanner Brilliance iCT 256, Philips Healthcare, Best, The Netherlands) prior to the catheter ablation procedure. A detailed description of the CT protocol can be found in the paragraph entitled "3.1.4 Coronary CTA acquisition".

3.2.3 Image analysis

Commercially available Philips IntelliSpace Portal v.6.2, (Philips Healthcare) software was used for the measurement of LAWT and PVs. Eleven separate LA locations were chosen for the assessment of the maximum wall thickness areas (right, middle, and left regions of the atrium and mid-posterior and infero-posterior areas).

Based on literature data, these eleven locations are considered the most useful sites to assess the LAWT (97-103). Furthermore, based on Hayashi et al., the left lateral ridge and mitral isthmus were also analyzed (102). Each location is represented in Figure 6. For roof thickness measurement of the LA, an oblique coronal plane was set parallel to the superior PV or posterior wall (Number 1, 4, 7 in Figure 6 and 7) while to evaluate the mid-posterior and infero-posterior wall (Number 2, 5, 8, 3, 6, 9 in Figure 6 and 7) an oblique axial plane perpendicular to the posterior LA wall was obtained. The right and left roofs of the LAWT and the right and left infero-posterior regions were evaluated 10 mm farther from the LA-PV connection. At the mitral isthmus, the wall thickness was measured by setting an axial plane that is displayed as Number 10 in Figure 6 and 7. The wall thickness of the LA ridge was assessed at 5 mm inside the left superior PV centre by setting an oblique perpendicular plane view to the superior left lateral ridge (Number 11 in Figure 6 and 7). The mean and maximal LAWT was calculated for the right (Number 1-3) and left side (Number 7-9) based on the thickest part of the given segment and for all measured segments.

DOI:10.14753/SE.2024.2997

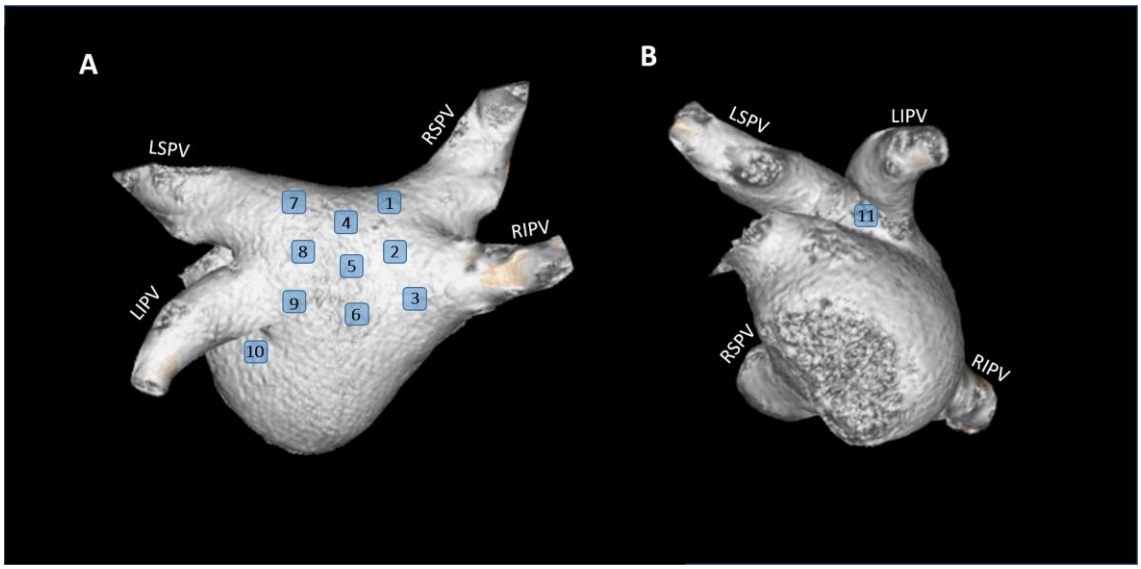

Figure 6. Volume-rendered 3D CCTA images demonstrate the 11 locations where LAWT was measured in the left atrium. (Figure from (127).)

On panel **A**, the LA is in a posterior view, while panel **B** displays the left lateral view of the LA. The numbers represent the following left atrial areas: 1: right roof, 2: right mid-posterior, 3: right infero-posterior, 4: middle part of the roof, 5: middle part of the mid-posterior, 6: middle part of the infero-posterior, 7: left of the roof, 8: left of the mid-posterior, 9: left of the infero-posterior, 10: mitral isthmus, 11: left lateral ridge.

Abbreviations: 3D: three-dimensional, CCTA: coronary computed tomography angiography, LA: left atrium, LAWT: left atrial wall thickness, LIPV: left inferior pulmonary vein, LSPV: left superior pulmonary vein, RIPV: right inferior pulmonary vein, RSPV: right superior pulmonary vein.

DOI:10.14753/SE.2024.2997

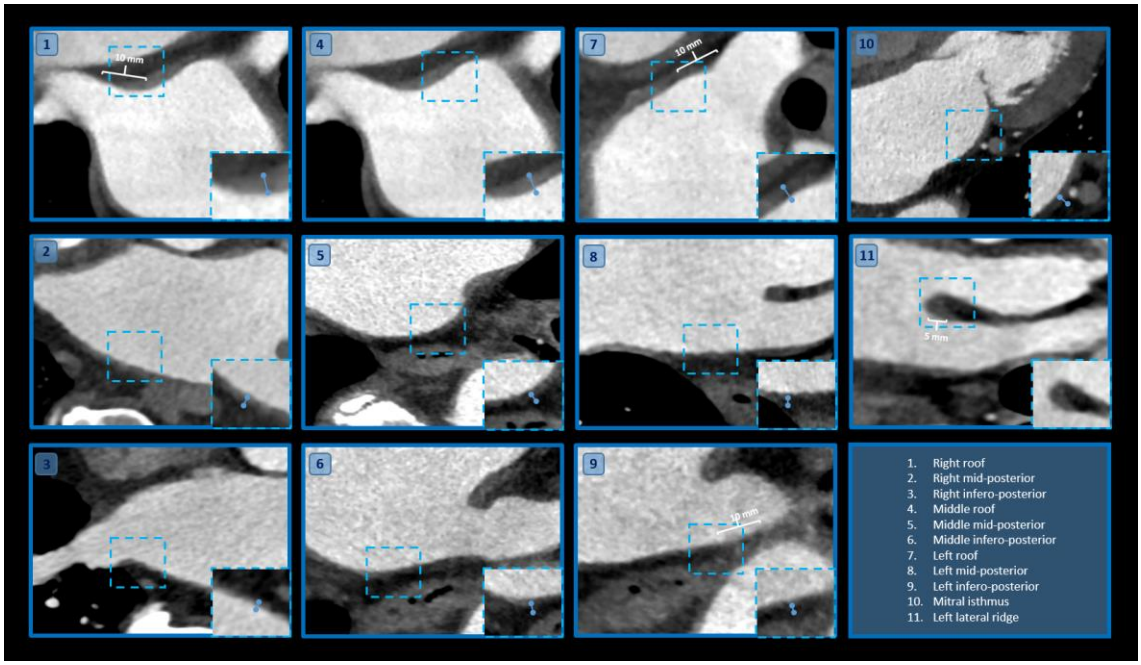

Figure 7. LAWT measurement areas at 11 points are depicted in CCTA images. (Figure from (127).)

Left atrial wall thickness (LAWT) was evaluated at 11 sites based on Hayashi et al. as shown on the CT images. The numbers indicate the exact locations for LAWT assessment as illustrated in Figure 6. The dashed squares represent the region of interest, and they are enlarged in the right-hand corner of each image. The size of the measured LAWT is depicted with a blue line between the two dots. The roof and the infero-posterior wall thickness (Number 1, 3, 7 and 9) were measured at a 10 mm distance from the junction of the LA and PV. At the ridge, the LAWT was measured at the centre of the left superior PV (5 mm from the LA wall).

Abbreviations: CCTA: coronary computed tomography angiography, LA: left atrium, LAWT: left atrial wall thickness, PV: pulmonary vein

The anatomy and diameter of the PVs were also evaluated in this patient population based on their CCTA scans. A PV anatomy was considered normal when at both sides of the LA, two-two distinct pulmonary veins were present (right superior and inferior and left superior and inferior). Figure 8. displays the typical pulmonary vein anatomy. The common trunk was defined in the case of the fusion/connection of the superior and inferior veins of a given side.

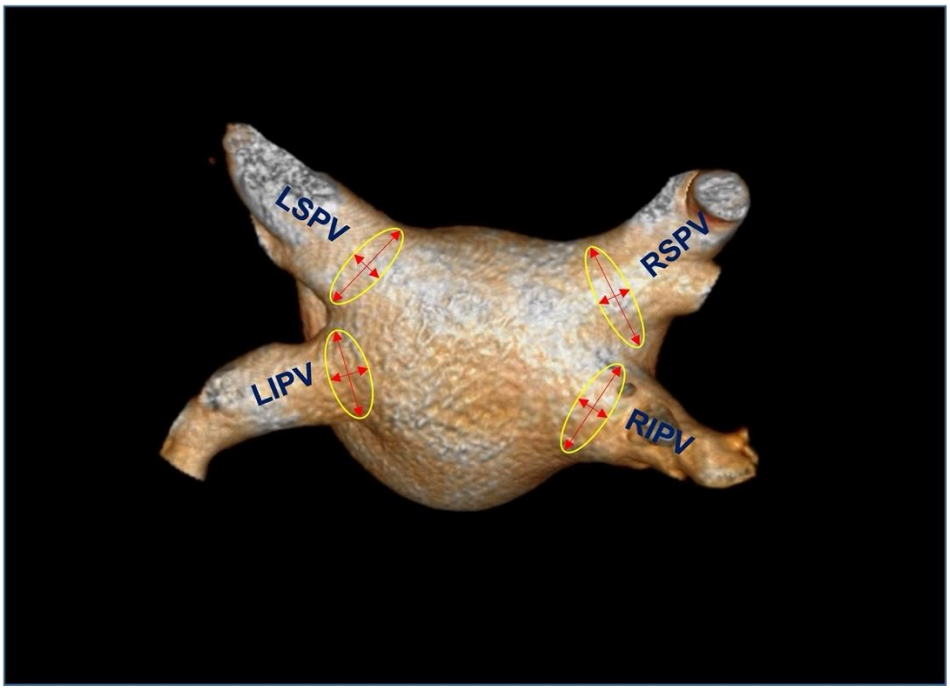

Figure 8. Volume-rendered images demonstrate a typical PV anatomy with left inferior and superior PVs and right inferior and superior PVs. (Figure was based on illustration from (127).)

The red circles represent the area of the ostium of each PV, whereas the blue arrows show the maximum and minimum orifice diameters.

Abbreviations: LIPV: left inferior pulmonary vein, LSPV: left superior pulmonary vein, RIPV: right inferior pulmonary vein, RSPV: right superior pulmonary vein

After selecting a PV orifice at the angle where the PVs left the LA curvature, the centreline was adjusted manually (104). Subsequently, areas and effective diameters were measured perpendicular to the vessel based on the minimum and maximum diameters of the given orifice (21). The assessments were carried out in the common ostium in the case of a right or left common trunk.

3.2.4 Pulmonary vein isolation procedure

The indication of AF ablation and periprocedural anticoagulation were in line with the current guideline (105). PVI was carried out using the CARTO3 electroanatomical mapping system (Biosense Webster, Inc., Baldwin Park, CA, USA) with radiofrequency energy using the point-by-point technique. The aim of every procedure was to reach electrical isolation of all PVs from the LA with contiguous and circumferential lines of

ablation. Firstly, with a multipolar mapping catheter (Lasso® NAV Eco, Biosense Webster, Inc., Baldwin Park, CA, USA), a fast anatomical map from the LA was generated. Secondly, using the ThermoCool SmartTouch® (Biosense Webster, Inc., Baldwin Park, CA, USA) ablation catheter and a steerable sheath (Agilis, Abbott), radiofrequency ablations were applied in a point-by-point manner. The modified CLOSE protocol was used to guide the ablations: ablation index (AI) target value was 500 on the anterior and 400 on the posterior wall, inter-lesion distance at all sites was < 6 mm, and target contact force 10-40 g. (Figure 9.) During the ablation of the left or right-sided PVs, the mapping catheter was left in the contralateral PVs, enabling the operating physician to evaluate the results of first-pass isolation objectively. After finishing the circumferential ablation line around the given PV, in order to assess entrance and exit blocks, hence the acute success of the PVI, the mapping catheter was placed in the vein. When local PV potentials were absent on the mapping catheter, the entrance block was confirmed, whereas the exit block was assessed by pacing at several sites inside the PVs. When both entrance and exit block was present first-pass isolation was stated. The absence of first-pass isolation was defined by the persistence of PV conduction. In such cases, the ablation was continued until both the entrance and exit blocks were achieved. After an ablation site was finished, the mapping catheter was left in those PVs, and the ablation was continued at the other sides. In order to assess acute PV reconnection, each PV was evaluated repeatedly after 20 minutes. In uncomplicated cases, patients were discharged the day after the procedure.

DOI:10.14753/SE.2024.2997

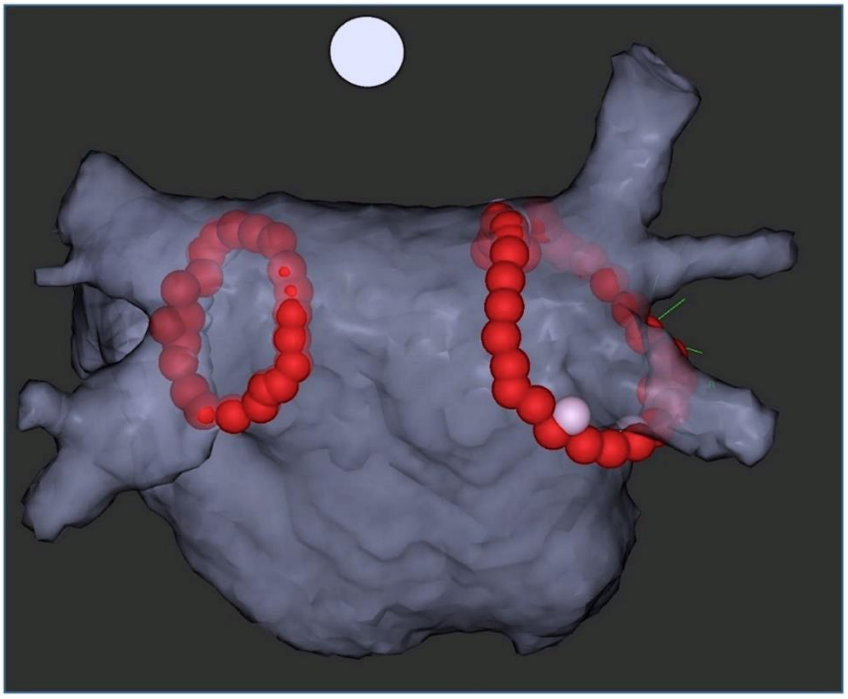

Figure 9. Electroanatomical map of the LA after PV isolation carried out with the modified CLOSE protocol (postero-anterior view). (Figure was basd on illustration from (127).)

All red ablation tags indicate an ablation index value >500 on the anterior wall and >400 on the posterior wall. The inter-tag distance is <6 mm between all neighboring points. The white circle displays the postero-anterior orientation.

Abbreviations: LA: left atrium, PV: pulmonary vein

3.2.5 Statistical analysis

Each analysis was conducted by STATA v13.0. Categorical parameters are presented as frequency (percentages), while continuous variables are represented as mean (standard deviation). For the comparison of LAWT and different LA wall territories or for the assessment of the differences between PVs with the absence or presence of first-pass isolation, an independent sample t-test was used. After that, in order to identify predictors of procedural success of right or left PVs, logistic regression was applied. To evaluate the reproducibility of the measurements, including intra- and inter-observer agreement intraclass correlation coefficient (ICC) was used in 20 patients by a single reader. A two-sided p-value less than 0.05 was considered statistically significant.

DOI:10.14753/SE.2024.2997

4 RESULTS

4.1 Pericoronary adipose tissue analysis

4.1.1 Patient characteristics

4.1.1.1 Zero calcium score group

For the assessment of stable chest pain, 4120 consecutive patients underwent CCTA examination (Philips Brilliance scanner) between 2016 and 2019. Among this patient population, 1839 patients had a zero calcium score. We excluded 187 patients based on exclusion criteria. Overall, 1652 patients were analyzed in the Zero calcium score group who met all the inclusion and exclusion criteria (Figure 10.).

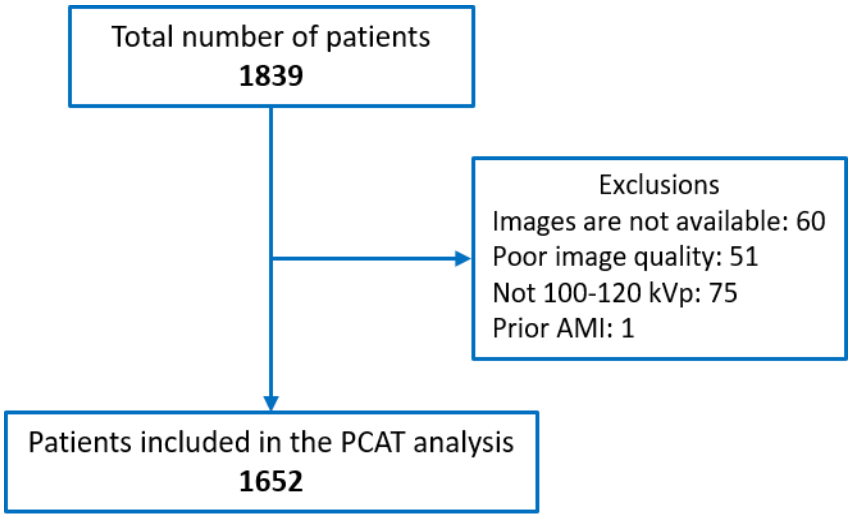

Figure 10. Patient flow charts of the Zero calcium score study group. (Own work.)

Abbreviations: AMI: acute myocardial infarction, kVp: kilovoltage peak, PCAT: pericoronary adipose tissue.

The mean age of the patients was 51±11 years, and 871 patients (53%) were female. Overall, 649 (39%) individuals had a plaque. The summary of patient characteristics and CCTA findings is in Table 1.

DOI:10.14753/SE.2024.2997

Table 1. Patient characteristics of the Zero calcium score study group.

Parameters	**Zero calcium score group n=1652**
Clinical characteristics	
Age [years]	51 ± 11
BMI [kg/m^2]	27.5 ± 5.0
Male sex n (%)	781 (47)
Hypertension n (%)	753 (46)
Diabetes n (%)	115 (7)
Dyslipidemia n (%)	486 (29)
Smoking n (%)	258 (16)
CCTA acquisition parameters	
CT scanner	Philips – Brilliance iCT 256
Heart rate [beats/min]	60 ± 9
Tube voltage [kVp]	
100 kVp n (%)	716 (43)
120 kVp n (%)	936 (57)
Tube current [mAs]	277 ± 37
Contrast volume (106)	89 ± 8
Radiation dose of CCTA [DLP]	248 ± 78
Total effective dose [mSv]	4.2 ± 1.4
Attenuation parameters	
Aorta SD [HU]	29 ± 8
RCA [HU]	577 ± 134
CNR	25 ± 8
SNR	21 ± 8
Coronary artery disease characteristics	
Presence of plaque n (%)	649 (39)
Presence of coronary calcium n (%)	0 (0)
Coronary calcium [score]	0 ± 0
Presence of obstructive stenosis n (%)	15 (1)
SSS [n]	1 ± 2
SIS [n]	1 ± 1
Presence of HRP n (%)	58 (4)
PCAT analysis	
PCAT attenuation [HU]	-92 ± 9
PCAT gradient [%]	-1 ± 12

Continuous variables are presented as mean (SD), while categorical parameters are counts and percentages.

Abbreviations: BMI: body mass index, CNR: contrast to noise ratio, CCTA: coronary CT angiography, DLP: dose length product, HU: Hounsfield Unit, HRP: High-risk plaque, kVp: kilovoltage peak, mAs: milliampere-second, mSv: millisievert, PCAT: pericoronary adipose tissue, RCA: right coronary artery, SD: standard deviation, SIS: segment involvement score, SNR: signal to noise ratio, SSS: segment stenosis score.

DOI:10.14753/SE.2024.2997

4.1.1.2 Zero calcium score group – different scanner

In order to establish the 20% of the number of Zero calcium score group using a different scanner (GE CardioGraph), 398 images were analyzed and 330 suitable scans were selected for PCAT evaluations (Figure 11.).

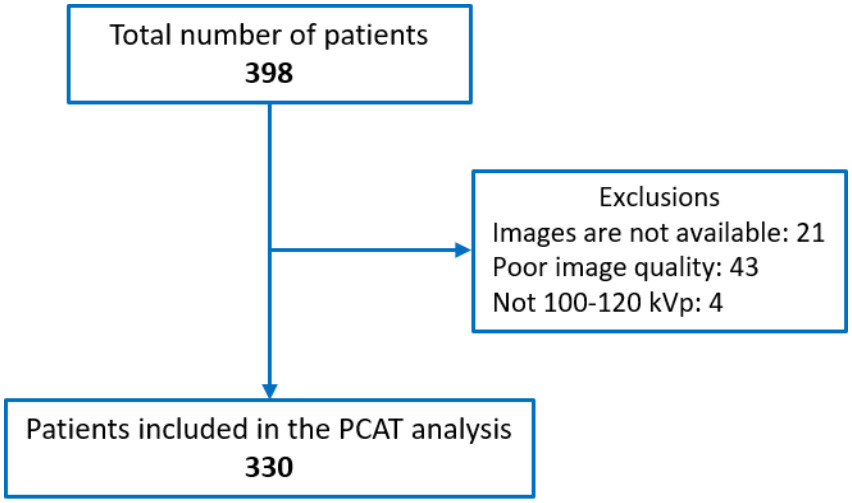

Figure 11. Patient flow charts of the Zero calcium core study group with a different scanner. (Own work.)

Abbreviations: AMI: acute myocardial infarction, kVp: kilovoltage peak PCAT: pericoronary adipose tissue.

The average age was 52±12 years, among them 53% (174/330) were males. Overall, 137 individuals had coronary plaque (Table 2.).

Table 2. Patient characteristics of the Zero calcium score study group with a different scanner.

Parameters	**Zero calcium score group – different scanner n=330**
Clinical characteristics	
Age [years]	52 ± 12
BMI [kg/m^2]	27.5 ± 4.6
Male sex n (%)	174 (53)
Hypertension n (%)	170 (52)
Diabetes n (%)	4 (1)
Dyslipidemia n (%)	93 (28)
Smoking n (%)	48 (15)
CCTA acquisition parameters	
CT scanner	GE – CardioGraphe
Heart rate [beats/min]	65.3 ± 13.0
Tube voltage [kVp]	
100 kVp n (%)	32 (10)
120 kVp n (%)	298 (90)
Tube current [mAs]	210 ± 102
Contrast volume (106)	85 ± 5
Radiation dose of CCTA [DLP]	291 ± 133
Total effective dose [mSv]	4.1 ± 1.9
Attenuation parameters	
Aorta SD [HU]	30 ± 11
RCA [HU]	405 ± 92
CNR	18 ± 7
SNR	15 ± 6
Coronary artery disease characteristics	
Presence of plaque n (%)	137 (42)
Presence of coronary calcium n (%)	0 (0)
Coronary calcium [score]	0 ± 0
Presence of obstructive stenosis n (%)	3 (1)
SSS [n]	1 ± 2
SIS [n]	1 ± 2
Presence of HRP n (%)	3 (1)
PCAT analysis	
PCAT attenuation [HU]	-77 ± 12
PCAT gradient [%]	22 ± 20

Continuous variables are presented as mean (SD), while categorical parameters are counts and percentages.

Abbreviations: BMI: body mass index, CNR: contrast to noise ratio, CCTA: coronary CT angiography, DLP: dose length product, GE: General Electric, HU: Hounsfield Unit, HRP: High-risk plaque, kVp: kilovoltage peak, mAs: milliampere-second, mSv: millisievert, PCAT: pericoronary adipose tissue, RCA: right coronary artery, SD: standard deviation, SIS: segment involvement score, SNR: signal to noise ratio, SSS: segment stenosis score.

DOI:10.14753/SE.2024.2997

4.1.1.3 Moderate to severe CAD group

Overall, 402 scans (Philips Brilliance scanner) were screened to achieve 330 scans suitable for PCAT measurements (Figure 12).

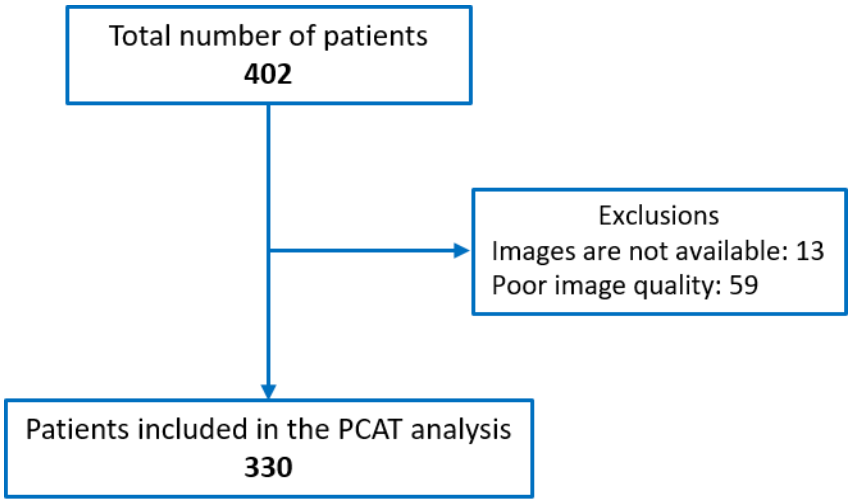

Figure 12. Patient flow charts of the Moderate to severe CAD study group. (Own work.)

Abbreviations: PCAT: pericoronary adipose tissue.

The average age was 63±10 years, and 61% (200/330) were males. Everyone had at least one obstructive plaque per inclusion criteria, and in 43 patients (13%), there was at least one high-risk plaque (Table 3).

Table 3. Patient characteristics of the Moderate to severe CAD study group.

Parameters	**Moderate to severe CAD group n=330**
Clinical characteristics	
Age [years]	63 ± 10
BMI [kg/m^2]	28.7 ± 4.5
Male sex n (%)	200 (61)
Hypertension n (%)	242 (73)
Diabetes n (%)	46 (14)
Dyslipidemia n (%)	138 (42)
Smoking n (%)	51 (16)
CCTA acquisition parameters	
CT scanner	Philips – Brilliance iCT 256
Heart rate [beats/min]	63 ± 13
Tube voltage [kVp]	
100 kVp n (%)	35 (11)
120 kVp n (%)	295 (89)
Tube current [mAs]	255 ± 89
Contrast volume (106)	90 ± 8
Radiation dose of CCTA [DLP]	329 ± 126
Total effective dose [mSv]	4.6 ± 1.7
Attenuation parameters	
Aorta SD [HU]	33 ± 12
RCA [HU]	481 ± 132
CNR	19 ± 8
SNR	16 ± 7
Coronary artery disease characteristics	
Presence of plaque n (%)	330 (100)
Presence of coronary calcium n (%)	283 (86)
Coronary calcium [score]	296 ± 437
Presence of obstructive stenosis n (%)	330 (100)
SSS [n]	9 ± 6
SIS [n]	5 ± 3
Presence of HRP n (%)	43 (13)
PCAT analysis	
PCAT attenuation [HU]	-82 ± 14
PCAT gradient [%]	17 ± 24

Continuous variables are presented as mean (SD), while categorical parameters are counts and percentages.

Abbreviations: BMI: body mass index, CAD: coronary artery disease, CNR: contrast to noise ratio, CCTA: coronary CT angiography, DLP: dose length product, HU: Hounsfield Unit, HRP: High-risk plaque, kVp: kilovoltage peak, mAs: milliampere-second, mSv: millisievert, PCAT: pericoronary adipose tissue, RCA: right coronary artery, SD: standard deviation, SIS: segment involvement score, SNR: signal to noise ratio, SSS: segment stenosis score.

4.1.2 Predictors of PCAT attenuation in the Zero calcium score group

In individuals with zero calcium score (Philips Brilliance Scanner), the range between PCAT values was -123 HU and -51 HU. Average PCAT attenuation was -92 ± 9 HU, whereas the median value was: -93 HU (25^{th} percentile: -99 HU; 75^{th} percentile: -87 HU). Within this study group in patients with no plaque (n=1003), the PCAT attenuation range was -123 HU to -51 HU with an average of -93 ± 9 HU and the median of -94 HU (25^{th} percentile: -100 HU; 75^{th} percentile: -88 HU).

4.1.2.1 Univariable analysis

Among CAD characteristics, the presence of NCP, segment stenosis score (SSS), segment involvement score (SIS), and high-risk plaque were associated with an increasing PCAT attenuation (2.3, 0.6, 1.0, 5.6 HU, respectively; $p<0.001$ for all), whereas there was no evidence of an association between PCAT attenuation and the presence of obstructive stenosis (1.3 HU, p=0.58). Detailed results are depicted in Table 4.

4.1.2.2 Multivariable analysis

After the correction of all factors in the multivariable analysis, among the clinical characteristics of the patients and their image acquisition parameters, male sex, 120 kVp instead of 100 kVp, SNR, and pixel spacing were independently associated with higher PCAT attenuation values (1.4 HU p=0.003, 7.7 HU $p<0.001$, 1.4 HU $p<0.001$, 32.4 HU $p<0.001$; respectively). While the following decreased PCAT attenuation independently: each kg/m^2 increase in BMI, beat/minute in heart rate, mAs in tube current, unit in CNR (-0.4 HU, -0.2 HU, -0.02 HU, -1.3 HU; $p<0.001$ for all; respectively). Moreover, none of the CAD characteristics was associated with PCAT attenuation [presence of NCP (0.1 HU, p=0.93), presence of obstructive stenosis (1.1 HU, p=0.71), SSS (-0.4 HU, p=0.39), SIS (0.8 HU, p=0.18), high-risk plaque (1.9 HU, p=0.10)]. Detailed results are shown in Table 4.

DOI:10.14753/SE.2024.2997

Table 4. The relationship between clinical characteristics, CCTA acquisition parameters, coronary artery disease characteristics, and PCAT attenuation in the Zero calcium score study group.

Predictors	Zero calcium score group (n=1652)					
	Univariable model			Multivariable model		
	HU	95% CI	p	HU	95% CI	p
Clinical characteristics						
Age [y]	0.1	[0.0; 0.1]	**0.001**	0.0	[-0.1; 0.0]	0.23
Male sex	2.6	[1.7; 3.5]	**<0.001**	1.4	[0.5; 2.3]	**0.003**
BMI [kg/m^2]	0.1	[0.0; 0.2]	0.14	-0.4	[-0.5; -0.3]	**<0.001**
Hypertension [mmHg]	1.1	[0.2; 2.0]	**0.01**	0.3	[-0.6; 1.1]	0.53
Diabetes	0.7	[-1.1; 2.4]	0.46	0.7	[-1.0; 2.3]	0.42
Dyslipidemia	0.5	[-0.5; 1.5]	0.30	0.1	[-0.8; 1.0]	0.88
Smoking	0.3	[-0.9; 1.6]	0.62	0.1	[-1.0; 1.2]	0.92
CCTA acquisition parameters						
Non-sinus rhythm	1.3	[-1.9; 4.4]	0.44	2.6	[-0.3; 5.5]	0.08
Heart rate [beats/minute]	-0.2	[-0.3; -0.2]	**<0.001**	-0.2	[-0.2; -0.1]	**<0.001**
Poor image quality	-3.6	[-5.4; -1.8]	**<0.001**	-1.3	[-3.0; 0.5]	0.15
Tube voltage 120 kVp	6.2	[5.4; 7.1]	**<0.001**	7.7	[6.7; 8.7]	**<0.001**
Tube current [mAs]	-0.02	[-0.03; -0.004]	**0.01**	-0.02	[-0.03; -0.01]	**<0.001**
CNR	0.0	[-0.1; 0.1]	0.94	-1.3	[-1.7; -1.0]	**<0.001**
SNR	0.0	[0.0; 0.1]	0.48	1.4	[1.0; 1.7]	**<0.001**
Pixel Spacing [mm^3]	30.5	[22.5; 38.6]	**<0.001**	32.4	[24.9; 39.9]	**<0.001**
Coronary artery disease characteristics						
Presence of plaque	2.3	[1.4; 3.3]	**<0.001**	0.1	[-1.2; 1.4]	0.93
Presence of obstructive stenosis	1.3	[-3.4; 6.1]	0.58	1.1	[-4.5; 6.6]	0.71
SSS [n]	0.6	[0.3; 0.8]	**<0.001**	-0.4	[-1.1; 0.4]	0.39
SIS [n]	1.0	[0.6; 1.4]	**<0.001**	0.8	[-0.4; 2.0]	0.18
Presence of HRP	5.6	[3.2; 8.1]	**<0.001**	1.9	[-0.3; 4.2]	0.10

Univariable and multivariable linear regression models demonstrating the effects of clinical characteristics, CCTA acquisition setting and CAD characteristics on PCAT

attenuation. Significant predictors are marked in bold. All variables were entered into the multivariable models.

Abbreviations: BMI: body mass index, CAD: coronary artery disease, CNR: contrast to noise ratio, CTA: coronary CT angiography, HRP: High-risk plaque, kVp: kilovoltage peak, mAs: milliampere-second, PCAT: pericoronary adipose tissue, SIS: Segment involvement score, SNR: Signal to noise ratio, SSS: Segment Stenosis Score.

4.1.2.3 Sensitivity analysis

In the Main group: Zero calcium score group (Philips Brilliance scanner), 1003 patients had no CAD. Within this subpopulation in the univariable model, the same patient and imaging characteristics were found to be associated with PCAT attenuation as the whole Zero calcium score group, except for hypertension and tube current showed no significance. The same patient and image acquisition parameters were significant in the multivariable analysis. The results of the analysis are represented in Supplementary Table 2 (85).

4.1.3 Predictors of PCAT gradient in the Zero calcium score group

The range between the PCAT gradient values was -31% to 75% in patients with zero calcium scores (Philips Brilliance scanner). The average PCAT gradient value among individuals with a calcium score of zero was: -1±12%, whereas the median value was: -2% (25^{th} percentile: -9%; 75^{th} percentile: 6%).

4.1.3.1 Univariable analysis

A significant association was found between all CAD parameters and PCAT gradient: the presence of NCP (-2.2 % p<0.001), the presence of obstructive stenosis (7.5% p=0.01), SSS (0.9% p<0.001), SIS (1.4% p<0.001), high-risk plaque (5.3% p<0.001) (Table 5.).

4.1.3.2 Multivariable analysis

In the multivariable analysis after correcting for all factors, age (0.1 % p<0.001), male sex (3.1 % p<0.001), non-sinus rhythm (5.6% p=0.01), 120 kVp (4.0% p<0.001) SNR (1.3% p<0.001), and pixel spacing (36.5% p<0.001) were all independently linked with higher PCAT gradient values. Contrarily, each beat per minute increase in heart rate (-0.1% p=0.02), each increase in mAs (-0.02% p=0.003), and CNR (-1.4% p<0.001) were independently associated with lower PCAT gradient values. Moreover, none of the CAD

parameters showed evidence of any association with PCAT gradient: the presence of NCP (0.2 % p=0.79), presence of obstructive stenosis (4.0% p=0.28), SSS (0.0% p=0.94) SIS (0.4% p=0.65) and presence of high-risk plaque (1.8% p=0.25). Detailed results are displayed in Table 5.

Table 5. The relationship between clinical characteristics, CCTA acquisition parameters, coronary artery disease characteristics, and PCAT gradient in the Zero calcium score study group.

Predictors	Zero calcium score group (n=1652)					
	Univariable model			Multivariable model		
	%	95% CI	p	%	95% CI	p
Clinical characteristics						
Age [y]	0.1	[0.1; 0.2]	**<0.001**	0.1	[0.1; 0.2]	**<0.001**
Male sex	3.1	[2.0; 4.2]	**<0.001**	3.1	[1.8; 4.3]	**<0.001**
BMI [kg/m^2]	0.4	[0.3; 0.5]	**<0.001**	-0.1	[-0.2; 0.1]	0.38
Hypertension [mmHg]	2.2	[1.1; 3.4]	**<0.001**	0.2	[-1.0; 1.3]	0.78
Diabetes	1.6	[-0.6; 3.9]	0.16	0.1	[-2.1; 2.2]	0.97
Dyslipidemia	1.8	[0.6; 3.1]	**0.004**	0.8	[-0.5; 2.0]	0.22
Smoking	0.8	[-0.8; 2.3]	0.35	0.9	[-0.6; 2.4]	0.25
CCTA acquisition parameters						
Non-sinus rhythm	4.8	[0.7; 8.8]	**0.02**	5.6	[1.7; 9.5]	**0.01**
Heart rate [beats/minute]	-0.1	[-0.2; -0.1]	**<0.001**	-0.1	[-0.15; -0.01]	**0.02**
Poor image quality	-3.2	[-5.5; -0.8]	**0.008**	-2.2	[-4.5; 0.1]	0.07
Tube voltage 120 kVp	5.4	[4.3; 6.6]	**<0.001**	4.0	[2.7; 5.3]	**<0.001**
Tube current [mAs]	0.0	[0.0; 0.0]	0.82	-0.02	[-0.04; -0.01]	**0.003**
CNR	-0.2	[-0.3; -0.1]	**<0.001**	-1.4	[-1.8; -0.9]	**<0.001**
SNR	-0.2	[-0.3; -0.1]	**<0.001**	1.3	[0.8; 1.8]	**<0.001**
Pixel Spacing [mm^3]	41.1	[30.9; 51.4]	**<0.001**	36.5	[26.4; 46.6]	**<0.001**
Coronary artery disease characteristics						
Presence of plaque	-2.2	[2.0; 4.4]	**<0.001**	0.2	[-1.5; 2.0]	0.79
Presence of obstructive stenosis	7.5	[1.5; 13.5]	**0.01**	4.0	[-3.4; 11.5]	0.28
SSS [n]	0.9	[0.6; 1.2]	**<0.001**	0.0	[-1.0; 1.1]	0.94

SIS [n]	1.4	[0.9; 1.8]	**<0.001**	0.4	[-1.2; 2.0]	0.65
Presence of HRP	5.3	[2.2; 8.4]	**<0.001**	1.8	[-1.3; 4.9]	0.25

Univariable and multivariable linear regression models demonstrating the effects of clinical characteristics, CCTA acquisition setting, and CAD characteristics on PCAT gradient. Significant predictors are marked in bold. All variables were entered into the multivariable models.

Abbreviations: BMI: body mass index, CAD: coronary artery disease, CNR: contrast to noise ratio, CTA: coronary CT angiography, HRP: High-risk plaque, kVp: kilovoltage peak, mAs: milliampere-second, PCAT: pericoronary adipose tissue, SIS: Segment involvement score, SNR: signal to noise ratio, SSS: segment stenosis score.

4.1.3.3 Sensitivity analysis

For patients who had a calcium score of zero and had no CAD (n=1003) in the Main group (Zero calcium score group Philips Brilliance scanner), the same parameters were found to have a significant association with PCAT gradient in the univariable analyses as in the whole patient population with zero calcium score. Only poor image quality and heart rate were non-significant. In the multivariable analysis, the same patient and image acquisition parameters were significant, apart from heart rate. The results of the analysis are represented in Supplementary Table 3 (85).

4.1.4 Validation group: Zero calcium score group – different scanner

Comparing PCAT attenuation values, it was lower in the main Zero calcium score group (Philips Brilliance scanner) than in the Zero calcium score group -different scanner (GE CardioGraphe scanner) (-92 ± 9 vs. -77 ± 12, $p<0.001$). The attenuation values ranged between -105 HU and -49 HU, whereas gradient values ranged between -21% and 90%.

4.1.4.1 Univariable analysis

No association was found between plaque markers and PCAT attenuation, while only the presence of plaque was associated with higher PCAT gradient values (5.3%, $p<0.02$) (Table 6.).

4.1.4.2 Multivariable analysis

After correcting for patient and image acquisition parameters, the univariate association between the presence of plaque and PCAT gradient disappeared. In terms of PCAT attenuation, BMI (-0.4 HU, p=0.01), heart rate (-0.2 HU, p<0.001), poor image quality (-5.2 HU, p=0.02) and pixel spacing (80.9 HU, p=0.02) remained significant, whereas only age (0.2%, p=0.03) male sex (9.1%, p<0.001) and poor image quality (-7.8%, p=0.04) were significant regarding PCAT gradient.

DOI:10.14753/SE.2024.2997

Table 6. The relationship between clinical characteristics, CCTA acquisition parameters, coronary artery disease characteristics, and PCAT attenuation/gradient in the Zero calcium score study group with a different scanner.

Predictors	Zero calcium score group – different scanner (n=330)											
	PCAT attenuation						PCAT gradient					
	Univariable model			Multivariable model			Univariable model			Multivariable model		
	HU	95% CI	p	HU	95% CI	p	%	95% CI	p	%	95% CI	p
Clinical characteristics												
Age [y]	0.1	[-0.04; 0.2]	0.27	0.1	[-0.02; 0.2]	0.09	0.1	[-0.04; 0.3]	0.12	0.2	[0.03; 0.4]	**0.03**
Male sex	0.9	[-1.6; 3.5]	0.47	2.6	[-0.1; 5.3]	0.06	6.8	[2.6; 11.0]	**0.002**	9.1	[4.5; 13.7]	**<0.001**
BMI [kg/m^2]	-0.4	[-0.6; -0.1]	**0.01**	-0.4	[-0.7; -0.1]	**0.01**	-0.2	[-0.7; 0.2]	0.32	-0.4	[-0.9; 0.03]	0.06
Hypertension [mmHg]	0.1	[-2.4; 2.7]	0.93	0.6	[-2.1; 3.3]	0.67	1.5	[-2.8; 5.7]	0.49	-0.1	[-4.7; 4.4]	0.96
Diabetes	-1.3	[-13.0; 10.3]	0.82	2.4	[-8.8; 13.7]	0.67	-7.6	[-27.0; 11.8]	0.44	-4.4	[-23.5; 14.7]	0.65
Dyslipidemia	-1.0	[-3.8; 1.8]	0.48	-0.7	[-3.5; 2.0]	0.61	-1.2	[-5.9; 3.5]	0.63	-0.4	[-5.1; 4.3]	0.85
Smoking	0.8	[-2.8; 4.4]	0.66	1.5	[-1.9; 4.9]	0.39	-1.8	[-7.8; 4.2]	0.55	-0.2	[-6.1; 5.6]	0.93
CCTA acquisition parameters												
Non-sinus rhythm	-4.5	[-13.4; 4.3]	0.31	4.9	[-4.7; 14.4]	0.32	-5.2	[-19.9; 9.6]	0.49	7.7	[-8.5; 23.9]	0.35
Heart rate [beats/minute]	-0.2	[-0.3; -0.1]	**<0.001**	-0.2	[-0.3; -0.1]	**<0.001**	-0.3	[-0.4; -0.1]	**0.002**	-0.3	[-0.5; -0.1]	0.005
Poor image quality	-7.4	[-11.7; -3.1]	**<0.001**	-5.2	[-9.5; -0.9]	**0.02**	-10.1	[-17.3; -2.9]	**0.01**	-7.8	[-15.1; -0.5]	**0.04**
Tube voltage 120 kVp	0.2	[-0.1; 0.4]	0.14	0.2	[-0.1; 0.4]	0.17	0.4	[0.02; 0.7]	**0.04**	0.3	[-0.1; 0.6]	0.19
Tube current [mAs]	-0.01	[-0.02; -0.0002]	**0.04**	-0.01	[-0.02; 0.002]	0.12	-0.01	[-0.03; 0.01]	0.36	-0.01	[-0.03; 0.01]	0.38
CNR	0.4	[0.2; 0.6]	**<0.001**	0.3	[-0.8; 1.4]	0.59	0.5	[0.1; 0.8]	**0.004**	0.4	[-1.4; 2.2]	0.64
SNR	0.4	[0.2; 0.6]	**<0.001**	0.1	[-1.1; 1.3]	0.90	0.5	[0.2; 0.9]	**0.003**	0.03	[-2.0; 2.0]	0.98
Pixel Spacing [mm^3]	49.3	[-20.4; 119.1]	0.16	80.9	[13.2; 148.5]	**0.02**	16.1	[-100.6; 132.7]	0.79	63.3	[-51.7; 178.2]	0.28
Coronary artery disease characteristics												
Presence of plaque	2	[-0.6; 4.5]	0.13	3.6	[-0.2; 7.3]	0.06	5.3	[1.0; 9.6]	**0.02**	5.1	[-1.2; 11.5]	0.11
Presence of obstructive stenosis	9.9	[-3.5; 23.3]	0.15	13.1	[-2.0; 28.2]	0.09	14.0	[-8.3; 36.4]	0.22	8.2	[-17.5; 33.9]	0.53
SSS [n]	-0.1	[-0.7; 0.6]	0.88	-0.5	[-2.8; 1.8]	0.66	0.7	[-0.4; 1.8]	0.21	0.3	[-3.6; 4.1]	0.88
SIS [n]	-0.1	[-0.9; 0.8]	0.84	-0.4	[-3.3; 2.4]	0.77	0.8	[-0.6; 2.2]	0.25	-1.5	[-6.3; 3.4]	0.56
Presence of HRP	-3.3	[-16.7; 10.1]	0.62	-0.2	[-14.0; 13,7]	0.98	10.2	[-12.1; 32.6]	0.37	10.0	[-13.5; 33.5]	0.40

Univariable and multivariable linear regression models demonstrating the effects of clinical characteristics, CTA acquisition setting and CAD characteristics on PCAT attenuation/gradient. Significant predictors are marked in bold. All variables were entered into the multivariable models.

Abbreviations: BMI: body mass index, CAD: coronary artery disease, CNR: contrast to noise ratio, CTA: coronary CT angiography, HRP: High-risk plaque, kVp: kilovoltage peak, mAs: milliampere-second, PCAT: pericoronary adipose tissue, SIS: Segment involvement score, SNR: Signal to noise ratio, SSS: Segment Stenosis Score.

4.1.5 Validation group: Moderate to severe CAD group

PCAT values in the Moderate to severe CAD group (Philips Brilliance scanner) ranged between -82 HU and -50 HU, whereas the gradient values ranged between -22% and 116%.

4.1.5.1 Univariable analysis

Regarding plaque markers, SSS and SIS were associated with PCAT attenuation (0.5 HU, p<0.001; 1.1 HU, p<0.001, respectively). In the case of PCAT gradient, similarly, only SSS and SIS were significantly associated (1.0%, p<0.001, 2.3%, p<0.001, respectively). However, several patient and image acquisition parameters are also significantly linked with PCAT markers (Table 7).

4.1.5.2 Multivariable analysis

After the correction of all patient and image acquisition characteristics, only the presence of high-risk plaque had an association with PCAT attenuation (3.7 HU, p=0.04). In contrast, none of the plaque markers were associated with PCAT gradients similar to the main cohort. Nonetheless, in parallel to the initial cohort, BMI (-0.4 HU, p=0.02) and several image acquisition parameters were associated with PCAT attenuation, including [tube voltage (0.5 HU, p<0.001), tube current (-0.04 HU, p<0.001), CNR (-1.5 HU, p=0.002) SNR (1,6 HU, p=0.004) pixel spacing (100.0 HU, p<0.001)]. In contrast, only image acquisition settings showed a significant association with PCAT gradient: tube voltage (0.4%, p=0.02), tube current (-0.1%, p<0.001), CNR (-2.3%, p=0.01) SNR (2.6%, p=0.02) pixel spacing (157.4%, p<0.001) (Table 7).

Representative images from all three groups showing how different heart rates influence PCAT attenuation and PCAT gradient values are shown in Figure 13.

DOI:10.14753/SE.2024.2997

Table 7. The relationship between clinical characteristics, CCTA acquisition parameters, coronary artery disease characteristics, and PCAT attenuation/gradient in the Moderate to severe CAD study group.

Predictors	Moderate to severe CAD group – (n=330)											
	PCAT attenuation						PCAT gradient					
	Univariable model			Multivariable model			Univariable model			Multivariable model		
	HU	95% CI	p	HU	95% CI	p	%	95% CI	p	%	95% CI	p
Clinical characteristics												
Age [y]	0.01	[-0.1; 0.2]	0.84	-0.1	[-0.2; 0.1]	0.44	0.2	[-0.1; 0.4]	0.14	0.1	[-0.2; 0.3]	0.47
Male sex	3.0	[0.001; 6.0]	0.05	1.1	[-1.6; 3.9]	0.41	5.6	[0.3; 10.9]	**0.04**	4.0	[-1.2; 9.1]	0.13
BMI [kg/m^2]	-0.3	[-0.6; 0.05]	0.09	-0.4	[-0.7; -0.1]	**0.02**	-0.1	[-0.7; 0.4]	0.63	-0.2	[-0.7; 0.4]	0.55
Hypertension [mmHg]	-0.1	[-3.4; 3.2]	0.94	-0.9	[-3.7; 1.9]	0.53	3.2	[-2.6; 9.1]	0.28	0.5	[-4.8; 5.8]	0.84
Diabetes	0.3	[-4.0; 4.5]	0.90	-1.4	[-4.9; 2.1]	0.42	1.2	[-6.3; 8.7]	0.76	-3.4	[-9.9; 3.2]	0.31
Dyslipidemia	1.3	[-1.7; 4.2]	0.41	2.1	[-0.5; 4.6]	0.11	3.5	[-1.7; 8.8]	0.19	3.8	[-0.9; 8.5]	0.12
Smoking	0.1	[-3.9; 4.2]	0.95	-0.03	[-3.4; 3.3]	0.99	-0.1	[-7.3; 7.0]	0.97	0.03	[-6.2; 6.2]	0.99
CCTA acquisition parameters												
Non-sinus rhythm	-8.9	[-18.4; 0.6]	0.07	0.8	[-8.5; 10.0]	0.87	-17.6	[-34.4; -0.9]	**0.04**	-0.8	[-18.1; 16.5]	0.93
Heart rate [beats/minute]	-0.1	[-0.2; 0.03]	0.12	-0.1	[-0.2; 0.1]	0.32	-0.2	[-0.4; -0.012]	**0.04**	-0.1	[-0.3; 0.1]	0.21
Poor image quality	-5.7	[-11.6; 0.1]	0.05	-0.6	[-5.4; 4.2]	0.80	-11.0	[-21.4; -0.7]	**0.04**	-2.8	[-11.9; 6.2]	0.54
Tube voltage 120 kVp	0.5	[0.3; 0.7]	**<0.001**	0.5	[0.3; 0.7]	**<0.001**	0.7	[0.2; 1.1]	**0.002**	0.4	[0.1; 0.8]	**0.02**
Tube current [mAs]	-0.1	[-0.1; -0.05]	**<0.001**	-0.04	[-0.1; -0.02]	**<0.001**	-0.1	[-0.1; -0.1]	**<0.001**	-0.1	[-0.1; -0.03]	**<0.001**
CNR	-0.1	[-0.3; 0.1]	0.23	-1.5	[-2.5; -0.5]	**0.002**	-0.2	[-0.5; 0.1]	0.26	-2.3	[-4.2; -0.5]	**0.01**
SNR	-0.1	[-0.3; 0.2]	0.56	1.6	[0.5; 2.7]	**0.004**	-0.1	[-0.5; 0.3]	0.57	2.6	[0.5; 4.6]	**0.02**
Pixel Spacing [mm^3]	129.6	[103.5; 155.7]	**<0.001**	100.0	[73.9; 126.1]	**<0.001**	211.9	[164.8; 259.0]	**<0.001**	157.4	[108.6; 206.1]	**<0.001**
Coronary artery disease characteristics												
Presence of plaque	-	-	-	-	-	-	-	-	-	-	-	-
Presence of obstructive stenosis	3.5	[-0.2; 7.2]	0.06	2.3	[-1.5; 6.2]	0.24	6.4	[-0.1; 13.0]	0.05	2.0	[-5.2; 9.2]	0.58
SSS [n]	0.5	[0.2; 0.7]	**<0.001**	-0.2	[-0.8; 0.3]	0.46	1.0	[0.6; 1.4]	**<0.001**	-0.1	[-1.1; 1.0]	0.92
SIS [n]	1.1	[0.6; 1.6]	**<0.001**	0.9	[-0.2; 1.9]	0.09	2.3	[1.5; 3.2]	**<0.001**	1.4	[-0.6; 3.3]	0.17
Presence of HRP	2.9	[-1.5; 7.2]	0.19	3.7	[0.1; 7.2]	**0.04**	2.7	[-5.0; 10.4]	0.49	3.5	[-3.1; 10.2]	0.30

Univariable and multivariable linear regression models demonstrating the effects of clinical characteristics, CTA acquisition setting and CAD characteristics on PCAT attenuation/gradient. Significant predictors are marked in bold. All variables were entered into the multivariable models.

Abbreviations: BMI: body mass index, CAD: coronary artery disease, CNR: contrast to noise ratio, CTA: coronary CT angiography, HRP: High-risk plaque, kVp: kilovoltage peak, mAs: milliampere-second, PCAT: pericoronary adipose tissue, SIS: Segment involvement score, SNR: Signal to noise ratio, SSS: Segment Stenosis Score.

DOI:10.14753/SE.2024.2997

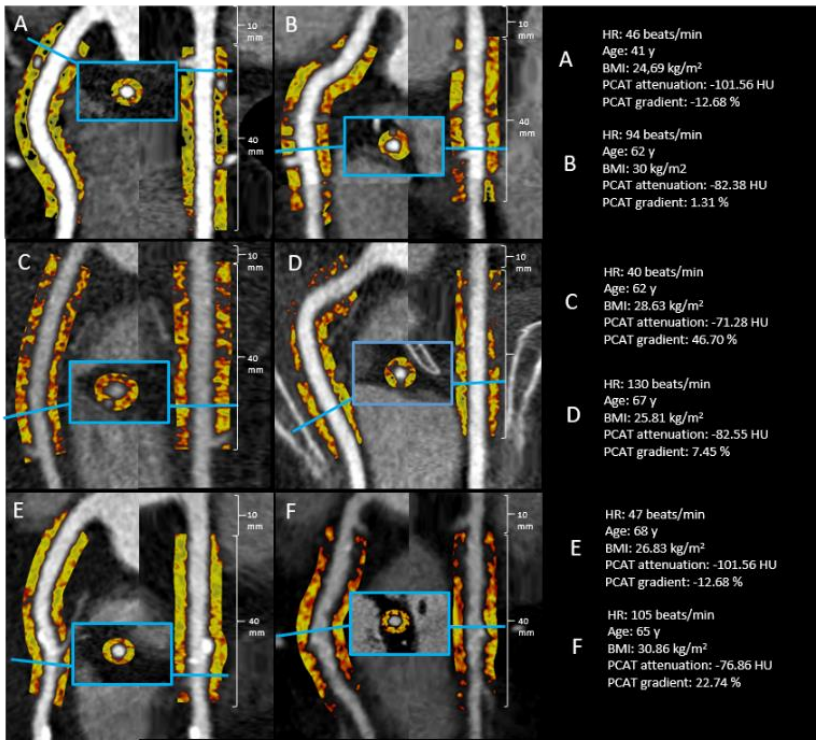

Figure 13. Representative images showing differences in PCAT attenuation and PCAT gradient in patients with different heart rates. (Figure from (126).)

Panels **A** and **B** show two representative images from the Zero calcium score group. Patients were scanned on a Philips - Brilliance iCT 256 and had a calcium score of zero. Panels **C** and **D** show two representative cases from the Zero calcium score - different scanner group. Patients were scanned on a GE - CardioGraphe and had a calcium score of zero. Panels **E** and **F** show two representative images from the Moderate to severe CAD group. Patients were scanned on a Philips - Brilliance iCT 256 and had obstructive CAD. Patients within all three cohorts had a wide range of PCAT attenuation and gradient values.

Abbreviations: BMI: body mass index, CAD: coronary artery disease, HR: heart rate, HU: Hounsfield unit, PCAT: pericoronary adipose tissue.

4.1.6 Cardiovascular outcome analysis

In the Zero calcium score group, during the average 3.0-year follow-up time, two patients had AMI, with PCAT attenuation and gradient values of -93 HU and -79 HU and -1% and 19%, respectively. In the Zero calcium score validation cohort with a different scanner, no events occurred within the average follow-up time of 0.7 years, whereas in

DOI:10.14753/SE.2024.2997

the Moderate to severe CAD group, there were seven events with an average of 2.2 years. The PCAT attenuation ranged between -88 HU and -64 HU, and the gradient values were between 7% to 51%.

4.2 Left atrial wall thickness and pulmonary vein analysis

4.2.1 Patient characteristics

Overall, the study population for analysis comprised 94 patients. The mean age was 62±13 years, the mean BMI was 28.1±3.5 kg/m^2, and 39.4% were female. A total of 1034 LAWT values were measured, and 376 PV ostium diameters and areas were analyzed. The flow chart and the table, including the baseline characteristics of the study population, are summarized in Figure 14. and Table 8., respectively.

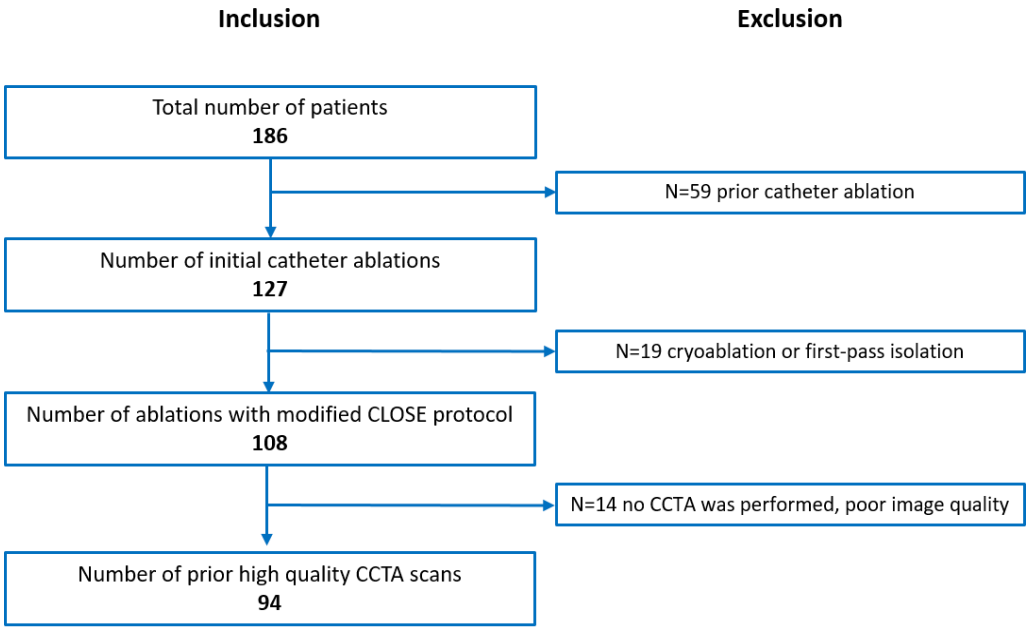

Figure 14. Study design. (Own work.)

Abbreviation: CCTA: coronary CT angiography

DOI:10.14753/SE.2024.2997

Table 8. Patient characteristics.

Parameters	Total N=94	Successful first-pass isolation in all PVs N=51	Absence of first-pass isolation in at least one PV N=43	p value
Antropometric, comoribities				
Age (years), (mean ± SD)	63 ± 13	63 ± 10	62 ± 15	0.06
Female sex, n (%)	37 (39.40)	23 (45.10)	14 (32.60)	0.21
Body mass index (kg/m^2), (mean ± SD)	28.14 ± 3.49	27.91 ± 3.56	28.44 ± 3.43	0.81
Body surface area (m^2), (mean ± SD)	2.04 ± 0.19	2.04 ± 0.20	2.06 ± 0.20	0.14
Diabetes, n (%)	14 (14.90)	5 (9.80)	0 (0.0)	0.06
Hypertension, n (%)	61 (64.90)	36 (70.60)	25 (58.10)	0.20
Hyperlipidemia, n (%)	26 (27.70)	19 (37.30)	7 (16.30)	**0.03**
Prior Stroke/TIA, n (%)	4 (4.30)	2 (3.90)	2 (4.70)	0.86
Persistent AF, n (%)	36 (38.30)	17 (33.30)	19 (44.20)	0.28
CHA_2DS_2-VASc score, (mean ± SD)	2.11 ± 1.46	2.03 ± 1.36	2.10 ± 1.57	0.71
Procedural parameters				
LAT (min), (mean ± SD)	61.87 ± 15.63	62.08 ± 17.29	61.62 ± 13.57	0.89
Procedure time (min), (mean ± SD)	81.16 ± 19.29	75.31 ± 14.21	88.44 ± 22.27	**0.01**
Fluoroscopy time (min), (mean ± SD)	214.15 ± 177.28	192.69 ± 172.03	239.18 ± 182.17	0.61
Fluoroscopy dose (mGym^2), (mean ± SD)	0.34 ± 1.13	0.22 ± 0.443	0.49 ± 1.61	0.06
Echocardiographic parameters				
Ejection fraction (%), (mean ± SD)	57.90 ± 8.00	58.28 ± 7,57	57.38 ± 8.51	0.63
LAA flow, cm/s	57.08 ± 24.24	57.58 ± 24.19	56.37 ± 24.71	0.40
CT derived parameter				
LAV (ml), (mean ± SD)	101.61 ± 39.82	99.67 ± 35.43	104.02 ± 45.03	0.08

Significant values are marked in bold.

Abbreviations: AF: atrial fibrillation, LAA: left atrial appendage, LAT: left atrial time, LAV: left atrial volume, PV: pulmonary vein, SD: standard deviation, TIA: transient ischemic attack.

4.2.2 Left atrial measurement

The mean LAWT value was 1.35±0.76 (ranging from 0.1 to 4.2 mm). Table 9. shows the results of LAWT measurements.

Table 9. The LAWT values in millimeters in 11 locations.

LA locations	Mean	SD	Standard Error	95% CI for mean		Minimum	Maximum
				Lower Bound	Upper Bound		
1	1.79	0.81	0.08	1.63	1.96	0.20	4.20
2	1.93	0.79	0.08	1.77	2.09	0.10	4.00
3	1.56	0.75	0.07	1.41	1.72	0.10	3.10
4	1.21	0.60	0.06	1.09	1.33	0.10	2.80
5	1.29	0.66	0.06	1.16	1.43	0.20	3.20
6	0.97	0.54	0.05	0.86	1.08	0.10	2.50
7	1.01	0.52	0.05	0.89	1.11	0.10	2.40
8	1.01	0.59	0.06	0.89	1.13	0.20	2.80
9	0.83	0.49	0.05	0.73	0.94	0.10	2.30
10	1.24	0.67	0.06	1.10	1.38	0.10	2.70
11	1.95	0.77	0.08	1.79	2.11	0.20	4.00
Total	1.35	0.76	0.02	1.30	1.39	0.10	4.20

1: right roof, 2: right mid-posterior, 3: right infero-posterior, 4: middle roof, 5: middle mid-posterior, 6: middle infero-posterior, 7: left roof, 8: left mid-posterior, 9: left infero-posterior, 10: mitral isthmus, 11: left lateral ridge

Abbreviations: CI: confidence interval, LA: left atrium, LAWT: left atrial wall thickness, SD: standard deviation.

With a mean value of 0.83±0.49 mm, the left infero-posterior mean thickness was the lowest and was significantly smaller in comparison to the right roof, right mid-posterior, right infero-posterior, middle roof, middle mid-posterior, and the mitral isthmus and left lateral ridge LA locations ($p<0.01$). The left lateral ridge represented the largest LAWT, with a mean value of 1.95±0.77 mm, and was significantly larger than other LA locations ($p<0.01$).

Regional differences were assessed with the combination of several measurement points. We found that LAWT on the right side (roof, mid-posterior, infero-posterior) was significantly larger in contrast to the middle (roof, mid-posterior, infero-posterior) and left side (roof, mid-posterior, infero-posterior) (all $p<0.01$). The infero-posterior region (right infero-posterior, middle infero-posterior, left infero-posterior) was substantially

DOI:10.14753/SE.2024.2997

thinner than the mean middle (right mid-posterior, middle mid-posterior, left mid-posterior) and mean roof total (right roof, middle roof, left roof ($p=0.01$ and $p=0.08$, respectively). PV diameters and areas are summarized in Table 10.

DOI:10.14753/SE.2024.2997

Table 10. CCTA-based assessment of LA-PV parameters.

	First-pass on left side	Unsuccessful first-pass on left side	p value	First-pass on right side	Unsuccessful first-pass on right side	p value
PV diameter (mm), (mean ± SD)						
LIPV	17.64 ± 5.89	16.43 ± 3.95	0.31	NA	NA	NA
LSPV	18.60 ± 3.14	17.19 ± 3.85	0.19	NA	NA	NA
RSPV	NA	NA	NA	21.34 ± 3.19	19.90 ± 3.71	**0.04**
RIPV	NA	NA	NA	18.04 ± 3.06	17.29 ± 2.61	0.23
PV area (mm2), (mean ± SD)						
LIPV	269.67 ± 220.16	224.11 ±116.93	0.33	NA	NA	NA
LSPV	280.98 ± 98.39	250.00 ± 94.61	0.08	NA	NA	NA
RSPV	NA	NA	NA	371.63 ± 111.26	312.52 ± 122.66	0.09
RIPV	NA	NA	NA	266.86 ± 88.35	241.81 ± 62.15	0.31
LAWT (mm), (mean ± SD)						
Mean total	1.35 ± 0.46	1.32 ± 0.51	0.78	1.34 ± 0.46	1.32 ± 0.54	0.83
Mean roof	1.39 ± 0.59	1.21 ± 0.53	0.18	1.36 ± 0.56	1.27 ± 0.66	0.52
Mean mid-posterior	1.39 ± 0.60	1.41 ± 0.74	0.91	1.37 ± 0.65	1.45 ± 0.62	0.64
Mean infero-posterior	1.12 ± 0.52	1.09 ± 0.62	0.89	1.09 ± 0.55	1.18 ± 0.57	0.51
Mean left	1.21 ± 0.44	1.18 ± 0.49	0.74	NA	NA	NA
Mean right	NA	NA	NA	1.74 ± 0.66	1.79 ± 0.68	0.74

Significant values are marked in bold.

Abbreviations: CCTA: coronary CT angiography, CT: computer tomography, LA-PV: Left Atrial – Pulmonary Veins LAWT: left atrial wall thickness, LIPV: left inferior pulmonary vein, LSPV: left superior pulmonary vein, NA: not applicable, PV: pulmonary vein, RIPV: right inferior pulmonary vein, RSPV: right superior pulmonary vein, SD: standard deviation.

4.2.3 The effect of clinical and CT-derived parameters on the first-pass isolation rate

In 100% of the PVs, complete electrical isolation was achieved. There were no periprocedural complications. Successful first-pass isolation was achieved in 67 cases on the right side and 71 on the left. Successful first-pass isolation of every PV was captured in 51 patients. No acute reconnection was administered during the 20 min post-ablation waiting period. As for anthropometrics and clinical risk factors, no association was detected with the first-pass isolation success rate, based on univariate regression analysis, in any case of first-pass isolation. Where first-pass isolation was achieved on both sides, shorter procedural time was found (p=0.03).

We also showed that LAWT did not affect the first-pass isolation rate during PVI, guided by our standardized ablation protocol.

Among all analyzed parameters, only the RSPV diameter was linked with the success rate of right-sided first-pass isolation, as a wider RSPV diameter resulted in easier first-pass isolation (OR 1.01, p=0.04). The success rate of first-pass isolation was not influenced by other CCTA and echocardiography-derived parameters (all p>0.05) (Table 11.).

Table 11. Univariate logistic regression analysis for the detection of predictors of achieving first-pass isolation.

Parameters	First-pass isolation in all PVs				First-pass isolation in case of right-sided PVs				First-pass isolation in case of left-sided PVs			
	p value	OR	95% CI		p value	OR	95% CI		p value	OR	95% CI	
Age	0.75	1.00	0.97	1.03	0.18	1.02	0.98	1.06	0.76	1.00	0.97	1.04
Female sex	0.21	0.58	0.25	1.36	0.21	0.51	0.17	1.46	0.77	0.87	0.34	2.18
Body mass index	0.13	1.10	0.97	1.24	0.38	1.06	0.92	1.23	0.49	1.04	0.91	1.20
Diabetes	0.07	0.32	0.09	1.13	0.51	0.65	0.18	2.37	0.14	0.40	0.12	1.35
Hypertension	0.21	1.72	0.73	4.06	0.82	1.11	0.41	3.0	0.23	1.75	0.70	4.38
Hyperlipidemia	0.02	3.05	1.13	8.20	0.09	3.03	0.81	11.30	0.45	1.48	0.52	4.24
Prior Stroke/TIA	0.86	0.83	0.11	6.20	0.94	0.92	0.09	9.38	0.86	1.21	0.12	12.26
Paroxysmal/persistent AF	0.28	1.58	0.68	3.65	0.80	1.12	0.42	2.99	0.75	1.15	0.46	2.87

CHA_2DS_2-VASc	0.65	0.92	0.66	1.29	0.69	1.08	0.72	1.60	0.28	0.82	0.57	1.17
Ablation parameters												
LAT	0.88	1.00	0.98	1.03	0.99	1.00	0.97	1.03	0.91	1.00	0.97	1.03
Procedure time	**0.03**	0.95	0.93	0.98	0.16	0.98	0.96	1.00	0.031	0.97	0.94	0.99
Fluoroscopy time	0.21	0.99	0.99	1.00	0.29	0.99	0.99	1.00	0.756	1.00	0.99	1.00
Echocardiographic parameters												
Ejection fraction, (mean ± SD)	0.62	1.01	0.95	1.07	0.21	1.0	0.97	1.10	0.71	0.98	0.92	1.05
LAA flow	0.83	1.00	0.98	1.02	0.20	0.98	0.96	1.00	0.29	1.01	0.98	1.03
CT derived parameters												
LAV, (mean ± SD)	0.60	0.99	0.98	1.00	0.47	0.99	0.98	1.00	0.62	1.00	0.99	1.01
PV diameter, (mean ± SD)												
LIPV	0.29	1.00	0.99	1.00	NA	NA	NA	NA	0.32	1.00	0.99	1.00
LSPV	0.10	1.00	0.99	1.00	NA	NA	NA	NA	0.19	1.00	0.99	1.00
RSPV	0.16	1.00	.99	1.00	**0.04**	1.01	1.00	1.01	NA	NA	NA	NA
RIPV	0.06	1.00	1.00	1.01	0.22	1.00	0.99	1.01	NA	NA	NA	NA
PV area												
LIPV	0.33	1.04	0.96	1.12	NA	NA	NA	NA	0.33	1.04	0.95	1.15
LSPV	0.12	1.11	0.97	1.27	NA	NA	NA	NA	0.09	1.13	0.98	1.32
RSPV	0.07	1.13	0.99	1.29	0.08	1.15	0.97	1.35	NA	NA	NA	NA
RIPV	0.05	1.15	0.99	1.33	0.30	1.09	0.92	1.29	NA	NA	NA	NA
LAWT, (mean ± SD)												
Mean total	0.35	0.66	0.27	1.59	0.82	1.12	0.40	3.10	0.77	1.15	0.44	2.99
Mean roof	0.56	1.22	0.60	2.49	0.51	1.31	0.56	3.05	0.17	1.74	0.77	3.93
Mean mid-posterior	0.09	0.56	0.28	1.09	0.63	0.83	0.39	1.76	0.90	0.95	0.47	1.93
Mean infero-posterior	0.16	0.58	0.27	1.25	0.50	0.74	0.31	1.78	0.89	1.05	0.46	2.41
Mean left	0.53	1.18	0.68	2.05	NA	NA	NA	NA	0.73	1.18	0.43	3.19
Mean right	0.64	0.88	0.52	1.48	0.73	0.88	0.42	1.83	NA	NA	NA	NA
Mitral isthmus	0.34	0.74	0.40	1.37	0.84	1.07	0.52	2.21	0.67	0.86	0.44	1.70
Left lateral ridge	0.32	1.31	0.76	2.24	0.05	2.01	0.99	4.05	0.93	1.02	0.57	1.84

Abbreviations: AF: atrial fibrillation, CI: confidence interval, CT: computer tomography, LAA: left atrial appendage, LAT: left atrial time, LAV: left atrial volume, LAWT: left

atrial wall thickness, LIPV: left inferior pulmonary vein, LSPV: left superior pulmonary vein, PV: pulmonary vein, RIPV: right inferior pulmonary vein, RSPV: right superior pulmonary vein, SD: standard deviation, OR: odds ratio, TIA: transient ischemic attack.

In terms of wall thickness, reproducibility was measured in 20 patients at 11 regions of interest (20×11 measurements); furthermore, the diameter and area of each PV were also evaluated. The intra- and inter-reader intraclass correlation coefficient (ICC) for the LAWT assessment were 0.98 (CI 0.97–0.98) and 0.92 (CI 0.79–0.97), respectively. The minimum and maximum range of the intra-reader area and diameter ICC were between 0.94 and 0.99 and 0.98–0.99, respectively, whereas theinter–reader area and diameter ICC's minimum and maximum range were between 0.78–0.92 and 0.80–0.94, respectively.

5 DISCUSSION

5.1 Pericoronary adipose tissue analysis

PCAT attenuation and gradient have been proven to be associated with several cardiovascular conditions as markers of perivascular inflammation. However, due to the fact that PCAT marker analysis is based on HU values, patient and imaging characteristics can potentially alter these values. In our primary cohort, 1652 patients with zero calcium scores demonstrated a wide range of PCAT attenuation and gradient values. Nonetheless, markers of CAD proved to be associated with PCAT markers. However, a great number of patient and image acquisition parameters, such as male sex, heart rate, tube voltage, and current and pixel spacing, were also significantly associated with PCAT attenuation. Whereas, regarding our univariable results, PCAT attenuation and gradient showed an association with NCP characteristics, similar to the previous analysis in the scientific literature, although after correcting for patient and imaging characteristics, this link did not persist. Importantly, similar results were observed in our two validation cohorts (Validation group I.: Zero calcium score – different scanner, Validation group II.: Moderate to severe CAD group).

Based on a study with ex vivo and in vivo models, Antonopoulos et al. demonstrated that at the time of MACE as a response to inflammation in the vasculature and vulnerable plaques, there are phenotypic changes in PCAT, thus in PCAT attenuation values (3). The association between inflammation and PCAT values was strengthened by Goeller et al. as a positive correlation was found between PCAT attenuation and pro-inflammatory serum markers (IL-7 and MCP-1), whereas a negative association was demonstrated between PCAT attenuation and anti-inflammatory cytokines (IL-4, -10, -13); however, these correlations were weak as the Pearson correlation coefficient range was -0.12 to 0.23 (107). In addition, in stable patients with high-risk plaque features on their CCTA images, PCAT attenuation showed an association with 18F-sodium fluoride uptake on PET-CT images, demonstrating another association with a proven marker of inflammation (41). As to the association between PCAT attenuation and coronary plaque in patients with acute coronary syndrome, based on Goeller at al., the PCAT attenuation values around the culprit lesions were higher as compared to non-culprit lesions (91). However, our findings demonstrate that there are certain parameters that must be taken into consideration before drawing any conclusions about the use of PCAT markers.

First, based on our study, a large variability of PCAT attenuation and gradient values was demonstrated in the patient population with uniformly low cardiovascular risk, referred to CCTA. A great number of evidence has been defined that patients with zero calcium scores have a low risk of developing adverse events (108-110). Therefore, it could be evident that the PCAT values would be universally low with low variability, mainly in patients with zero calcium score and with no plaque. However, in our group, with 1652 patients, PCAT attenuation and PCAT gradient exhibited a wide range of values. The reason for this might be explained by our second finding that PCAT markers are significantly influenced by patient and image acquisition parameters. Most of the prior studies about PCAT markers use the original definition of PCAT attenuation, which was initially called the fat attenuation index. This index was developed by Antonopoulos et al. using no correction factors applied for possible confounders (3). Few studies used some factors, but the number of variables that were included in these models varied largely (Supplementary Table 1. (85)) (111-113).

To tackle the limitations mentioned above, in the CRISP-study, Oikonomou et al. used a modified PCAT attenuation parameter to take into consideration the possible patient and imaging-related parameters and to have a prediction in later outcomes (11). These corrected differences in HU values ranged between 100 and 120 kVp using a correction factor that was based on a 17-patient population study where the patients were scanned on a dual-source CT. The average attenuation was simply divided by freehand drawn region of interest of the pericardium (100 and 120 kVp, (-96.1/-86.2=1.11485)) (114, 115). The purpose of the modified PCAT attenuation marker was to define the optimal cut-off value for the identification of individuals at risk of all-cause mortality. However, it is important to highlight that in these early studies, several parameters that could independently affect PCAT attenuation values were not included in the correction factor. Moreover, beyond image acquisition parameters (for instance, CNR, SNR), heart rate significantly influences PCAT attenuation values. Hence the robust estimation of PCAT attenuation and the determination of normal ranges of PCAT marker values might be challenging. In the CORE320 trial, a correction for PCAT attenuation was used by adding adjacent lumen attenuation values to take into consideration the patient and image acquisition parameters. However, after correction, the association between PCAT and MACE was not found (115). In addition, in our study, the average PCAT attenuation

value was 15 HU higher when simply using a different CT scanner among the patient groups with zero calcium score patients.

Using PCAT metrics as an independent factor in cardiovascular risk stratification might be more challenging than previously thought. This view is strengthened by our findings based on the association between NCP characteristics and PCAT values. After adjusting patient and imaging parameters, the link between plaque characteristics and PCAT markers disappeared (116, 117).

5.2 Left atrial wall thickness and pulmonary vein analysis

The main finding of our study showed that in drug-refractory AF patients, using the AI with standardized ablation protocol results in a high acute procedural success rate which is independent of CT-derived LAWT. In terms of PV anatomy, RSPV diameter may have an influence on the rate of first-pass isolation. LAWT and PV diameter measurements were highly reproducible.

Recent improvements in ablation techniques, pre-ablation imaging, and catheter types have helped develop effective and safe therapies in the treatment of AF (83). Nakagawa et al. were one of the first to introduce a novel ablation quality marker based on a canine study (118). AI can be seen as a surrogate measure and quality marker of radiofrequency lesion creation (119). Based on several studies, it is proved to be a valuable aid for an effective PVI as it integrates power, contact force, and time in a non-linear weighted formula (119, 120). In an in vitro study, the AI reliability was validated using different contact angles, radiofrequency power, and contact force settings, with a good correlation with lesion depth, volume, and width (121). Moreover, El Haddad et al. showed a substantial difference, in a clinical study, in the minimum value of AI for durably isolated PV segments when comparing the anterior and posterior parts of the circle. This demonstrates that the wall thickness in different parts of the PV antrum might play a role in the efficacy of PVI. It has been presented that a higher AI value is needed in the anterior segments to avoid possible reconnections (122). Although, it is essential to highlight that a wide range of optimal AI target values on the anterior and posterior wall has been presented in the literature (15, 77, 120, 123).

Even though CCTA is a reliable tool to assess LAWT because of its high temporal and spatial resolution, there is no gold-standard measurement for atrial wall thickness (124-

126). It has been shown that there is an inter- and intra- patient variability across persistent vs. paroxysmal AF in terms of LAWT (4, 101). Furthermore, the role of LAWT in terms of AF recurrence in PVI procedures has been investigated in several studies (127-130). However, these study results are controversial regarding the locations of LA's thickest region and the LAWT's role in procedural efficacy (97, 129). More importantly, the ablation techniques that were used were less advanced in these studies.

Mulder et al. were the first to analyze the association between LAWT and acute PV reconnection in patients who underwent AF ablation with AI guidance. According to their findings, in both the anterior and posterior atrial regions, local wall thickness affected the occurrence of acute PV reconnection (22). These study results are in contrast with our findings as we did not find any link between LAWT (mean wall thickness of all 11 regions) and the acute procedural outcome despite the substantial difference in different LA regions. This inconsistency can be explained by the procedural endpoint differences, as in our research, we evaluated the effect of LAWT on the first pass isolation rate. As there was no acute PV reconnection in our study, we could not even use it as an endpoint. The lack of acute reconnection can be explained by the use of the modified highly effective CLOSE protocol, with slightly higher minimal target contact force values in contrast with the study results by Mulder et al. (e.g. 10 g vs. 5 g) (22) and with the usage of a steerable sheath for ablation that might lead to a more stable catheter-tissue contact during the procedure.

El Haddad et al. introduced a novel approach for the enclosure of the PVs with contiguous and optimized radiofrequency lesions in order to achieve optimal lesion depth and continuity. These criteria were used in 130 patients with a high rate of first-pass isolation (122). Moreover, it was proven that its effectiveness was higher than PVI - AI strategy with also a higher incidence rate of first-pass isolation (17).

We used AI target value of 500 on the anterior wall and 400 on the posterior wall, which was associated with a high first-pass PVI rate and the absence of acute reconnection. With the usage of the previously mentioned AI target values, even when a thicker atrial wall was present, large enough lesions were created for successful first-pass isolation in case of different LAWT values (131). Hence, choosing our standardized approach may be applicable in order to create ablation lines with good quality, independently from the wall thickness. Notably, recent study results demonstrated that LAWT-based, individualized

AI values might have similar promising results, even with lower AI targets (132). However, this can be considered a time-consuming approach and does not differ in safety and efficacy.

Regarding the PV anatomy, out of all assessed parameters, RSPV diameter was linked with higher successful right-sided PVI on first-pass isolation rate. In spite of the fact that the right pulmonary vein region has some challenges in terms of PVI due to its epicardial connection with the right atrium and carina (133, 134), the size of the RSPV diameter might positively influence the PVI outcome. In our present study, we concluded that the wider the RSPV diameter is, the higher the likelihood of first-pass isolation. This can be explained by the freedom in the navigation of the catheter in case of not very narrow RSPV.

It is important to highlight that even though our results demonstrate that the LAWT measurement by CCTA does not have an influence on the acute success rate of AF ablation when using the modified CLOSE protocol, the role of CCTA before ablation is well established and provides valuable information for patient selection, procedural planning and the assessment of LA. Finally, it is essential to mention that compared to previous results, procedural safety was excellent with the current standardized ablation protocol (135).

5.3 Limitations

5.3.1 Pericoronary adipose tissue analysis

First, our main study group with zero coronary calcium score, thus low cardiovascular risk, was scanned using the same CT scanner with the same imaging protocol in a single centre, which could lead to a selection bias. However, we analyzed two validation cohorts to overcome this limitation and found similar results. Second, PCAT volumes were segmented by two readers with the same software, which could artificially reduce variation. Although, despite these facts, a substantial variation in PCAT metrics was found, which might be even larger when including more readers and different software. Third, one CCTA reconstruction algorithm was used in the patient groups. However, reconstruction algorithms can be considered an additional factor that needs to be taken into consideration in future PCAT analyses.

5.3.2 Left atrial wall thickness and pulmonary vein analysis

It was a relatively low patient-numbered, single-centre study. However, it firstly evaluated the association between the procedural success of first-pass isolation using a standardized ablation protocol. Then, in every patient, LAWT was assessed in 11 LA segments which resulted in a detailed assessment of the LA, evaluating its role in current AF management with the use of radiofrequency ablation. However, the central focus of the study was the assessment of the acute procedural success of the modified CLOSE protocol in regard to CT-derived LAWT measurements, and more studies are needed to evaluate the long-term procedural success of the modified CLOSE protocol. Due to the clinical CCTA protocol, LA volume was derived from the diastolic phase in the majority of cases; thus, it did not represent the maximal LA volume for a given patient and limited the conclusion of this parameter.

DOI:10.14753/SE.2024.2997

6 CONCLUSION

6.1 Pericoronary adipose tissue analysis

Based on our results, PCAT attenuation and gradient represent a wide range of values in the low cardiovascular-risk patient population (calcium score=0). PCAT markers are significantly influenced by different patient characteristics and image acquisition parameters. After correcting for these characteristics, the association between CAD and PCAT markers disappears, highlighting the importance of correcting for all possible confounders before evaluating the additive value of PCAT markers. Therefore, extensive correction for possible confounders is needed in future studies (85).

6.2 Left atrial wall thickness and pulmonary vein analysis

Using the standardized ablation protocol in persistent and paroxysmal AF patients leads to a high first-pass isolation rate with a high acute procedural success independent of the LAWT. Regarding RSPV, a larger diameter showed a link with right-sided successful first-pass isolation (136).

DOI:10.14753/SE.2024.2997

7 SUMMARY

7.1 Pericoronary adipose tissue analysis

CCTA-based PCAT markers (PCAT attenuation and gradient) as coronary inflammation biomarkers seem to play an essential role in the identification of patients at CAD risk. Although, PCAT markers might be affected by several patient and image acquisition parameters that are taken into account differently in the scientific literature. Therefore, our aim was to determine the effect of patient and imaging characteristics on the association between a low-cardiovascular-risk patient population and PCAT markers. In our retrospective, single-centre analysis, we enrolled stable chest pain patients with zero calcium scores on CCTA. The images were analyzed for the presence of NCP, obstructive stenosis, SSS, SIS, and HRP. Overall, 1652 patients' scans were analyzed with an addition of 330-330 patients' scans as validation cohorts. Based on our study results, patient and image acquisition parameters have a significant effect on PCAT markers, and they represent a wide range of values in the low cardiovascular-risk patient population. The association between PCAT markers and CAD characteristics after the correction of the above-mentioned parameters disappeared. This highlights the importance of evaluating PCAT markers by correcting for all possible confounders in the future.

7.2 Left atrial wall thickness and pulmonary vein analysis

A novel contact-force guided ablation technique called the modified CLOSE protocol for the enclosure of pulmonary veins is used for treating AF. Using this technique in our prospective, single-centre study, the aim was to define whether LAWT has an influence on the success rate of first-pass PVI. Symptomatic, drug-refractory AF patients were enrolled consecutively who underwent initial radiofrequency catheter ablation with the use of the modified CLOSE protocol after a pre-procedural CCTA. Our analysis was based on 1034 LAWT and 376 PV measurements in 94 patients. Based on our study results, with the modified CLOSE protocol, a high acute procedural success was present in persistent and paroxysmal AF patients, independently from CCTA-derived LAWT. Furthermore, regarding PV anatomy, a larger RSPV diameter had a positive influence on the right-sided first-pass isolation rate.

DOI:10.14753/SE.2024.2997

8 ÖSSZEFOGLALÁS

8.1 Perikoronáriás zsírszövet elemzés

A szí CT-alapú perikoronáriás zsírszövet attenuáció és gradiens a koszorúér-gyulladás biomarkerének tekinthető és fontos szerepet játszhatnak a koszorúér betegség kockázatával rendelkező egyének azonosításában. Vizsgálatunk célja volt, hogy meghatározzuk a beteg- és képalkotó paraméterek hatását a perikoronáriás zsírszövet markerekre egy alacsony kardiovaszkuláris kockázattal rendelkező betegpopulációban. Retrospektív, elemzésünkbe olyan stabil mellkasi fájdalomban szenvedő betegeket vontunk be (n=1652), akiknél a szív CT leltük alapján a kalciumpontszám nulla volt. A CT felvételeket nem calcificalt plakk, obstruktív szűkület, szegment sztenózis pontszám, szegment érintettségi pontszám és magas rizikójú plakkok jelenléte szempontjából elemeztük, kiegészítve 330-330 beteg CT felvételének elemzésével, mint validációs kohorszokkal. Vizsgálati eredményeink alapján a beteg és a képfelvételi paraméterek jelentős hatással vannak a perikoronáriás zsírszövet markerekre, és az alacsony kardiovaszkuláris kockázatú betegpopulációban széles értéktartományt képviselnek. A perikoronáriás zsírszövet markerek és a koszorúér betegség jellemzők közötti összefüggés a fent említett paraméterek korrekcióját követően eltűnt. Ez rávilágít annak fontosságára, hogy a jövőben a perikoronáriás zsírszövet markereket az összes lehetséges zavaró tényezőre korrigálva értékeljük.

8.2 A bal pitvari falvastagság és a tüdővéna elemzése

A pitvarfibrilláció kezelésére egy új, kontakt-erővel irányított ablációs technikát, a módosított CLOSE protokollt alkalmazzák a tüdővénák izolálására. Prospektív vizsgálatunkban célul tűztük ki, annak elemzését, hogy a bal pitvari falvastagság és a tüdővéna anatómia befolyásolja-e az új ablációs technika akut sikerességét. A betegpopulációba tünetmentes, gyógyszer-refrakter pitvarfibrilláló betegek kerültek, akiknél a CLOSE protokollal végrehajtott tüdővéna izolációt megelőzően szív CT vizsgálatot is végeztünk. Elemzésünk 94 beteg, 1034 bal pitvari falvastagság - és 376 tüdővéna mérésén alapult. Vizsgálati eredményeink alapján a módosított CLOSE protokoll alkalmazásával a pitvarfibrillációs betegeknél magas akut sikeresség volt tapasztalható, függetlenül a bal pitvari falvastagságtól. Továbbá, a tüdővénák anatómiáját tekintve a nagyobb, jobb felső véna átmérő pozitív hatással volt a jobb oldali tüdővéna izoláció sikerességére.

9 REFERENCES

1. Kumar V, Weerakoon S, Dey AK, Earls JP, Katz RJ, Reiner JS, et al. The evolving role of coronary CT angiography in Acute Coronary Syndromes. Journal of cardiovascular computed tomography. 2021;15(5):384-93.
2. Baessato F, Guglielmo M, Muscogiuri G, Baggiano A, Fusini L, Scafuri S, et al. The Incremental Role of Coronary Computed Tomography in Chronic Coronary Syndromes. Journal of clinical medicine. 2020;9(12).
3. Antonopoulos AS, Sanna F, Sabharwal N, Thomas S, Oikonomou EK, Herdman L, et al. Detecting human coronary inflammation by imaging perivascular fat. Sci Transl Med. 2017;9(398).
4. Beinart R, Abbara S, Blum A, Ferencik M, Heist K, Ruskin J, et al. Left atrial wall thickness variability measured by CT scans in patients undergoing pulmonary vein isolation. Journal of cardiovascular electrophysiology. 2011;22(11):1232-6.
5. Mensah GA, Moran AE, Roth GA, Narula J. The global burden of cardiovascular diseases, 1990-2010. Global heart. 2014;9(1):183-4.
6. Ralapanawa U, Sivakanesan R. Epidemiology and the Magnitude of Coronary Artery Disease and Acute Coronary Syndrome: A Narrative Review. Journal of epidemiology and global health. 2021;11(2):169-77.
7. Emfietzoglou M, Mavrogiannis MC, Samaras A, Rampidis GP, Giannakoulas G, Kampaktsis PN. The role of cardiac computed tomography in predicting adverse coronary events. Frontiers in cardiovascular medicine. 2022;9:920119.
8. Abdelrahman KM, Chen MY, Dey AK, Virmani R, Finn AV, Khamis RY, et al. Coronary Computed Tomography Angiography From Clinical Uses to Emerging Technologies: JACC State-of-the-Art Review. Journal of the American College of Cardiology. 2020;76(10):1226-43.
9. Moss AJ, Williams MC, Newby DE, Nicol ED. The Updated NICE Guidelines: Cardiac CT as the First-Line Test for Coronary Artery Disease. Current cardiovascular imaging reports. 2017;10(5):15.
10. Lima TP, Assuncao AN, Bittencourt MS, Liberato G, Arbab-Zadeh A, Lima JAC, et al. Coronary computed tomography plaque-based scores predict long-term cardiovascular events. European radiology. 2023;33(8):5436-45.
11. Oikonomou EK, Marwan M, Desai MY, Mancio J, Alashi A, Hutt Centeno E, et al. Non-invasive detection of coronary inflammation using computed tomography and prediction of residual cardiovascular risk (the CRISP CT study): a post-hoc analysis of prospective outcome data. Lancet (London, England). 2018;392(10151):929-39.
12. Arbab-Zadeh A, Fuster V. The myth of the "vulnerable plaque": transitioning from a focus on individual lesions to atherosclerotic disease burden for coronary artery disease risk assessment. Journal of the American College of Cardiology. 2015;65(8):846-55.
13. Haïssaguerre M, Jaïs P, Shah DC, Takahashi A, Hocini M, Quiniou G, et al. Spontaneous initiation of atrial fibrillation by ectopic beats originating in the pulmonary veins. The New England journal of medicine. 1998;339(10):659-66.
14. Jaïs P, Hocini M, Macle L, Choi KJ, Deisenhofer I, Weerasooriya R, et al. Distinctive electrophysiological properties of pulmonary veins in patients with atrial fibrillation. Circulation. 2002;106(19):2479-85.
15. Taghji P, El Haddad M, Phlips T, Wolf M, Knecht S, Vandekerckhove Y, et al. Evaluation of a Strategy Aiming to Enclose the Pulmonary Veins With Contiguous and

Optimized Radiofrequency Lesions in Paroxysmal Atrial Fibrillation: A Pilot Study. JACC Clinical electrophysiology. 2018;4(1):99-108.
16. Phlips T, Taghji P, El Haddad M, Wolf M, Knecht S, Vandekerckhove Y, et al. Improving procedural and one-year outcome after contact force-guided pulmonary vein isolation: the role of interlesion distance, ablation index, and contact force variability in the 'CLOSE'-protocol. Europace : European pacing, arrhythmias, and cardiac electrophysiology : journal of the working groups on cardiac pacing, arrhythmias, and cardiac cellular electrophysiology of the European Society of Cardiology. 2018;20(Fi_3):f419-f27.
17. Berte B, Hilfiker G, Moccetti F, Schefer T, Weberndörfer V, Cuculi F, et al. Pulmonary vein isolation using ablation index vs. CLOSE protocol with a surround flow ablation catheter. Europace : European pacing, arrhythmias, and cardiac electrophysiology : journal of the working groups on cardiac pacing, arrhythmias, and cardiac cellular electrophysiology of the European Society of Cardiology. 2020;22(1):84-9.
18. Szegedi N, Vecsey-Nagy M, Simon J, Szilveszter B, Herczeg S, Kolossváry M, et al. Orientation of the right superior pulmonary vein affects outcome after pulmonary vein isolation. European heart journal Cardiovascular Imaging. 2022;23(4):515-23.
19. Wei W, Ge JB, Zou Y, Lin L, Cai Y, Liu XB, et al. Anatomical characteristics of pulmonary veins for the prediction of postoperative recurrence after radiofrequency catheter ablation of atrial fibrillation. PloS one. 2014;9(4):e93817.
20. Hauser TH, Essebag V, Baldessin F, McClennen S, Yeon SB, Manning WJ, et al. Prognostic value of pulmonary vein size in prediction of atrial fibrillation recurrence after pulmonary vein isolation: a cardiovascular magnetic resonance study. Journal of cardiovascular magnetic resonance : official journal of the Society for Cardiovascular Magnetic Resonance. 2015;17(1):49.
21. Chen J, Yang ZG, Xu HY, Shi K, Long QH, Guo YK. Assessments of pulmonary vein and left atrial anatomical variants in atrial fibrillation patients for catheter ablation with cardiac CT. European radiology. 2017;27(2):660-70.
22. Mulder MJ, Kemme MJB, Hagen AMD, Hopman L, van de Ven PM, Hauer HA, et al. Impact of local left atrial wall thickness on the incidence of acute pulmonary vein reconnection after Ablation Index-guided atrial fibrillation ablation. International journal of cardiology Heart & vasculature. 2020;29:100574.
23. Nagy E, Jermendy AL, Merkely B, Maurovich-Horvat P. Clinical importance of epicardial adipose tissue. Archives of medical science : AMS. 2017;13(4):864-74.
24. Iacobellis G. Epicardial and pericardial fat: close, but very different. Obesity (Silver Spring, Md). 2009;17(4):625; author reply 6-7.
25. Sacks HS, Fain JN. Human epicardial adipose tissue: a review. American heart journal. 2007;153(6):907-17.
26. Iacobellis G, Corradi D, Sharma AM. Epicardial adipose tissue: anatomic, biomolecular and clinical relationships with the heart. Nat Clin Pract Cardiovasc Med. 2005;2(10):536-43.
27. Iacobellis G, Willens HJ, Barbaro G, Sharma AM. Threshold values of high-risk echocardiographic epicardial fat thickness. Obesity (Silver Spring, Md). 2008;16(4):887-92.
28. Iacobellis G, Ribaudo MC, Zappaterreno A, Iannucci CV, Leonetti F. Relation between epicardial adipose tissue and left ventricular mass. The American journal of cardiology. 2004;94(8):1084-7.

29. Iacobellis G, Leonetti F. Epicardial adipose tissue and insulin resistance in obese subjects. J Clin Endocrinol Metab. 2005;90(11):6300-2.
30. Shah RV, Anderson A, Ding J, Budoff M, Rider O, Petersen SE, et al. Pericardial, But Not Hepatic, Fat by CT Is Associated With CV Outcomes and Structure: The Multi-Ethnic Study of Atherosclerosis. JACC Cardiovascular imaging. 2017;10(9):1016-27.
31. Hassan M, Said K, Rizk H, ElMogy F, Donya M, Houseni M, et al. Segmental peri-coronary epicardial adipose tissue volume and coronary plaque characteristics. European heart journal Cardiovascular Imaging. 2016;17(10):1169-77.
32. Duncan BB, Chambless LE, Schmidt MI, Szklo M, Folsom AR, Carpenter MA, et al. Correlates of body fat distribution. Variation across categories of race, sex, and body mass in the atherosclerosis risk in communities study. The Atherosclerosis Risk in communities (ARIC) Study Investigators. Ann Epidemiol. 1995;5(3):192-200.
33. Queiroz M, Sena CM. Perivascular adipose tissue in age-related vascular disease. Ageing Res Rev. 2020;59:101040.
34. Britton KA, Fox CS. Perivascular adipose tissue and vascular disease. Clin Lipidol. 2011;6(1):79-91.
35. Antonopoulos AS, Margaritis M, Verheule S, Recalde A, Sanna F, Herdman L, et al. Mutual Regulation of Epicardial Adipose Tissue and Myocardial Redox State by PPAR-gamma/Adiponectin Signalling. Circ Res. 2016;118(5):842-55.
36. Antonopoulos AS, Margaritis M, Coutinho P, Digby J, Patel R, Psarros C, et al. Reciprocal effects of systemic inflammation and brain natriuretic peptide on adiponectin biosynthesis in adipose tissue of patients with ischemic heart disease. Arterioscler Thromb Vasc Biol. 2014;34(9):2151-9.
37. Margaritis M, Antonopoulos AS, Digby J, Lee R, Reilly S, Coutinho P, et al. Interactions between vascular wall and perivascular adipose tissue reveal novel roles for adiponectin in the regulation of endothelial nitric oxide synthase function in human vessels. Circulation. 2013;127(22):2209-21.
38. Antonopoulos AS, Margaritis M, Coutinho P, Shirodaria C, Psarros C, Herdman L, et al. Adiponectin as a link between type 2 diabetes and vascular NADPH oxidase activity in the human arterial wall: the regulatory role of perivascular adipose tissue. Diabetes. 2015;64(6):2207-19.
39. Takaoka M, Suzuki H, Shioda S, Sekikawa K, Saito Y, Nagai R, et al. Endovascular injury induces rapid phenotypic changes in perivascular adipose tissue. Arterioscler Thromb Vasc Biol. 2010;30(8):1576-82.
40. Ohyama K, Matsumoto Y, Amamizu H, Uzuka H, Nishimiya K, Morosawa S, et al. Association of Coronary Perivascular Adipose Tissue Inflammation and Drug-Eluting Stent-Induced Coronary Hyperconstricting Responses in Pigs: (18)F-Fluorodeoxyglucose Positron Emission Tomography Imaging Study. Arterioscler Thromb Vasc Biol. 2017;37(9):1757-64.
41. Kwiecinski J, Dey D, Cadet S, Lee SE, Otaki Y, Huynh PT, et al. Peri-Coronary Adipose Tissue Density Is Associated With (18)F-Sodium Fluoride Coronary Uptake in Stable Patients With High-Risk Plaques. JACC Cardiovascular imaging. 2019;12(10):2000-10.
42. Garvey CJ, Hanlon R. Computed tomography in clinical practice. BMJ (Clinical research ed). 2002;324(7345):1077-80.
43. Dawson P, Lees WR. Multi-slice technology in computed tomography. Clinical radiology. 2001;56(4):302-9.

44. DenOtter TD, Schubert J. Hounsfield Unit. StatPearls. Treasure Island (FL): StatPearls Publishing
Copyright © 2022, StatPearls Publishing LLC.; 2022.
45. Seeram E. Computed Tomography: A Technical Review. Radiologic technology. 2018;89(3):279ct-302ct.
46. Obaid DR, Calvert PA, Gopalan D, Parker RA, Hoole SP, West NE, et al. Atherosclerotic plaque composition and classification identified by coronary computed tomography: assessment of computed tomography-generated plaque maps compared with virtual histology intravascular ultrasound and histology. Circulation Cardiovascular imaging. 2013;6(5):655-64.
47. Detrano R, Guerci AD, Carr JJ, Bild DE, Burke G, Folsom AR, et al. Coronary calcium as a predictor of coronary events in four racial or ethnic groups. The New England journal of medicine. 2008;358(13):1336-45.
48. Agatston AS, Janowitz WR, Hildner FJ, Zusmer NR, Viamonte M, Jr., Detrano R. Quantification of coronary artery calcium using ultrafast computed tomography. Journal of the American College of Cardiology. 1990;15(4):827-32.
49. Hsia J, Klouj A, Prasad A, Burt J, Adams-Campbell LL, Howard BV. Progression of coronary calcification in healthy postmenopausal women. BMC Cardiovascular Disorders. 2004;4(1):21.
50. Schmermund A, Baumgart D, Möhlenkamp S, Kriener P, Pump H, Grönemeyer D, et al. Natural history and topographic pattern of progression of coronary calcification in symptomatic patients: An electron-beam CT study. Arterioscler Thromb Vasc Biol. 2001;21(3):421-6.
51. Budoff MJ, Young R, Lopez VA, Kronmal RA, Nasir K, Blumenthal RS, et al. Progression of coronary calcium and incident coronary heart disease events: MESA (Multi-Ethnic Study of Atherosclerosis). Journal of the American College of Cardiology. 2013;61(12):1231-9.
52. Elias-Smale SE, Proença RV, Koller MT, Kavousi M, van Rooij FJ, Hunink MG, et al. Coronary calcium score improves classification of coronary heart disease risk in the elderly: the Rotterdam study. Journal of the American College of Cardiology. 2010;56(17):1407-14.
53. McClelland RL, Jorgensen NW, Budoff M, Blaha MJ, Post WS, Kronmal RA, et al. 10-Year Coronary Heart Disease Risk Prediction Using Coronary Artery Calcium and Traditional Risk Factors: Derivation in the MESA (Multi-Ethnic Study of Atherosclerosis) With Validation in the HNR (Heinz Nixdorf Recall) Study and the DHS (Dallas Heart Study). Journal of the American College of Cardiology. 2015;66(15):1643-53.
54. Bittner DO, Takx RAP, Staziaki PV, Janjua S, Neilan TG, Meyersohn NM, et al. Identification of coronary artery calcification can optimize risk stratification in patients with acute chest pain. International journal of cardiology. 2017;249:473-8.
55. Mittal TK, Pottle A, Nicol E, Barbir M, Ariff B, Mirsadraee S, et al. Prevalence of obstructive coronary artery disease and prognosis in patients with stable symptoms and a zero-coronary calcium score. European heart journal Cardiovascular Imaging. 2017;18(8):922-9.
56. Bergström G, Persson M, Adiels M, Björnson E, Bonander C, Ahlström H, et al. Prevalence of Subclinical Coronary Artery Atherosclerosis in the General Population. Circulation. 2021;144(12):916-29.

57. Maurovich-Horvat P, Ferencik M, Voros S, Merkely B, Hoffmann U. Comprehensive plaque assessment by coronary CT angiography. Nature reviews Cardiology. 2014;11(7):390-402.
58. Leipsic J, Abbara S, Achenbach S, Cury R, Earls JP, Mancini GJ, et al. SCCT guidelines for the interpretation and reporting of coronary CT angiography: a report of the Society of Cardiovascular Computed Tomography Guidelines Committee. Journal of cardiovascular computed tomography. 2014;8(5):342-58.
59. Min JK, Shaw LJ, Devereux RB, Okin PM, Weinsaft JW, Russo DJ, et al. Prognostic value of multidetector coronary computed tomographic angiography for prediction of all-cause mortality. Journal of the American College of Cardiology. 2007;50(12):1161-70.
60. Bekkers E, Roos J. Coronary CTA: stenosis classification and quantification, including automated measures. Journal of cardiovascular computed tomography. 2009;3 Suppl 2:S109-15.
61. Thilo C, Gebregziabher M, Mayer FB, Berghaus TM, Zwerner PL, Schoepf UJ. Can non-calcified coronary artery plaques be detected on non-contrast CT calcium scoring studies? Academic radiology. 2011;18(7):858-65.
62. Motoyama S, Kondo T, Sarai M, Sugiura A, Harigaya H, Sato T, et al. Multislice computed tomographic characteristics of coronary lesions in acute coronary syndromes. Journal of the American College of Cardiology. 2007;50(4):319-26.
63. Maurovich-Horvat P, Schlett CL, Alkadhi H, Nakano M, Otsuka F, Stolzmann P, et al. The napkin-ring sign indicates advanced atherosclerotic lesions in coronary CT angiography. JACC Cardiovascular imaging. 2012;5(12):1243-52.
64. Karanasos A, Ligthart JM, Witberg KT, Regar E. Calcified nodules: an underrated mechanism of coronary thrombosis? JACC Cardiovascular imaging. 2012;5(10):1071-2.
65. Glagov S, Weisenberg E, Zarins CK, Stankunavicius R, Kolettis GJ. Compensatory enlargement of human atherosclerotic coronary arteries. The New England journal of medicine. 1987;316(22):1371-5.
66. Gauss S, Achenbach S, Pflederer T, Schuhbäck A, Daniel WG, Marwan M. Assessment of coronary artery remodelling by dual-source CT: a head-to-head comparison with intravascular ultrasound. Heart (British Cardiac Society). 2011;97(12):991-7.
67. Maurovich-Horvat P, Hoffmann U, Vorpahl M, Nakano M, Virmani R, Alkadhi H. The napkin-ring sign: CT signature of high-risk coronary plaques? JACC Cardiovascular imaging. 2010;3(4):440-4.
68. Li D, Zhang L, Kneller J, Nattel S. Potential ionic mechanism for repolarization differences between canine right and left atrium. Circ Res. 2001;88(11):1168-75.
69. Wijesurendra RS, Casadei B. Mechanisms of atrial fibrillation. Heart (British Cardiac Society). 2019;105(24):1860-7.
70. Heeringa J, van der Kuip DA, Hofman A, Kors JA, van Herpen G, Stricker BH, et al. Prevalence, incidence and lifetime risk of atrial fibrillation: the Rotterdam study. European heart journal. 2006;27(8):949-53.
71. Friberg J, Scharling H, Gadsbøll N, Jensen GB. Sex-specific increase in the prevalence of atrial fibrillation (The Copenhagen City Heart Study). The American journal of cardiology. 2003;92(12):1419-23.
72. Stewart S, Hart CL, Hole DJ, McMurray JJ. A population-based study of the long-term risks associated with atrial fibrillation: 20-year follow-up of the Renfrew/Paisley study. The American journal of medicine. 2002;113(5):359-64.

73. Chen SA, Hsieh MH, Tai CT, Tsai CF, Prakash VS, Yu WC, et al. Initiation of atrial fibrillation by ectopic beats originating from the pulmonary veins: electrophysiological characteristics, pharmacological responses, and effects of radiofrequency ablation. Circulation. 1999;100(18):1879-86.
74. Khan R. Identifying and understanding the role of pulmonary vein activity in atrial fibrillation. Cardiovascular research. 2004;64(3):387-94.
75. Tsai CF, Tai CT, Hsieh MH, Lin WS, Yu WC, Ueng KC, et al. Initiation of atrial fibrillation by ectopic beats originating from the superior vena cava: electrophysiological characteristics and results of radiofrequency ablation. Circulation. 2000;102(1):67-74.
76. Szegedi N, Salló Z, Perge P, Piros K, Nagy VK, Osztheimer I, et al. The role of local impedance drop in the acute lesion efficacy during pulmonary vein isolation performed with a new contact force sensing catheter-A pilot study. PLoS One. 2021;16(9):e0257050.
77. Lee SR, Choi EK, Lee EJ, Choe WS, Cha MJ, Oh S. Efficacy of the optimal ablation index-targeted strategy for pulmonary vein isolation in patients with atrial fibrillation: the OPTIMUM study results. J Interv Card Electrophysiol. 2019;55(2):171-81.
78. Osorio J, Hunter TD, Rajendra A, Zei P, Morales G. First pass isolation predicts clinical success after contact force guided paroxysmal atrial fibrillation ablation. European Heart Journal. 2020;41(Supplement_2).
79. Sandorfi G, Rodriguez-Mañero M, Saenen J, Baluja A, Bories W, Huybrechts W, et al. Less Pulmonary Vein Reconnection at Redo Procedures Following Radiofrequency Point-by-Point Antral Pulmonary Vein Isolation With the Use of Contemporary Catheter Ablation Technologies. JACC Clinical electrophysiology. 2018;4(12):1556-65.
80. Osorio J, Hunter TD, Rajendra A, Zei P, Silverstein J, Morales G. Predictors of clinical success after paroxysmal atrial fibrillation catheter ablation. Journal of cardiovascular electrophysiology. 2021;32(7):1814-21.
81. Kircher S, Sommer P. Electrophysiological Evaluation of Pulmonary Vein Isolation. Journal of atrial fibrillation. 2013;6(3):934.
82. Salló Z, Perge P, Balogi B, Orbán G, Piros K, Herczeg S, et al. Impact of High-Power and Very High-Power Short-Duration Radiofrequency Ablation on Procedure Characteristics and First-Pass Isolation During Pulmonary Vein Isolation. Frontiers in cardiovascular medicine. 2022;9:935705.
83. Szegedi N, Vecsey-Nagy M, Simon J, Szilveszter B, Herczeg S, Kolossváry M, et al. Orientation of the right superior pulmonary vein affects outcome after pulmonary vein isolation. Eur Heart J Cardiovasc Imaging. 2021.
84. Hauser TH, Essebag V, Baldessin F, McClennen S, Yeon SB, Manning WJ, et al. Prognostic value of pulmonary vein size in prediction of atrial fibrillation recurrence after pulmonary vein isolation: a cardiovascular magnetic resonance study. Journal of Cardiovascular Magnetic Resonance. 2015;17(1):49.
85. Boussoussou M, Vattay B, Szilveszter B, Simon J, Lin A, Vecsey-Nagy M, et al. The effect of patient and imaging characteristics on coronary CT angiography assessed pericoronary adipose tissue attenuation and gradient. Journal of cardiovascular computed tomography. 2023;17(1):34-42.
86. Simon J, Száraz L, Szilveszter B, Panajotu A, Jermendy Á, Bartykowszki A, et al. Calcium scoring: a personalized probability assessment predicts the need for additional or alternative testing to coronary CT angiography. European radiology. 2020;30(10):5499-506.

87. Karády J, Panajotu A, Kolossváry M, Szilveszter B, Jermendy Á L, Bartykowszki A, et al. The effect of four-phasic versus three-phasic contrast media injection protocols on extravasation rate in coronary CT angiography: a randomized controlled trial. Eur Radiol. 2017;27(11):4538-43.
88. Hadamitzky M, Achenbach S, Al-Mallah M, Berman D, Budoff M, Cademartiri F, et al. Optimized prognostic score for coronary computed tomographic angiography: results from the CONFIRM registry (COronary CT Angiography EvaluatioN For Clinical Outcomes: An InteRnational Multicenter Registry). J Am Coll Cardiol. 2013;62(5):468-76.
89. Shaw LJ, Blankstein R, Bax JJ, Ferencik M, Bittencourt MS, Min JK, et al. Society of Cardiovascular Computed Tomography / North American Society of Cardiovascular Imaging - Expert Consensus Document on Coronary CT Imaging of Atherosclerotic Plaque. J Cardiovasc Comput Tomogr. 2021;15(2):93-109.
90. Ferencik M, Nomura CH, Maurovich-Horvat P, Hoffmann U, Pena AJ, Cury RC, et al. Quantitative parameters of image quality in 64-slice computed tomography angiography of the coronary arteries. Eur J Radiol. 2006;57(3):373-9.
91. Goeller M, Achenbach S, Cadet S, Kwan AC, Commandeur F, Slomka PJ, et al. Pericoronary Adipose Tissue Computed Tomography Attenuation and High-Risk Plaque Characteristics in Acute Coronary Syndrome Compared With Stable Coronary Artery Disease. JAMA Cardiol. 2018;3(9):858-63.
92. Goeller M, Tamarappoo BK, Kwan AC, Cadet S, Commandeur F, Razipour A, et al. Relationship between changes in pericoronary adipose tissue attenuation and coronary plaque burden quantified from coronary computed tomography angiography. Eur Heart J Cardiovasc Imaging. 2019;20(6):636-43.
93. Lin A, Kolossváry M, Yuvaraj J, Cadet S, McElhinney PA, Jiang C, et al. Myocardial Infarction Associates With a Distinct Pericoronary Adipose Tissue Radiomic Phenotype: A Prospective Case-Control Study. JACC Cardiovasc Imaging. 2020;13(11):2371-83.
94. Tzolos E, McElhinney P, Williams MC, Cadet S, Dweck MR, Berman DS, et al. Repeatability of quantitative pericoronary adipose tissue attenuation and coronary plaque burden from coronary CT angiography. J Cardiovasc Comput Tomogr. 2021;15(1):81-4.
95. Jánosi A, Ofner P. [National Myocardial Infarction Registry of Hungary]. Orv Hetil. 2014;155(19):740-4.
96. Sinka Lászlóné Adamik E, Hári P, Póth A, Zorándi Á, Bradák A, Gál J, et al. [Quality assurance of national internet-based patient register data: Experiences during the operation of the Hungarian Myocardial Infarction Registry, 2010–2020]. Orv Hetil. 2021;162(2):61-8.
97. Suenari K, Nakano Y, Hirai Y, Ogi H, Oda N, Makita Y, et al. Left atrial thickness under the catheter ablation lines in patients with paroxysmal atrial fibrillation: insights from 64-slice multidetector computed tomography. Heart Vessels. 2013;28(3):360-8.
98. Imada M, Funabashi N, Asano M, Uehara M, Ueda M, Komuro I. Anatomical remodeling of left atria in subjects with chronic and paroxysmal atrial fibrillation evaluated by multislice computed tomography. Int J Cardiol. 2007;119(3):384-8.
99. Hoffmeister PS, Chaudhry GM, Mendel J, Almasry I, Tahir S, Marchese T, et al. Evaluation of left atrial and posterior mediastinal anatomy by multidetector helical computed tomography imaging: relevance to ablation. J Interv Card Electrophysiol. 2007;18(3):217-23.

100. Pan NH, Tsao HM, Chang NC, Chen YJ, Chen SA. Aging dilates atrium and pulmonary veins: implications for the genesis of atrial fibrillation. Chest. 2008;133(1):190-6.
101. Nakamura K, Funabashi N, Uehara M, Ueda M, Murayama T, Takaoka H, et al. Left atrial wall thickness in paroxysmal atrial fibrillation by multislice-CT is initial marker of structural remodeling and predictor of transition from paroxysmal to chronic form. Int J Cardiol. 2011;148(2):139-47.
102. Hayashi H, Hayashi M, Miyauchi Y, Takahashi K, Uetake S, Tsuboi I, et al. Left atrial wall thickness and outcomes of catheter ablation for atrial fibrillation in patients with hypertrophic cardiomyopathy. J Interv Card Electrophysiol. 2014;40(2):153-60.
103. Takahashi K, Okumura Y, Watanabe I, Nagashima K, Sonoda K, Sasaki N, et al. Relation Between Left Atrial Wall Thickness in Patients with Atrial Fibrillation and Intracardiac Electrogram Characteristics and ATP-Provoked Dormant Pulmonary Vein Conduction. J Cardiovasc Electrophysiol. 2015;26(6):597-605.
104. Jazayeri MA, Vanga SR, Vuddanda V, Turagam M, Parikh V, Lavu M, et al. Impact of Radiofrequency Ablation of Atrial Fibrillation on Pulmonary Vein Cross Sectional Area: Implications for the Diagnosis of Pulmonary Vein Stenosis. J Atr Fibrillation. 2017;10(1):1531.
105. Kirchhof P, Benussi S, Kotecha D, Ahlsson A, Atar D, Casadei B, et al. 2016 ESC Guidelines for the Management of Atrial Fibrillation Developed in Collaboration With EACTS. Rev Esp Cardiol (Engl Ed). 2017;70(1):50.
106. Corban MT, Eshtehardi P, Suo J, McDaniel MC, Timmins LH, Rassoul-Arzrumly E, et al. Combination of plaque burden, wall shear stress, and plaque phenotype has incremental value for prediction of coronary atherosclerotic plaque progression and vulnerability. Atherosclerosis. 2014;232(2):271-6.
107. Goeller M, Achenbach S, Herrmann N, Bittner DO, Kilian T, Dey D, et al. Pericoronary adipose tissue CT attenuation and its association with serum levels of atherosclerosis-relevant inflammatory mediators, coronary calcification and major adverse cardiac events. J Cardiovasc Comput Tomogr. 2021;15(5):449-54.
108. Budoff MJ, Shaw LJ, Liu ST, Weinstein SR, Mosler TP, Tseng PH, et al. Long-term prognosis associated with coronary calcification: observations from a registry of 25,253 patients. J Am Coll Cardiol. 2007;49(18):1860-70.
109. Blaha MJ, Blumenthal RS, Budoff MJ, Nasir K. Understanding the utility of zero coronary calcium as a prognostic test: a Bayesian approach. Circ Cardiovasc Qual Outcomes. 2011;4(2):253-6.
110. Blaha M, Budoff MJ, Shaw LJ, Khosa F, Rumberger JA, Berman D, et al. Absence of coronary artery calcification and all-cause mortality. JACC Cardiovasc Imaging. 2009;2(6):692-700.
111. Kanaji Y, Hirano H, Sugiyama T, Hoshino M, Horie T, Misawa T, et al. Pre-percutaneous Coronary Intervention Pericoronary Adipose Tissue Attenuation Evaluated by Computed Tomography Predicts Global Coronary Flow Reserve After Urgent Revascularization in Patients With Non-ST-Segment-Elevation Acute Coronary Syndrome. J Am Heart Assoc. 2020;9(17):e016504.
112. Hoshino M, Yang S, Sugiyama T, Zhang J, Kanaji Y, Yamaguchi M, et al. Peri-coronary inflammation is associated with findings on coronary computed tomography angiography and fractional flow reserve. J Cardiovasc Comput Tomogr. 2020;14(6):483-9.

113. Honold S, Wildauer M, Beyer C, Feuchtner G, Senoner T, Jaschke W, et al. Reciprocal communication of pericoronary adipose tissue and coronary atherogenesis. Eur J Radiol. 2021;136:109531.
114. Okayama S, Soeda T, Takami Y, Kawakami R, Somekawa S, Uemura S, et al. The influence of effective energy on computed tomography number depends on tissue characteristics in monoenergetic cardiac imaging. Radiol Res Pract. 2012;2012:150980.
115. Chatterjee D, Shou BL, Matheson MB, Ostovaneh MR, Rochitte C, Chen MY, et al. Perivascular fat attenuation for predicting adverse cardiac events in stable patients undergoing invasive coronary angiography. J Cardiovasc Comput Tomogr. 2022.
116. Sugiyama T, Kanaji Y, Hoshino M, Yamaguchi M, Hada M, Ohya H, et al. Determinants of Pericoronary Adipose Tissue Attenuation on Computed Tomography Angiography in Coronary Artery Disease. J Am Heart Assoc. 2020;9(15):e016202.
117. Raggi P, Gadiyaram V, Zhang C, Chen Z, Lopaschuk G, Stillman AE. Statins Reduce Epicardial Adipose Tissue Attenuation Independent of Lipid Lowering: A Potential Pleiotropic Effect. J Am Heart Assoc. 2019;8(12):e013104.
118. Nakagawa H, Ikeda A, Govari A, Papaioannou T, Constantine G, Bar-Tal M, et al. Abstract 12104: Prospective Study Using a New Formula Incorporating Contact Force, Radiofrequency Power and Application Time (Force-Power-Time Index) for Quantifying Lesion Formation to Guide Long Continuous Atrial lesions in the Beating Canine Heart. Circulation. 2013;128(suppl_22):A12104-A.
119. Das M, Loveday JJ, Wynn GJ, Gomes S, Saeed Y, Bonnett LJ, et al. Ablation index, a novel marker of ablation lesion quality: prediction of pulmonary vein reconnection at repeat electrophysiology study and regional differences in target values. EP Europace. 2016;19(5):775-83.
120. Solimene F, Schillaci V, Shopova G, Urraro F, Arestia A, Iuliano A, et al. Safety and efficacy of atrial fibrillation ablation guided by Ablation Index module. J Interv Card Electrophysiol. 2019;54(1):9-15.
121. Kawaji T, Hojo S, Kushiyama A, Nakatsuma K, Kaneda K, Kato M, et al. Limitations of lesion quality estimated by ablation index: An in vitro study. J Cardiovasc Electrophysiol. 2019;30(6):926-33.
122. El Haddad M, Taghji P, Phlips T, Wolf M, Demolder A, Choudhury R, et al. Determinants of Acute and Late Pulmonary Vein Reconnection in Contact Force-Guided Pulmonary Vein Isolation: Identifying the Weakest Link in the Ablation Chain. Circulation Arrhythmia and electrophysiology. 2017;10(4).
123. Hussein A, Das M, Riva S, Morgan M, Ronayne C, Sahni A, et al. Use of Ablation Index-Guided Ablation Results in High Rates of Durable Pulmonary Vein Isolation and Freedom From Arrhythmia in Persistent Atrial Fibrillation Patients: The PRAISE Study Results. Circ Arrhythm Electrophysiol. 2018;11(9):e006576.
124. Budoff MJ, Dowe D, Jollis JG, Gitter M, Sutherland J, Halamert E, et al. Diagnostic performance of 64-multidetector row coronary computed tomographic angiography for evaluation of coronary artery stenosis in individuals without known coronary artery disease: results from the prospective multicenter ACCURACY (Assessment by Coronary Computed Tomographic Angiography of Individuals Undergoing Invasive Coronary Angiography) trial. J Am Coll Cardiol. 2008;52(21):1724-32.
125. Meijboom WB, Meijs MF, Schuijf JD, Cramer MJ, Mollet NR, van Mieghem CA, et al. Diagnostic accuracy of 64-slice computed tomography coronary angiography: a prospective, multicenter, multivendor study. J Am Coll Cardiol. 2008;52(25):2135-44.

126. Paech DC, Weston AR. A systematic review of the clinical effectiveness of 64-slice or higher computed tomography angiography as an alternative to invasive coronary angiography in the investigation of suspected coronary artery disease. BMC Cardiovasc Disord. 2011;11:32.
127. Zuo K, Li K, Liu M, Li J, Liu X, Liu X, et al. Correlation of left atrial wall thickness and atrial remodeling in atrial fibrillation: Study based on low-dose-ibutilide-facilitated catheter ablation. Medicine (Baltimore). 2019;98(15):e15170.
128. Nakatani Y, Sakamoto T, Yamaguchi Y, Tsujino Y, Kataoka N, Nishida K, et al. Impacts of the body size on the left atrial wall thickness and atrial fibrillation recurrence after catheter ablation. Heart Vessels. 2019;34(8):1351-9.
129. Nakatani Y, Sakamoto T, Yamaguchi Y, Tsujino Y, Kataoka N, Kinugawa K. Heterogeneity in the left atrial wall thickness contributes to atrial fibrillation recurrence after catheter ablation. Heart Vessels. 2018;33(12):1549-58.
130. Inoue J, Skanes AC, Gula LJ, Drangova M. Effect of Left Atrial Wall Thickness on Radiofrequency Ablation Success. J Cardiovasc Electrophysiol. 2016;27(11):1298-303.
131. Okamatsu H, Koyama J, Sakai Y, Negishi K, Hayashi K, Tsurugi T, et al. High-power application is associated with shorter procedure time and higher rate of first-pass pulmonary vein isolation in ablation index-guided atrial fibrillation ablation. J Cardiovasc Electrophysiol. 2019;30(12):2751-8.
132. Teres C, Soto-Iglesias D, Penela D, Jáuregui B, Ordoñez A, Chauca A, et al. Personalized paroxysmal atrial fibrillation ablation by tailoring ablation index to the left atrial wall thickness: the 'Ablate by-LAW' single-centre study-a pilot study. Europace. 2021.
133. Garg L, Pothineni NVK, Daw JM, Hyman MC, Arkles J, Tschabrunn CM, et al. Impact of Left Atrial Bipolar Electrogram Voltage on First Pass Pulmonary Vein Isolation During Radiofrequency Catheter Ablation. Front Physiol. 2020;11:594654.
134. Yoshida K, Baba M, Shinoda Y, Harunari T, Tsumagari Y, Koda N, et al. Epicardial connection between the right-sided pulmonary venous carina and the right atrium in patients with atrial fibrillation: A possible mechanism for preclusion of pulmonary vein isolation without carina ablation. Heart Rhythm. 2019;16(5):671-8.
135. Szegedi N, Széplaki G, Herczeg S, Tahin T, Salló Z, Nagy VK, et al. Repeat procedure is a new independent predictor of complications of atrial fibrillation ablation. Europace. 2019;21(5):732-7.
136. Boussoussou M, Szilveszter B, Vattay B, Kolossváry M, Vecsey-Nagy M, Salló Z, et al. The effect of left atrial wall thickness and pulmonary vein sizes on the acute procedural success of atrial fibrillation ablation. The international journal of cardiovascular imaging. 2022.

10 BIBLIOGRAPHY OF THE CANDIDATE

10.1 Bibliography related to the present thesis

1. **Boussoussou M**, Vattay B, Szilveszter B, Simon J, Lin A, Vecsey-Nagy M, et al. The effect of patient and imaging characteristics on coronary CT angiography assessed pericoronary adipose tissue attenuation and gradient. Journal of Cardiovascular Computed Tomography. 2022. **IF: 5,17**
2. **Boussoussou M**, Szilveszter B, Vattay B, Kolossváry M, Vecsey-Nagy M, Salló Z, et al. The effect of left atrial wall thickness and pulmonary vein sizes on the acute procedural success of atrial fibrillation ablation. Int J Cardiovasc Imaging. 2022. **IF: 2,316**

10.2 Bibliography not related to the present thesis

1. **Boussoussou M**, Édes István F, Nowotta F, Vattay B, Vecseys-Nagy M, Drobni Zs et al. Coronary CT-based FFR in patients with acute myocardial infarction might predict follow-up invasive FFR: The XPECT-MI study. Journal of cardiovascular computed tomography. 2023;17(4):269-76. **IF: 5,4**
2. Maurovich-Horvat P, Bosserdt M, Kofoed KF, Rieckmann N, Benedek T, Donnelly P, … **Boussoussou M,** et al. CT or Invasive Coronary Angiography in Stable Chest Pain. N Engl J Med. 2022;386(17):1591-602. **IF: 176,079**
3. Panajotu A, Vecsey-Nagy M, Jermendy Á L, **Boussoussou M**, Vattay B, Kolossváry M, et al. Coronary CTA Amidst the COVID-19 Pandemic: A Quicker Examination Protocol with Preserved Image Quality Using a Dedicated Cardiac Scanner. Diagnostics (Basel, Switzerland). 2023;13(3). **IF: 3,6**
4. Vattay B, Szilveszter B, **Boussoussou M**, Vecsey-Nagy M, Lin A, Konkoly G, et al. Impact of virtual monoenergetic levels on coronary plaque volume components using photon-counting computed tomography. European radiology. 2023. **IF: 5,9**
5. Vecsey-Nagy M, Varga-Szemes A, Emrich T, Zsarnoczay E, Nagy N, Fink N, … **Boussoussou M**, et al. Calcium scoring on coronary computed angiography tomography with photon-counting detector technology: Predictors of performance. Journal of cardiovascular computed tomography. 2023. **IF: 5,4**
6. Vecsey-Nagy M, Jokkel Z, Jermendy Á L, Nagy M, Boussoussou M, Vattay B, et al. The Impact of Novel Reconstruction Algorithms on Calcium Scoring: Results

on a Dedicated Cardiac CT Scanner. Diagnostics (Basel, Switzerland). 2023;13(4). **IF: 3,6**

7. Vattay B, Borzsák S, **Boussoussou M**, Vecsey-Nagy M, Jermendy Á L, Suhai FI, et al. Association between coronary plaque volume and myocardial ischemia detected by dynamic perfusion CT imaging. Front Cardiovasc Med. 2022;9:974805. **IF: 5,846**
8. Vattay B, Nagy AI, Apor A, Kolossváry M, Manouras A, Vecsey-Nagy M, … **Boussoussou M,** et al. The Predictive Value of Left Atrial Strain Following Transcatheter Aortic Valve Implantation on Anatomical and Functional Reverse Remodeling in a Multi-Modality Study. Front Cardiovasc Med. 2022;9:841658. **IF: 5,846**
9. Vecsey-Nagy M, Szilveszter B, Kolossváry M, **Boussoussou M**, Vattay B, Merkely B, et al. Correlation between Coronary Artery Calcium- and Different Cardiovascular Risk Score-Based Methods for the Estimation of Vascular Age in Caucasian Patients. J Clin Med. 2022;11(4). **IF: 4,964**
10. Vecsey-Nagy M, Szilveszter B, Kolossváry M, **Boussoussou M**, Vattay B, Gonda X, et al. Cyclothymic affective temperament is independently associated with left ventricular hypertrophy in chronic hypertensive patients. J Psychosom Res. 2022;160:110988. **IF: 4,620**
11. Vecsey-Nagy M, Jermendy Á L, Kolossváry M, Vattay B, **Boussoussou M**, Suhai FI, et al. Heart Rate-Dependent Degree of Motion Artifacts in Coronary CT Angiography Acquired by a Novel Purpose-Built Cardiac CT Scanner. J Clin Med. 2022;11(15). **IF: 4,964**
12. Papp S, Bárczi G, Karády J, Kolossváry M, Drobni ZD, Simon J, … **Boussoussou M,** et al. Coronary plaque burden of the left anterior descending artery in patients with or without myocardial bridge: A case-control study based on coronary CT-angiography. Int J Cardiol. 2021;327:231-5. **IF: 4,039**
13. Szilveszter B, Vattay B, **Bossoussou M**, Vecsey-Nagy M, Simon J, Merkely B, et al. CAD-RADS may underestimate coronary plaque progression as detected by serial CT angiography. Eur Heart J Cardiovasc Imaging. 2022;23(11):1530-9. **IF: 9,13**

14. Vecsey-Nagy M, Szilveszter B, Kolossváry M, **Boussoussou M**, Vattay B, Gonda X, et al. Association between affective temperaments and severe coronary artery disease. J Affect Disord. 2021;295:914-9. **IF: 6,533**
15. Vecsey-Nagy M, Jermendy Á L, Suhai FI, Panajotu A, Csőre J, Borzsák S, … **Boussoussou M,** et al. Model-based adaptive filter for a dedicated cardiovascular CT scanner: Assessment of image noise, sharpness and quality. Eur J Radiol. 2021;145:110032. **IF: 4,531**
16. Vecsey-Nagy M, Szilveszter B, Kolossváry M, **Boussoussou M**, Vattay B, Gonda X, et al. The association between accelerated vascular aging and cyclothymic affective temperament in women. J Psychosom Res. 2021;145:110423. **IF: 4,620**
17. **Boussoussou M**, Boussoussou N, Merész G, Rakovics M, Entz L, Nemes A. Atmospheric fronts as minor cardiovascular risk factors, a new approach to preventive cardiology. J Cardiol. 2020;75(2):196-202. **IF: 3,159**
18. Simon J, Száraz L, Szilveszter B, Panajotu A, Jermendy Á, Bartykowszki A, et al. Calcium scoring: a personalized probability assessment predicts the need for additional or alternative testing to coronary CT angiography. Eur Radiol. 2020;30(10):5499-506. **IF: 5,315**
19. Boussoussou N, **Boussoussou M**, Merész G, Rakovics M, Entz L, Nemes A. Complex effects of atmospheric parameters on acute cardiovascular diseases and major cardiovascular risk factors: data from the Cardiometeorology(SM) study. Sci Rep. 2019;9(1):6358. **IF: 3,988**

Hungarian journal articles:

1. **Boussoussou M**, Vattay B, Szilveszter B, Kolossváry M, Simon J, Vecsey-Nagy M, et al. Functional assessment of coronary plaques using CT based hemodynamic simulations: Current status, technical principles and clinical value. Imaging. 2021;13(1):37-48.
2. Vattay B, **Boussoussou M**, Borzsák S, Vecsey-Nagy M, Simon J, Kolossváry M, et al. Myocardial perfusion imaging using computed tomography: Current status, clinical value and prognostic implications. Imaging. 2021;13(1):49-60.

3. Boussoussou N, **Boussoussou M**, Nemes A. Historical overview of medical meteorology - the new horizon in medical prevention. Orv Hetil. 2017;158(5):187-91. **IF: 0,322**
4. Boussoussou N, **Boussoussou M**, Entz L. Akut cardiovascularis kórképek vizsgálata különböző légköri paraméterek tükrében. Orv Hetil. 2014;155(27): 1078-1082. **IF: 0,322**
5. Simon J, Herczeg S, Borzsák S, Csőre J, Kardos AS, Mérges G, … **Boussoussou M,** et al. Extracardiac findings on cardiac computed tomography in patients undergoing atrial fibrillation catheter ablation. Imaging. 2022;14(1):52-9.

DOI:10.14753/SE.2024.2997

11 ACKNOWLEDGEMENTS

The present thesis and the research work behind it would have never been possible without my colleagues and family's valuable help and overwhelming support.

First of all, I would like to express my gratitude to Prof. Dr. Béla Merkely, who created a scientific and working environment at the Semmelweis University Heart and Vascular Centre with endless possibilities for evolving and becoming a better physician and researcher. I am also thankful to Prof. Dr. Pál Maurovich-Horvat, who supported me and trusted in me from the beginning and let me join the Cardiovascular Imaging Research Group, where I had the chance to work with Dr. Bálint Szilveszter, Dr. Márton Kolossváry, Dr. Borbála Vattay, and Dr. Milán Vecsey-Nagy. They became not just my trusted and appreciated colleagues but also my friends during the past years.

I would also like to express my sincere gratitude to Dr. Bálint Szilveszter, Dr. Márton Kolossváry, and Dr. Nándor Szegedi, who supported and guided me in my research and without whom this thesis would not have been possible.

I also wish to thank the co-workers of the Heart and Vascular Centre, especially the CT and electrophysiology laboratory team, for their contribution.

Last but not least, I owe an infinite debt of gratitude to my sister, Dr. Nora Boussoussou, my Parents, Ágota & Farid, my Grandparents, Katalin & József and the Rojo Granda family, Amelia, Luis, Lucía and Belén. They always encouraged and supported me and gave me every opportunity to pursue my dreams. Words cannot express my gratitude for all the love they have given me for so many years. Thank you! I love you to infinity and beyond!

12 SUPPLEMENTS

Supplementary Table 1. Main studies about PCAT attenuation, PCAT gradient, PCAT volume and CCTA (sorted chronologically by years)(85).

Author, year	DOI	Study design, N	Study aims	Scanner and Software	Adjustments for clinical or acquisition parameters	Main findings
Petra M. Gorter et al. 2008	10.1016/j.amjcard.2008.04.002	Cross-sectional, N=128	To evaluate the relation between EAT and PCAT and coronary atherosclerosis and CAC in patients with suspected CAD and whether this relation is modified by BMI.	*Scanner:* 64-detector CT Brilliance 64, Philips Medical Systems *Software:* Extended Brilliance Workspace and Easy Vision, Philips Medical Systems, Philips computed tomographic workstation	Age, gender, BMI	- EAT and PCAT were not associated with the severity of coronary atherosclerosis (p=.6, p=.7 respectively) and CAC in patients with suspected CAD (p=.6, p=.4 respectively). - Patients with BMI<27 kg/m^2, increased EAT and PCAT were related to more severe coronary atherosclerosis (p=.04, p=.06 respectively) and CAC (p=.02. p=.01 respectively).
Masaaki Konishi, et al. 2010	10.1016/j.atherosclerosis.2010.10.007	Cross-sectional, N=108	To evaluate the association between inflammation in PCAT and CAD by pathological examination and clinical evaluation with CCTA.	*Scanner:* 64-detector CT Brilliance-64 Phillips Medical Systems *Software:* Unknown	Dyslipidemia, $HBA1_C$	- PDG was greater in patients with CAD (22±16 HU) than those without CAD (16±10 HU, p=.046). - PFI was significantly larger in patients with CAD than those without CAD (6532±4927 vs.4037±2626 HUcm^3, p=.009). - PFI (OR [95% CI];1.234 [1.012–1.503] per 1000 HUcm^3, p=.037), - The presence of dyslipidemia (5.927 [1.302–26.978], p=.021), and HbA1c (4.946 [2.025–12.076], p<.001) were independently and significantly associated with the presence of CAD.
Amir A. Mahabadi et al. 2010	10.1016/j.atherosclerosis.2010.02.013	Cross-sectional, N=78, only LAD and LCX were analyzed	- To determine whether the amount of local PCAT volume is associated with the presence of plaque burden in the underlying coronary artery segment. - Whether this association is independent of overall pericardial fat volume and traditional cardiovascular risk factors.	*Scanner:* DSCT Somatom, Siemens Medical Solutions, *Software:* Unknown	Age, BMI, hyperlipidemia, diabetes, smoking, family history of CVD	- Per each doubling of PCAT volume: 2.5-fold increase in the presence of plaque in the underlying coronary segment in unadjusted models (95% CI [1.87–3.27], p<0.001) it has remained after adjustment for traditional cardiovascular risk factors (OR 3.07 [2.16–4.35], p<.001) and after additionally accounting for overall pericardial fat volume (OR 2.68 [1.90–3.79], p<.001). - Similar associations were found in all coronary artery segments independent of plaque type (calcified/non-calcified, p<.01 for all).
Pál Maurovich-Horvat et al. 2011	10.1016/j.atherosclerosis.2011.06.049	Cross-sectional, N=51 Group 1: patients with plaque, hs-CRP >2.0mg/L Groupe 2: patients without plaque, hs-CRP >2.0mg/L Group 3: patients with no plaque, hs-CRP<1mg/L	- To firstly assess the feasibility and reproducibility of a threshold-based method of PCAT volume quantification and determine the relationship of PCAT volume to the presence of coronary atherosclerotic plaque and hs-CRP levels on per-patient and per-vessel basis. - To determine the association between PCAT volumes and CAD (plaque vs. no plaque and plaque morphology).	*Scanner:* 4-slice MDCT Sensation 64, Siemens Medical Solution, *Software:* SurePlaque, Toshiba	BMI, hypertension, hyperlipidemia, vessel, distance, hs-CRP	- Distance-based PCAT volume measurements (proximal 40 mm of the coronary arteries): intra-observer ICC=0.997, inter-observer ICC=0.951. - In a patient-based analysis, PCAT volume differed significantly across the three groups (p<.001), and was greater in Group 1 than in Group 2 and 3, irrespective of hs-CRP levels (Group 2: high hs-CRP, p<.001, Group 3: low hs-CRP, p<.001). - In patients without plaque, no difference in PCAT volume between patients with high and low hs-CRP levels (p=.514). - Adjusted PCAT volumes were higher in subsegments with plaques than without (p<.001).

						- Adjusted PCAT volume was greatest in subsegments with mixed plaque followed by non-calcified plaque, calcified plaque, and the lowest volume in segments with no plaque (p<.001), no difference between calcified plaque and no plaque (p= 0.12), but a difference between mixed plaque and non-calcified plaque as compared with no plaque (both p <.001). - The difference in PCAT volumes remained significant across the three patient groups after adjustment for BMI, hypertension, and hyperlipidemia.
Marwan, Mohamed et al. 2017	10.1097 /RCT.00 0000000 0000589	Cross-sectional, N=29	To analyse PCAT CT attenuation in normal versus atherosclerotic coronary segments as defined by IVUS.	*Scanner:* DS CT Siemens Healthcare; *Software:* Unknown	None	- Segments with any coronary atherosclerotic plaque: mean PCAT attenuation: −34±14 HU. Segments without plaque: mean PCAT attenuation: −56±16 HU (p=.005). - Segments with fibrous vs lipid-rich plaque (defined by IVUS): PCAT density was not significantly different (−35±19 HU vs −36±16 HU, p=.8).
Ryo Okubo et al. 2017	10.1007 /s00380- 017- 0943-1	Cross-sectional, N=103, PCAT ratios were divided into low, mid and high tertile groups.	To evaluate the association between PCAT and vulnerable plaques.	*Scanner:* 64-slice CT scanner, Aquillion-64; Toshiba *Software:* None	Age, male gender, number of coronary risk factors, hypertension, diabetes, dyslipidemia, current smoking, BMI, LDL-cholesterol, HDL-cholesterol, EAT, PCAT	- Low, mid and high tertile groups: mean PCAT ratio: 0.79±0.11, 1.07±0.09, and 1.50±0.33, respectively (p<.001). - High tertile group: significantly lower mean plaque attenuation compared with the mid and low tertile groups (47.5±28.8 vs. 53.1±29.7 vs. 64.7±27.0, p=.04). - Vulnerable plaques were more frequent in the high tertile group than in the other two groups (52.9 vs. 31.4 vs. 26.5%, p=.06, respectively). - Significant frequency of vulnerable plaques with NRS in the high tertile group compared with the mid or low tertile group (61.8 vs. 37.1 vs. 32.4%, p=.03, respectively).
Alexios S Antonopoulos 2017	10.1126 /scitrans lmed.aal 2658	Case-control, longitudinal, N=273	To evaluate whether phenotypic changes in PVAT induced by vascular inflammation could be quantified using a new CCTA methodology.	*Scanner:* Unknown, *Software:* Aquarius Workstation V.4.4.11 TeraRecon	Age, gender, and cardiovascular risk factors: hypertension, dyslipidemia, diabetes, smoking,	- Association of FAI and distance from the vascular wall: significantly (p=.001) different in case and control groups. - Association of FAI_{PVAT} and patients with and without CAD, significant (p =.001) difference independently of the presence of obstructive RCA disease. No difference in $FAI_{non\text{-}PVAT}$ between CAD and non-CAD groups. - PVAT volume around RCA (independently of age, gender, and cardiovascular risk factors) was not associated with either the presence of CAD or the RCA calcium burden. - VPCI: weakly associated only with the calcium burden in RCA but not total CCS. - FAI_{PVAT} and CCS were related to the presence of CAD independently of each other and of age, gender, and other cardiovascular risk factors. - FAI_{PVAT} (but not total CCS in the entire coronary tree or CCS in the RCA): positively related with atherosclerotic plaque burden of the RCA (independently of age, gender, and cardiovascular risk factors). - FAI_{PVAT} was increased by 8.76±2.87 HU around the culprit lesion compared with FAI_{PVAT} proximal to the lesion (p<.0001). - [FAI_{PVAT}] was significantly (p<.001) increased around ruptured compared with stable plaques and had high diagnostic accuracy for detecting these areas of vascular inflammation.
Evangelos K Oikonomou, 2018	10.1016 /S0140- 6736(18)31114- 0	Longitudinal, N=1872	To evaluate whether, quantifying coronary artery inflammation, the perivascular FAI could predict future adverse events.	*Scanner:* 64-slice *Software:* Aquarius Workstation V.4.4.11 TeraRecon	Age, male sex, cardiovascular risk factors, tube voltage, modified Duke CAD index,	- The perivascular FAI was normally distributed around a mean of –75.1 HU (SD=8.6) in the derivation cohort. and –77.0 HU (SD=8.5) in the validation cohort. - After multivariable adjustment high perivascular FAI values (≥–70.1 HU vs <–70.1 HU) were associated with a higher prospective risk of all-cause mortality (adjusted HR 2.55, 95% CI [1.65–3.92]; p<.0001) and cardiac mortality (9.04, [3.35–24.40]; p<.0001).

					number of CCTA derived HRP	- In the subgroup of patients with CCS (n=1415 [76%]): FAI remained predictive for both endpoints after additional adjustment for CCS (adjusted HR 2.03, 95% CI [1.17–3.52]; p=.0122 for all-cause mortality and 12.83, [2.76–59.56]; p=.0011 for cardiac mortality). - Perivascular FAI values of ≥–70.1 HU were associated with increased risk of all-cause mortality (adjusted HR 3.69, 95% CI [2.26–6.02]; p<.0001); and cardiac mortality (5.62, [2.90–10.88]; p<.0001).
Markus Goeller et al. 2018	10.1001/jamacardio.2018.1997	Case-control, N=35	To evaluate the association between HRP characteristics and PCAT CT attenuation in patients with a first ACS and matched controls with stable CAD.	*Scanner:* DSCT Somatom Definition; Siemens Healthcare *Software:* AutoPlaque version 2.0	Age, male sex, number of cardiovascular risk factors: hypertension, Diabetes, current smoker	- PCAT attenuation was significantly higher around culprit lesions compared with non-culprit lesions in patients with ACS and in controls (including the highest-grade stenosis lesions) (p=.014, p=.013). - Multivariable logistic regression analysis: low-attenuation NCP burden (increase of 1%; OR, 1.43; 95% CI [1.2-1.8]; p<0.001), intermediate-attenuation NCP burden (increase of 1%; OR, 1.27; 95% CI [1.0-1.4]; p<.01), and PCAT CT attenuation (1 HU increase; OR, 1.2; 95% CI [1.0-1.3]; p=.01) were independently associated with the presence of culprit lesions.
Markus Goeller et al. 2019	10.1093/ehjci/jez013	Longitudinal, N=111	To investigate whether PCAT CT attenuation is related to progression of coronary plaque burden.	*Scanner:* DSCT Siemens Definition, Siemens Medical Solutions *Software:* Autoplaque version 2.0	Baseline PCAT attenuation, sex, number of CAD risk factors, LDL change, and statin use,	- Patients with an increase in NCP burden (n = 51) showed an increase in PCAT attenuation, whereas patients with a decrease in NCP burden (n = 60) showed a decrease 4.4 HU 95% CI [2.6–6.2] vs. -2.78 HU 95% CI [–4.6 - -1.0] HU, p<.0001. - Positive correlation between changes in mean PCAT CT attenuation and changes in NCP burden (r=0.55, p<.001), changes in LD-NCP burden (r=0.24, p=.01) and change in TP burden (r=0.52, p<.001) of the proximal RCA. Changes in CP burden did not correlate with changes in PCAT CT attenuation (r=0.10, p=.3). - Baseline PCAT CT attenuation: positively correlated with change in PCAT CT attenuation (r=0.55, p<.001). - Change in TP and NCP burden within the proximal RCA: change in TP and NCP burden throughout the entire coronary tree (changes of NCP burden: rho=0.329, p=.0005; changes of TP burden: rho=0.258, p= .0065). Weak correlation between change in PCAT CT attenuation around the proximal RCA and change in the TP burden and NCP burden in the entire coronary tree (changes in NCP burden: rho=0.197, p=.039; changes in TP burden: rho=0.219. p=.0217). - Multivariable logistic regression: adjusting for confounding variables increase in NCP burden was associated with increase in PCAT attenuation around the proximal RCA (p<.001). - PCAT CT attenuation correlated significantly with mean EAT attenuation at baseline and follow-up (r= 0.42 and 0.51, p<.001 for both). PCAT volume also correlated with EAT volume at baseline and follow-up (r=0.76 and 0.66, p<.001 for both). - Positive correlation between PCAT CT attenuation surrounding the proximal RCA at baseline and change in NCP burden (r=0.31, p=.001) and change in TP burden (r=0.30, p=.0013) within the proximal RCA. - Multivariable logistic regression: adjusted for confounding variables baseline PCAT CT attenuation around the proximal RCA was associated with increase in NCP burden within the proximal RCA [OR 1.32, 95% CI [1.03–1.69]; p=.03]. PCAT attenuation threshold of ≥-75 HU was associated with an increase in NCP burden (OR 3.07, 95% CI [1.4–7.0]; p<.008). - Baseline PCAT CT attenuation ≥-75 HU was the only covariate independently associated with progression of TP burden within the proximal RCA (OR 2.4, 95% CI [1.1–5.2]; p=.03.

Jacek Kwiecinski 2019	10.1016/j.jcmg.2018.11.032	Cross-sectional, N=41	To assess the association between increased lesion PCAT density and 18F-NaF uptake on PET in stable patients with HRPs shown on CCTA.	*Scanner:* DSCT Definition, Siemens Healthcare *Software:* AutoPlaque version2.0	In terms of TBR: lesion quantitative percent stenosis, total plaque, and NCP plaque volumes	- Lesions with increased activity of 18F-NaF had higher surrounding PCAT density than those without (-73 HU; IQR: -79 to -68 HU vs. -86 HU; IQR: -94 to -80 HU; p<.001) - Adjusted multivariable linear regression analyses: lesion PCAT density and LAP volume were associated with 18F-NaF TBR: ß =0.25 per 11 HU PCAT density increase (95% CI [0.17-0.34; p<.001); and ß =0.07 per 14 mm^3 LAP volume increase (95% CI [0.03-0.11]; p=.002), after adjustments for lesion quantitative percent stenosis, total plaque, and NCP plaque volumes. - Adjusted multivariable linear regression analyses: lesion 18F-NaF TBR and LAP volume were associated with lesion PCAT: ß=6.3 per 0.47 TBR increase (95% CI [4.6-7.8]; p<.001); and ß =0.84 per 14 mm^3 LAP volume increase (95% CI [0.02 - 1.66]; p=.029).
Nicola Gaibazzi et al. 2019	10.1161/JAHA.119.013235	Case-control N=212 (MINOCA/TTS=106; controls with atypical chest pain=106)	To assess the association between pericoronary FAI and MINOCA and TTS.	*Scanner:* DSCT Somatom Definition FLASH; Siemens Healthcare *Software:* Aquarius Workstation version 4.4.13; TeraRecon Inc.	Tube voltage	- Mean pFAI averaged for the 3 coronary arteries: MINOCA/TTS group: -68.37±8.29 HU, Control group: -78.03±6.20 HU. Statistically significant difference (p<.0001). - Association between mean FAI in each coronary artery between MINOCA/TTS and controls was p<.0001. - NCP (HRP in particular), were more frequently found (p<.01) in the MINOCA/TTS group compared with controls.
Youssef A Elnabawi et al. 2019	10.1001/jamacardio.2019.2589	Longitudinal, N=134	To evaluate the association between biologic therapy in patient with psoriasis and FAI.	*Scanner:* 320-detector row Aquilion ONE ViSION; Toshiba *Software:* Unknown	Adjusted for factors from the CariHeart algorithm	- Biologic therapy was associated with a significant decrease in FAI at 1 year (median FAI -71.22 HU [IQR -75.85 to -68.11 HU] at baseline vs -76.09 HU [IQR, −80.08 to −70.37 HU] at 1 year; p<.001) parallel with skin disease improvement (median PASI, 7.7 [IQR, 3.2-12.5] at baseline vs 3.2 [IQR, 1.8-5.7] at 1 year; p<.001). No change in FAI who did not receive biologic therapy (median FAI, -71.98 [IQR, -77.36 to -65.64] at baseline vs -72.66 [IQR, -78.21 to -67.44] at 1 year; p=.39).
Markus Goeller et al. 2020	10.1016/j.ejrad.2020.108874	Cross-sectional, N=300	To investigate the relationship between plaque characteristics and PCAT attenuation around RCA and to assess gender and ethnic differences in PCAT attenuation using a matched cohort of SA, EA and Caucasians.	*Scanner:* 64-slice DSCT scanner Siemens Medical Solutions *Software:* Autoplaque version 2.0	None	- PCAT CT attenuation was increased in patients with any plaque in the coronary tree (N=211) compared with patients with no plaque (N =89, -81.4 vs. -88.1 HU, p <.001). - PCAT CT attenuation was increased in patients with plaque within the RCA (N=148) compared with patients with no RCA-plaque (N=152, -78.7 vs. -87.9HU, p<.001). - Positive correlation between PCAT CT attenuation and the total volume of NCP (r=0.226, p<.001), LD-NCP (r=0.178, p=.002) and CP (r= 0.219, p<.001) and the total burden of NCP (r=0.283, p<.001), LD-NCP (r=0.202, p<.001) and CP (r=0.241, p<.001. - Positive correlation between PCAT CT attenuation and the total volumes of NCP (r=0.439, p<.001) and LD-NCP (r=0.391, p<.001) without significance for CP (r=0.109, p=0.059). - Within the RCA: positive correlation between PCAT attenuation and the burden of NCP (r=0.468, p<.001) and LD-NCP (r=.393, p<.001) without significance for CP (r=0.105, p=.069). - No significant difference in PCAT CT attenuation between matched ethnic groups was found.
Runlei Ma et al. 2020	10.1007/s00330-	Cross-sectional, N=192	To determine normal PCAT mean attenuation values for LAD, LCX, and RCA in patients without plaques on CCTA taking into account tube voltage influence.	*Scanner:* DSCT Somatom Force;	Age, gender, BMI, tube voltage	- Overall mean PCAT attenuation value: − 90.3±11.1 HU - Multivariable regression analysis: kV, age and gender were significantly associated with mean PCAT attenuation value (p<.05), BMI was not (p=.235)

	020-07069-0			Siemens Healthineers, *Software:* Aquarius Workstation V.4.4.11 TeraRecon		- Mean PCAT attenuation showed a positive linear association with tube voltage. - Mean (SD) PCAT attenuation of the 70 kV, 80 kV, 90 kV, 100 kV, and 120 kV groups was −95.6±9.6 HU, −90.2±11.5 HU, −87.3±9.9 HU, − 82.7±6.2 HU, and −79.3±6.8 HU, respectively (p<.001). - Post-hoc pairwise comparison of the kV groups: significant differences between each two groups except for the 80 kV and 90 kV (*p*=.222), and 100 kV and 120 kV groups (*p*=.267)
Shone Almeida et al. 2020	10.1016/j.jcct.2020.04.004	Cross-sectional, N=119	To compare pre-contrast coronary scans to post-contrast CCTA for quantification of PCAT volume and attenuation.	*Scanner:* 256-slice GE Revolution scanner *Software:* Autoplaq v2.18.08.23, TeraRecon	Vessel diameter	- Mean PCAT attenuation of pre- and post-contrast images was significantly different at −87.02±7.15 HU and −82.74±6.54 HU, respectively (p<.0001) with a mean difference for volume of 396 mm^3± 294.3(p<.0001). - High degree of correlation between pre- and post-contrast studies: r= 0.65 for attenuation and r= 0.93 for volume, p<.0001 for both. - Subgroup analysis: cases with CAC=0 and CAD-RADS=0: precontrast attenuation −85.59±7.53 HU and postcontrast −82.21±7.15, *r* = 0.67, p<.0001
Yu Du et al. 2020	10.1186/s12872-020-01499-w	Cross-sectional, N=45	To investigate the association of lesion-specific EAT volume and density with the presence of myocardial ischemia.	*Scanner:* 128-slice DSCT scanner Somatom Definition Flash Siemens Healthcare, cardiac risk analysis software Siemens *Software:* computer workstation *(*MMWP, Siemens Healthcare)	Location, and segmental information: proximal segment, plaque length, plaque calcification, reference vessel diameter	- Indexed total EAT volume was non-significantly greater in ischemic patients than non-ischemic patients (53.4 vs 47.6 ml/m2, p=.032). - Significant stenosis patients had higher total EAT volume (102.0 vs 85.9 ml, p=.061) and a higher indexed total EAT volume (53.4 vs 47.6 ml/m2, p=.046) than non-significant stenosis patients. - Total EAT volume was positively correlated with the BMI (r=0.381, p=.010), fasting blood glucose level (r=0.341, p=.022), and glycated serum protein level (r=0.434, p=.003). - Ischemic lesions (compared with non-ischemic lesions): higher lesion EAT volumes (0.64 vs 0.50 ml, p=.051) and a higher peri-lesion EAT volume index (0.34 vs 0.27 ml/m2, p=.045).
Yoshihisa Kanaji et al., 2020	10.1161/JAHA.120.016504	Longitudinal, N=183	To evaluate the relationship between pre-procedural PCAT inflammation and g-CFR after the urgent PCI in patients with first NSTEMI.	*Scanner:* 320-slice CT scanner Aquilion ONE; Canon Medical Systems Corporation, *Software:* Aquarius iNtuition Edition version 4.4.13; TeraRecon Inc	Age, BSA, Killip class, GRACE score, culprit lesion, TIMI flow grade at baseline, HDL-C, eGFR, peak CK-MB, NT-proBNP, hs-CRP, LVMI, area at risk mass volume, mean PCAT attenuation, RCA PCAT attenuation, EF, LGE volume	- Mean PCAT attenuation: only significant factor to predict g-CFR 1 month after urgent PCI (p<.001). - Optimal cut-off values of corrected mean PCAT attenuation and age for predicting impaired g-CFR: -65.6 HU (AUC 0.639; 95% CI [0.544-0.726]) for mean PCAT attenuation and 63 years (AUC 0.639; 95% CI [0.544-0.726]) for age.
Tomoyo Sugyama et al., 2020	10.1161/JAHA.120.016202	Cross-sectional, N=540	To investigate the determinants predicting increased PCAT attenuation in patients with known or suspected coronary artery disease.	*Scanner:* 320-slice CT scanner Aquilion ONE; Canon Medical Systems Corporation *Software:* Aquarius iNtuition Edition version 4.4.13.P3; TeraRecon Inc.	None	- Patients with angiographically significant epicardial stenosis (diameter stenosis >50%) in the RCA had a higher RCA-PCATA than those without significant stenosis in the RCA (−70.17±8.05 versus −73.07±8.51 HU, p<.001). - Patients with angiographically significant stenosis in the LAD had a higher LAD-PCATA than those without significant stenosis in the LAD (−70.84±7.89 versus −72.30±8.16 HU, p=.037). - Multivariable linear regression analysis revealed that the significant determinants of RCA-PCATA were male sex (β=4.965, p=.008).

						- Multivariable logistic regression analysis demonstrated that the significant determinants of elevated RCA-PCATA (≥−70.1 HU) were male sex (OR=3.665, p=.999). - Sex-related determinants of RCA-PCATA were NT-pro-BNP (β =<0.001, p=.026, Agatston-score in the RCA (ß=-0.002, p=.010), LV mass index (ß=0.041, p=.028) and the presence of significant stenosis in the RCA (ß=0.041, p=.028) and the presence of significant stenosis in the RCA (ß=4.006, p<.001) in male patients and LV ejection fraction (ß=-0.217, p=.010) and the presence of significant stenosis in the RCA (ß=3.835, p=.023) in female patients.
Masahiro Hoshino et al. 2020	10.1016/j.jcct.2020.02.002	Cross-sectional, N=187, only the LAD was analyzed	To investigate the association between FAI and whole vessel and lesion plaque quantification in stable patients with intermediate epicardial stenosis evaluated by FFR.	*Scanner:* Unknown *Software:* Aquarius iNtuition Edition version 4.4.13. P3; TeraRecon Inc.	Age, male sex, diameter stenosis, lesion length, V/M, whole vessel mass volume, LAP, FFNC at MLA, plaque burden, MLA, plaque eccentricity, FAI > -70.94	- Multivariable analysis: FAI and MLA were independent predictors of FFR≤0.64. - FAI was independently predictive for FFR ≤0.64, FFR < 0.75, but not for FFR≤0.80 in the multivariable model. - Male, positive remodelling (remodelling index > 1.05), lower MLA, higher whole target vessel total cardiac mass, and lower FFR were independent predictors of FAI values in the multivariable analysis.
Sarah Honold et al., 2021	10.1016/j.ejrad.2021.109531	Longitudinal, N=120, PCAT was measured within a 5 mm radius	To evaluate whether a change of coronary plaques is directly associated with alterations of the epicardial adipose tissue composition with serial cardiac CTs.	*Scanner:* 28-slice DSCT Definition FLASH, Siemens or 64-slice CTA Somatom, Siemens *Software:* AW Server 3.2, General Electric	Age, BMI	- Plaque analysis showed a mean plaque regression of -69.4±63.2 mm^3 and a mean progression of 80.2 ±104.3 mm^3. - Total EAT volume: Group with CAD regression: decreased by -15.6 ±37.2 mm^3. Stable group: increased by 2.7 ±30.6 mm^3. Progressive CAD group by 24.3 ±37.1 mm^3 (p=.003). - Per-vessel analysis: stable CAD (1.2±9.1 HU) and CAD progressive patients (3.5±8.2 HU, p<.0001): significant decrease of perivascular EAT. - Epicardial sulcus fat volume: similar change in patients with atherosclerosis decrease (-2.8±5.0 cm^3) compared with stable (-0.8±4.5 cm^3) and increase (2.9±6.3 cm3, p =.002).
Evangelos Tzolos et al. 2021	10.1016/j.jcct.2020.03.007	Cross-sectional, N=50	Repeatability of quantitative PCAT attenuation and coronary plaque burden from CCTA.	*Scanner:* 64- detector row scanner Brilliance 64, Philips Medical Systems *Software:* Autoplaque 2.5	None	- Intraobserver mean differences in PCAT attenuation and NCP plaque burden: -0.05 HU and 0.92% with LOA of ± 1.54 and ± 5.97%. - Intraobserver ICC for PCAT attenuation and NCP burden: 0.999 and 0.978 respectively. - Interobserver mean differences in PCAT attenuation and NCP plaque burden: 0.13 HU [LOA ± 1.67HU] and −0.23% (LOA±9.61%). - Interobserver ICC values for PCAT attenuation and NCP burden: 0.998 and 0.944 respectively.

Didi Wen, 2021	10.1016/j.ejrad.2021.109740	Cross-sectional, N=61	To investigate the diagnostic abilities of both PCAT CT attenuation and volume for the predication hemodynamic significance of coronary artery stenosis as evaluated by FFR.	*Scanner:* 128-slice DSCT Somatom Definition Flash, Siemens Healthcare, *Software:* ITK-SNAP	None	- PCAT CT attenuation and FFR: strong correlation (r=0.64 p<.001). - PCAT CT attenuation in the coronary arteries with FFR≤0.8: (-65.6±5.9 HU) significantly higher than those with FFR>0.8 (-75.3±5.4 HU, p=.0001). - PCAT volume in the coronary arteries with FFR≤0.8 (5.0±3.5 cm^3) and FFR>0.8 (5.5±3.7 cm^3, p=.511): no significant difference - PCAT CT attenuation and diameter stenosis: <50 % and ≥50 % (-73.6±5.8 HU vs. -68.9±7.7 HU, p=.005: significant difference. - Adding PCAT CT attenuation to CCTA significantly improved the specificity (34/37, 91.9 %, p=0.023).
Maria Cristina Pasqualetto, 2021	10.1016/j.ijcard.2021.05.040	Cross-sectional, N=202 only LAD was analyzed, subjects were divided into groups by CFVR-lad quartiles	To evaluate the relationship between coronary inflammation measured by PCAT CT attenuation and coronary microvascular function measured by CFVR-lad on SE in subjects with no or mild-to-moderate obstructive CAD on the LAD.	*Scanner:* DSCT system Somatom Definition FLASH, Siemens Healthcare, *Software:* Aquarius Workstation®V.4.4.13, TeraRecon Inc.	Age, sex, hypertension, hyperlipidemia, diabetes, smoking, obesity	- PCAT values among the groups showed a statistically significant difference among CFVR-lad groups (p<.001). - The relationship between PCAT and CFVR-lad showed a significant, and inverse relationship between the two variables in all groups (r=−0.32, p<.001).
Pepijn A van Diemen, 2021	10.1016/j.jcmg.2021.02.026	Cross-sectional, N=539	To assess the prognostic value of PCAT attenuation beyond quantitative CCTA–derived plaque volume and PET determined ischemia.	*Scanner:* 256-slice Brilliance iCT-scanner, Philips Healthcare *Software:* Comprehensive Cardiac Analysis, Philips Healthcare	Age, male sex, BMI, smoking, hypertension, diabetes, hyperlipidemia, family history of CAD, early revascularization, inactive on ischemia on PET, CAC score >59 AU, obstructive CAD, HRP, TPV >220 mm^3, CPV >110 mm^3, NCPV >85 mm^3, RCA PCAT attenuation above	- Among the three main coronary arteries only RCA PCAT attenuation (above scanner specific thresholds) was associated with worse prognosis (unadjusted HR: 2.84; 95% CI [1.44-5.63]; p =.003). - RCA PCAT attenuation remained prognostic after adjustment for imaging variables and clinical characteristics (adjusted HR: 2.45; 95% CI [1.23-4.93]; p=.011).

					scanner specific threshold		
Markus Goeller et al. 2021	10.1016/j.jcct.2021.03.005	Longitudinal, N=293	To investigate the association between RCA mean PCAT CT attenuation and different grades of coronary calcification, serum levels of atherosclerosis-relevant inflammatory and anti-inflammatory mediators and MACE.	*Scanner:* SOMATOM Sensation® 64 or SOMATOM Definition, Siemens Healthineers, *Software:* Autoplaque version 2.5,	In terms of MACE: age, gender, obstructive coronary stenosis and coronary calcium score, the highest quartile of RCA PCAT CT attenuation	- With increased RCA PCAT attenuation the serum levels of MCP-1 were increased ($p<0.01$), while anti-inflammatory mediator levels IL-4, IL-13 were significantly reduced (each $p<.05$). - Adipocytokine MCP-1 ($r=0.23$, $p<.01$) and pro-inflammatory mediator IL-7 ($r=0.12$, $p=.04$) showed a mild positive correlation with RCA PCAT attenuation, whereas anti-inflammatory mediators IL-4, -10 and -13 correlated inversely (each $r<-0.12$, each $p<0.05$). - RCA PCAT attenuation is an independent predictor of MACE (HR 2.01, $p=.044$).

The table represents a systematic search for original research articles, published until December 2021. The investigation was performed in several electronic databases (PubMed, Scopus, Medline, Embase, Web of Science, The Cochrane Library and ProQuest). MeSH terms and free text words in English were used: pericoronary adipose tissue, fat attenuation index, volumetric perivascular characterization index, coronary CT angiography.

Abbreviations: ^{18}F-NaF: ^{18}F-sodium fluoride, ACS: acute coronary syndrome, AU: Agatston-unit, AUC: area under the curve BMI: body mass index, BSA: body surface index, EAT: epicardial adipose tissue, CAD: coronary artery disease, CAC: coronary artery calcium, CCS: coronary calcium score, CFVR-lad: coronary flow velocity reserve on the left anterior descending coronary artery; CI: confidence interval, CK-MB: creatine kinase myocardial band, CP: calcified plaque, CPV/NCPV: calcified/noncalcified plaque volume, CRP: C-reactive protein, CCTA: coronary CT angiography, CVD: cardiovascular disease, DSCT: dual source CT, EF: ejection fraction, FFR: fractional flow reserve, GFR: estimated glomerular filtration rate, FAI: fat attenuation index, FFNC: fibrofatty and necrotic core component area, g-CFR: global coronary flow reserve, GRACE score: Global Registry of Acute Coronary Events score, $HbA1_C$: hemoglobin A 1c, HR: hazard ratio, HRP: high risk plaque, HU: Hounsfield Unit, HDL-cholesterol: high-density lipoprotein cholesterol, hs-CRP: high sensitivity CRP, ICC: intraclass correlation coefficients, IL: interleukin, IQR: interquartile range, IVUS: intravascular ultrasound, LAD: left anterior descending artery, LAP: low attenuation plaque, LD-NCP: low-density, non-calcified plaque, LCX: left circumflex artery, LDL-

cholesterol: low-density lipoprotein cholesterol, LM: left main, LVMI: left ventricular mass index, LOA: limits of agreement, MACE: major adverse cardiovascular event, MCP-1: monocyte chemoattractant protein-1, MINOCA: myocardial infarction with nonobstructive coronary arteries MLA: minimum lumen area, NCP: non-calcified plaque, NRS: napkin-ring sign, NT-proBNP: N-terminal prohormone of brain natriuretic peptide, PASI: Psoriasis Area and Severity Index, PCAT: pericoronary adipose tissue, PDG: pericardial CT density gradient, NSTEMI: non-ST segment elevation infarction, PET: positron emission tomography PFI: pericoronary fat inflammation index, PVAT: perivascular adipose tissue, RCA: right coronary artery, SE: stress echocardiography; TBR: target-to-background ratios, TIMI: thrombolysis in myocardial infarction, TP: total plaque, TPV: total plaque volume, TTS: Tako-Tsubo syndrome, V/M: Target vessel lumen volume/target vessel myocardial mass

DOI:10.14753/SE.2024.2997

Supplementary Table 2. The relationship between clinical characteristics, CCTA acquisition parameters, coronary artery disease characteristics and PCAT attenuation in the zero calcium score group without any CAD (85).

Predictors	Zero calcium score group without any CAD (n=1003)					
	Univariable model			Multivariable model		
	HU	95% CI	p	HU	95% CI	p
Clinical characteristics						
Age [y]	0.1	[0.03; 0.13]	**0.004**	0.0	[-0.1; 0.0]	0.62
Male sex	1.8	[0.6; 3.0]	**0.003**	1.2	[0.01; 2.37]	**0.04**
BMI [kg/m^2]	0.04	[-0.1; 0.2]	0.44	-0.4	[-0.6; -0.3]	**<0.001**
Hypertension [mmHg]	1.0	[-0.2; 2.2]	0.11	0.5	[-0.7; 1.6]	0.44
Diabetes	0.2	[-2.3; 2.7]	0.88	0.0	[-2.3; 2.3]	0.99
Dyslipidemia	0.4	[-0.9; 1.8]	0.52	-0.1	[-139; 1.2]	0.92
Smoking	0.9	[-0.8; 2.5]	0.32	0.5	[-1.0; 2.0]	0.49
CCTA acquisition parameters						
Non-sinus rhythm	2.7	[-0.9; 6.4]	0.14	3.3	[-0.2; 6.7]	0.06
Heart rate [beats/minute]	-0.2	[-0.2; -0.1]	**<0.001**	-0.1	[-0.2; -0.1]	**<0.001**
Poor image quality	-3.1	[-5.3; -0.9]	**0.005**	-1.6	[-3.8; 0.5]	0.13
Tube voltage 120 kVp	5.9	[4.7; 7.0]	**<0.001**	7.7	[6.4; 9.0]	**<0.001**
Tube current [mAs]	-0.01	[-0.03; 0.00]	0.06	0.0	[-0.03; -0.01]	**0.005**
CNR	-0.01	[-0.08; 0.06]	0.84	-1.2	[-1.7; -0.8]	**<0.001**
SNR	0.02	[-0.06; 0.09]	0.67	1.2	[0.7; 1.7]	**<0.001**
Pixel Spacing [mm^3]	36.4	[25.9; 47.0]	**<0.001**	36.9	[26.9; 47.0]	**<0.001**

Univariable and multivariable linear regression models demonstrating the effects of clinical characteristics, CTA acquisition setting and CAD characteristics on PCAT attenuation. Significant predictors are marked in bold. All variables were entered into the multivariable models.

Abbreviations: BMI: body mass index, CAD: coronary artery disease, CNR: contrast to noise ratio, CTA: coronary CT angiography, HRP: High-risk plaque, kVp: kilovoltage peak, mAs: milliampere-second, PCAT: pericoronary adipose tissue, SIS: Segment involvement score, SNR: Signal to noise ratio, SSS: Segment Stenosis Score.

DOI:10.14753/SE.2024.2997

Supplementary Table 3. The relationship between clinical characteristics, CCTA acquisition parameters, coronary artery disease characteristics and PCAT gradient in the zero calcium score group without any CAD (85).

Predictors	Zero calcium score group without any CAD (n=1003)					
	Univariable model			Multivariable model		
	%	95% CI	p	%	95% CI	p
Clinical characteristics						
Age [y]	0.1	[0.1; 0.2]	**<0.001**	0.1	[0.1; 0.2]	**<0.001**
Male sex	2.6	[1.2; 4.1]	**<0.001**	3.0	[1.5; 4.6]	**<0.001**
BMI [kg/m^2]	0.4	[0.2; 0.5]	**<0.001**	0.03	[-0.22; 0.16]	0.78
Hypertension [mmHg]	1.8	[0.4; 3.3]	**0.01**	-0.1	[-1.5; 1.4]	0.94
Diabetes	1.7	[-1.4; 4.7]	0.29	0.5	[-2.5; 3.5]	0.74
Dyslipidemia	1.6	[0.1; 3.3]	**0.048**	0.4	[-1.2; 2]	0.61
Smoking	1.4	[-0.6; 3.5]	0.18	1.5	[-0.4; 3.5]	0.12
CCTA acquisition parameters						
Non-sinus rhythm	6.4	[1.9; 10.9]	**0.005**	6.2	[1.8; 10.6]	**0.006**
Heart rate [beats/minute]	-0.1	[-0.1; 0.0]	0.25	0.0	[-0.1; 0.1]	0.46
Poor image quality	-2.1	[-4.7; 0.6]	0.13	-2.1	[-4.9; 0.6]	0.13
Tube voltage 120 kVp	5.0	[3.6; 6.4]	**<0.001**	3.6	[1.9; 5.2]	**<0.001**
Tube current [mAs]	-0.01	[-0.2; 0.1]	0.30	-0.03	[-0.05; -0.01]	**<0.001**
CNR	-0.2	[-0.3; -0.1]	**<0.001**	-1.5	[-2.0; -0.9]	**<0.001**
SNR	-0.2	[-0.3; -0.1]	**<0.001**	1.4	[0.8; 2.0]	**<0.001**
Pixel Spacing [mm^3]	42.7	[29.7; 55.8]	**<0.001**	35.5	[22.7; 48.4]	**<0.001**

Univariable and multivariable linear regression models demonstrating the effects of clinical characteristics, CTA acquisition setting and CAD characteristics on PCAT gradient. Significant predictors are marked in bold. All variables were entered into the multivariable models.

Abbreviations: BMI: body mass index, CAD: coronary artery disease, CNR: contrast to noise ratio, CTA: coronary CT angiography, HRP: High-risk plaque, kVp: kilovoltage peak, mAs: milliampere-second, PCAT: pericoronary adipose tissue, SIS: Segment involvement score, SNR: Signal to noise ratio, SSS: Segment Stenosis Score.

DOI:10.14753/SE.2024.2997
Journal of Cardiovascular Computed Tomography 17 (2023) 34–42

Contents lists available at ScienceDirect

Journal of Cardiovascular Computed Tomography

journal homepage: www.JournalofCardiovascularCT.com

Research paper

The effect of patient and imaging characteristics on coronary CT angiography assessed pericoronary adipose tissue attenuation and gradient

Melinda Boussoussou [a], Borbála Vattay [a], Bálint Szilveszter [a], Judit Simon [b], Andrew Lin [c], Milán Vecsey-Nagy [a], Gábor Konkoly [a], Béla Merkely [a], Pál Maurovich-Horvat [a,b], Damini Dey [c], Márton Kolossváry [d,a,*]

[a] Semmelweis University Heart and Vascular Center, 1122 Budapest, Városmajor street 68., Hungary
[b] Semmelweis University Medical Imaging Center, 1082 Budapest, Korányi Sándor street 2., Hungary
[c] Cedars-Sinai Medical Center, 8700 Beverly Blvd #2900A, Los Angeles, CA, 90048, USA
[d] Cardiovascular Imaging Research Center, Massachusetts General Hospital, Harvard Medical School, Boston, MA, USA

ARTICLE INFO

Keywords:
Imaging biomarker
Pericoronary adipose tissue
Fat attenuation index
Volumetric perivascular characterization index
Coronary CT angiography

ABSTRACT

Background: Coronary CT angiography (CCTA) pericoronary adipose tissue (PCAT) markers are promising indicators of inflammation.
Objective: To determine the effect of patient and imaging parameters on the associations between non-calcified plaque (NCP) and PCAT attenuation and gradient.
Methods: This was a single-center, retrospective analysis of consecutive patients with stable chest pain who underwent CCTA and had zero calcium scores. CCTA images were evaluated for the presence of NCP, obstructive stenosis, segment stenosis and involvement score (SSS, SIS), and high-risk plaque (HRP). PCAT markers were assessed using semi-automated software. Uni- and multivariable regression models correcting for patient and imaging characteristics between plaque and PCAT markers were evaluated.
Results: Overall, 1652 patients had zero calcium score (mean age: 51 years ± 11 [SD], 871 women); PCAT attenuation values ranged between −123 HU and −51 HU, and 649 patients had plaque. In univariable analysis, the presence of NCP, SSS, SIS, and HRP were associated with PCAT attenuation (2, 1, 1, 6 HU; respectively; $p < .001$ all); while obstructive stenosis was not (1 HU, $p = .58$). In multivariable analysis, none of the plaque markers were associated with PCAT attenuation (0 HU $p = .93$, 0 HU $p = .39$, 1 HU $p = .18$, 2 HU $p = .10$, 1 HU $p = .71$, respectively), while patient and imaging characteristics showed significant associations, such as: male sex (1 HU, $p = .003$), heart rate [1/min] (−0.2 HU, $p < .001$), 120 kVp (8 HU, $p < .001$) and pixel spacing [mm^3] (32 HU, $p < .001$). Similar results were observed for PCAT gradient.
Conclusion: PCAT markers were significantly associated with NCP, however the associations did not persist following correction for patient and imaging characteristics.

1. Introduction

Conventional cardiovascular risk factors (e.g.: age, hyperlipidemia, smoking) only account for a portion of cardiovascular risk.[1,2] This residual cardiovascular risk stimulates the search for markers capable of identifying patients susceptible to major adverse cardiac events. Imaging is a noninvasive alternative to blood-based markers for detecting pathological changes indicative of diseases.[3,4] Coronary CT angiography (CCTA), a noninvasive imaging modality, provides information regarding luminal stenosis, plaque structure, and the surrounding pericoronary adipose tissue (PCAT).[5]

Inflammation is increasingly being recognized as an equally important pathological mechanism next to lipoprotein accumulation and endothelial dysfunction to promote coronary artery disease (CAD).[5,6] Recently, PCAT assessed using CCTA has been identified as a surrogate marker of inflammation.[7] Inflammation inhibits local adipogenesis,

Abbreviations: CAD, coronary artery disease; CCTA, coronary CT angiography; HU, Hounsfield unit; NCP, non-calcified plaque; PCAT, pericoronary adipose tissue; SIS, segment involvement score; SSS, segment stenosis score.

* Corresponding author.
E-mail address: mkolossvary@mgh.harvard.edu (M. Kolossváry).

https://doi.org/10.1016/j.jcct.2022.09.006
Received 27 July 2022; Received in revised form 24 August 2022; Accepted 30 September 2022
Available online 5 October 2022

leading to smaller adipocytes with lower intracellular lipid content. This in turn results in higher Hounsfield unit (HU) values of PCAT on CCTA,[5] which can be captured by PCAT markers (PCAT attenuation and PCAT gradient). Mean PCAT attenuation is the average HU within radial distance of the vessel within the range of −190- and −30 HU, while PCAT gradient is defined as the relative change in PCAT HU values perpendicular to the vessel.[5] PCAT attenuation was developed to describe adipocyte and lipid content while PCAT gradient provides additional information regarding local stimuli and is superior in identifying non-calcified plaque (NCP) as compared to PCAT attenuation.[5] PCAT attenuation is correlated with 18F-sodium fluoride uptake on PET CT,[8] and associations were also found between PCAT attenuation and patients with any plaque versus patients with no plaque.[9] Based on these findings, PCAT markers may be used to differentiate between stages and characteristics of CAD. However, reported changes in PCAT metrics between patient groups are subtle (Supplementary table 1), and may be affected by patient and image acquisition characteristics.

Coronary calcium score is a well-established independent risk marker for major adverse cardiac events.[10] A zero calcium score is an indicator of low cardiovascular risk. However, even in these patients, there is a considerable prevalence and progression of NCP.[11,12] This NCP is commonly considered a result of inflammation and a more vulnerable phenotype than calcified plaque.[13]

Our aim was 1) to evaluate the associations between CAD markers (presence of plaque, presence of obstructive stenosis, segment stenosis score [SSS], segment involvement score [SIS], presence of high-risk plaque) and PCAT attenuation and gradient in patients with a low cardiovascular risk (calcium score = 0); 2) to evaluate to what degree patient and imaging characteristics influence PCAT markers; 3) to assess whether potential associations between NCP and PCAT markers persisted after correcting for patient and imaging characteristics; 4) to validate our findings in a cohort of individuals with zero calcium scores but imaged using a different CT scanner, and on a group of patients with moderate to severe stenosis on CCTA.

2. Materials and methods

2.1. Patients

In our single-center, retrospective, observational study done at a university teaching hospital, 4120 consecutive patients underwent CCTA between April 2016 and August 2019 for the assessment of stable chest pain. In a previous analysis of these patients, we examined the effect of clinical characteristics, image acquisition, and calcium score values on additional testing following CCTA.[14] In the current sub-analysis, only individuals who had a calcium score of zero were included (Zero calcium score group; n = 1652), which is an established indicator of low cardiovascular risk.

Our study inclusion criteria were 1) patients with suitable image quality for PCAT analysis and 2) zero calcium score on non-contrast CT images. Exclusion criteria were 1) images not accessible from the clinical PACS system, 2) poor image quality evaluated by a consensus read of BM and VB, both with 3 years of experience in CCTA, 3) CCTA acquired at a tube voltage other than 100 or 120 kVp (only a minority of CCTA were performed at 80 or 140 kVp), 4) prior known CAD.

2.2. Validation groups

To validate our findings, we retrospectively identified two additional validation groups consisting of 330 individuals each (20% of the Zero calcium score group, respectively). The first validation group (Zero calcium score group – different scanner; n = 330) consisted of individuals with identical inclusion and exclusion criteria but scanned using another scanner (CardioGraphe, GE Healthcare). The second validation (Moderate to severe CAD group; n = 330) group consisted of patients scanned on the same scanner as the main study group (Brilliance iCT 256, Philips Healthcare) but with moderate to severe (50–99%) stenosis.

2.3. Sensitivity analysis

To assess whether our findings regarding the association between patient and imaging characteristics and PCAT markers are true in individuals without any CAD, we conducted a sensitivity analysis in individuals from our main study group with zero calcium scores and no NCP.

2.4. Coronary CTA acquisition, plaque characterization, and image quality assessment

Details are provided in supplemental material. In brief, for CCTA data sets acquired using the Philips scanner, 0.8-mm section thickness and 0.4-mm spacing between the sections was used, while for the CardioGraphe 0.5-mm section thickness with continuous sections was reconstructed to a 512x512 matrix with varying field of views optimized cardiac evaluation. High-risk plaque features were defined as low-attenuation plaque, positive remodeling, spotty calcification, and napkin-ring sign using standard definitions.[15] An atherosclerotic lesion was identified as high-risk plaque when two or more high-risk plaque features were present.[13]

2.5. PCAT analysis

PCAT analysis was performed around the proximal segment of the right coronary artery using AutoPlaque (version 2.0, Cedars-Sinai Medical Center), as previously described.[8,16] PCAT analysis was performed in the 40 mm proximal RCA segment following the first 10 mm from the RCA ostium as a standardized model for the analysis of PCAT.[5,7,17] Adipose tissue is defined as voxels with HU values between −190 HU and −30 HU, therefore all PCAT markers were calculated after removing all voxels with values below or above these thresholds.[5] PCAT attenuation was defined as the average HU attenuation within a radial distance from the outer coronary artery wall equal to the average diameter of the vessel.[5] Given the average radius of the right coronary artery was 3.4 ± 0.3 mm in the zero calcium score group, PCAT attenuation was uniformly calculated using a 3-mm radial distance from the vessel wall for all individuals.[5,18,19] PCAT gradient was calculated as the percentage change in PCAT attenuation when comparing HU values within the 3 mm radius as described above to non-PCAT HU values at a 20 mm distance from the outer vessel wall, defined as: = 100%*(PCAT attenuation - non-PCAT attenuation)/|PCAT attenuation|.[5] All measurements were done blinded to all clinical data by BM and VB, both with 3 years of experience in coronary CTA.

2.6. Article search for PCAT manuscripts

We performed systematic search for original research article published until December 2021 to provide an overview of the effect sizes reported in the literature for PCAT markers. The search was performed in several electronic databases (PubMed, Scopus, Medline, Embase, Web of Science, The Cochrane Library and ProQuest). The following MeSH terms and free text words were used: pericoronary adipose tissue, fat attenuation index, volumetric perivascular characterization index, coronary CT angiography, to identify articles regarding PCAT. The data is reported in Supplementary table 1.

2.7. Cardiovascular outcome analysis

All patients were followed up using the Hungarian Myocardial Infarction registry to ascertain whether they experienced an acute

myocardial infarction following the CT examination.[20,21] The registry is continuously checked and validated by dedicated personnel resulting in more than 92% of events being registered as compared to the national healthcare provider reimbursement dataset.[22]

2.8. Statistical analysis

Continuous variables are presented as mean and standard deviation, while categorical parameters are presented as frequencies with percentages. We used linear regression models to identify clinical, imaging and CAD predictors of PCAT attenuation and PCAT gradient. We built multivariable models including all predictors into the regression model. Due to the limited number of events, survival analyses were not done. All analyses were conducted in R environment (v4.0.2). A $p < .05$ was considered significant.

The institutional review board approved our study protocol. Due to the retrospective nature of our analysis, written informed consent was waived. All procedures used in this study were in accordance with the Health Insurance Portability and Accountability Act, local and federal regulations, and the Declaration of Helsinki.

3. Results

3.1. Patient characteristics

3.1.1. Zero calcium score group

Between 2016 and 2019, 4120 consecutive patients underwent CCTA for the assessment of stable chest pain. 1839 patients had a calcium score of zero. From these individuals 187 patients were excluded from the analyses. Overall, we analyzed 1652 patients in the zero calcium score group who met all inclusion and exclusion criteria (Fig. 1). The mean age of patients was 51 ± 11 years, and 871 patients (53%) were female. Overall, 649 (39%) individuals had plaque. Patient characteristics and CCTA findings are summarized in Table 1.

3.1.2. Zero calcium score group – different scanner

Overall, 398 images were screened to have 330 scans suitable for PCAT measurements (Fig. 1). The average age was 52 ± 12 years and 53% (174/330) were males. Altogether, 137 individuals had coronary plaque (Table 1).

3.1.3. Moderate to severe CAD group

Overall, 402 scans were screened to achieve 330 scans suitable for PCAT measurements (Fig. 1). The average age was 63 ± 10 years and 61% (200/330) were males. Per inclusion criteria, everyone had at least one obstructive plaque. In 43 individuals (13%) there was at least one high risk plaque (Table 1).

3.2. Predictors of PCAT attenuation in the zero calcium score group

The PCAT attenuation values ranged between −123 HU and −51 HU in individuals with a calcium score of zero. Average PCAT attenuation was −92 ± 9 HU, while the median value was: −93 HU (25th percentile: −99 HU; 75th percentile: −87 HU). Among the 1003 individuals who had zero calcium score and no plaque, PCAT attenuation ranged between: −123 HU and −51 HU; the average was: −93 ± 9 HU, and the median was: −94 HU (25th percentile: −100 HU; 75th percentile: −88 HU).

3.2.1. Univariable analysis

Based on the univariable analyses, among CAD characteristics, the presence of NCP, SSS, SIS, and high-risk plaque were associated with an increasing PCAT attenuation (2, 1, 1, 6 HU respectively; $p < .001$ for all), while presence of obstructive stenosis showed no evidence of an association (1 HU, $p = .58$). Detailed results are shown in Table 2.

3.2.2. Multivariable analysis

After correcting for all factors, among clinical characteristics and image acquisition parameters, independently male sex, 120 kVp instead of 100 kVp, signal to noise ratio and pixel spacing were associated with higher PCAT attenuation values (1 HU $p = .003$, 8 HU $p < .001$, 1 HU $p < .001$, 32 HU $p < .001$; respectively). While each kg/m^2 increase in body mass index, beat/minute in heart rate, mAs in tube current, unit in contrast to noise ratio independently decreased PCAT attenuation (−0.4 HU, −0.2 HU, −0.02 HU, −1.3 HU; $p < .001$ for all; respectively). Furthermore, none of the CAD characteristics was associated with PCAT attenuation (presence of NCP (0 HU, $p = .93$) presence of obstructive stenosis (1 HU, $p = .71$), SSS (0 HU, $p = .39$), SIS (1 HU, $p = .18$), high-risk plaque (2 HU, $p = .10$)). Detailed results are presented in Table 2.

3.2.3. Sensitivity analysis

In the 1003 individuals with calcium score of zero and no CAD, in univariable results we found the same patient and image acquisition parameters to be associated with PCAT attenuation as the whole group, except for hypertension and tube current which were non-significant. In multivariable analysis, we found the same patient and imaging characteristics to be significant. Results are presented in Supplementary table 2.

3.3. Predictors of PCAT gradient in the zero calcium score group

The PCAT gradient values ranged between −31% and 75% in individuals with a calcium score of zero. The average PCAT gradient was: −1±12%, while the median value was: −2% (25th percentile: −9%; 75th percentile: 6%).

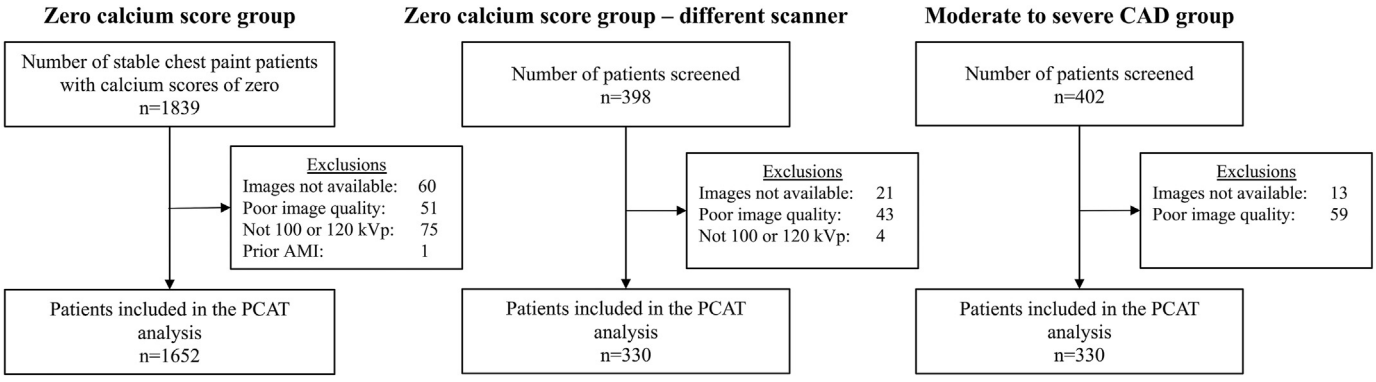

Fig. 1. Patient flow charts of the different study groups. Abbreviations: AMI: acute myocardial infarction, PCAT: pericoronary adipose tissue.

DOI:10.14753/SE.2024.2997 Journal of Cardiovascular Computed Tomography 17 (2023) 34–42

Table 1
Patient characteristics of the study groups.

Parameters	Zero calcium score group n = 1652	Zero calcium score group – different scanner n = 330	Moderate to severe CAD group n = 330
Clinical characteristics			
Age [years]	51 ± 11	52 ± 12	63 ± 10
BMI [kg/m^2]	27.5 ± 5.0	27.5 ± 4.6	28.7 ± 4.5
Male sex n (%)	781 (47)	174 (53)	200 (61)
Hypertension n (%)	753 (46)	170 (52)	242 (73)
Diabetes n (%)	115 (7)	4 (1)	46 (14)
Dyslipidemia n (%)	486 (29)	93 (28)	138 (42)
Smoking n (%)	258 (16)	48 (15)	51 (16)
CCTA acquisition parameters			
CT scanner	Philips - Brilliance iCT 256	GE - CardioGraphe	Philips - Brilliance iCT 256
Heart rate [beats/min]	60 ± 9	65.3 ± 13.0	63 ± 13
Tube voltage [kVp]			
100 kVp n (%)	716 (43)	32 (10)	35 (11)
120 kVp n (%)	936 (57)	298 (90)	295 (89)
Tube current [mAs]	277 ± 37	210 ± 102	255 ± 89
Contrast volume	89 ± 8	85 ± 5	90 ± 8
Radiation dose of CCTA [DLP]	248 ± 78	291 ± 133	329 ± 126
Total effective dose [mSv]	4.2 ± 1.4	4.1 ± 1.9	4.6 ± 1.7
Attenuation parameters			
Aorta SD [HU]	29 ± 8	30 ± 11	33 ± 12
RCA [HU]	577 ± 134	405 ± 92	481 ± 132
CNR	25 ± 8	18 ± 7	19 ± 8
SNR	21 ± 8	15 ± 6	16 ± 7
Coronary artery disease characteristics			
Presence of plaque n (%)	649 (39)	137 (42)	330 (100)
Presence of coronary calcium score n (%)	0 (0)	0 (0)	283 (86)
Coronary calcium [score]	0 ± 0	0 ± 0	296 ± 437
Presence of obstructive stenosis n (%)	15 (1)	3 (1)	330 (100)
SSS [n]	1 ± 2	1 ± 2	9 ± 6
SIS [n]	1 ± 1	1 ± 2	5 ± 3
Presence of HRP n (%)	58 (4)	3 (1)	43 (13)
PCAT analysis			
PCAT attenuation [HU]	−92 ± 9	−77 ± 12	−82 ± 14
PCAT gradient [%]	−1 ± 12	22 ± 20	17 ± 24

Continuous variables are presented as mean (SD), while categorical parameters are counts and percentages.
Abbreviations: BMI: body mass index, coronary, CNR: contrast to noise ratio, CCTA: coronary CT angiography, CV: cardiovascular, GE: General Electric, HU: Hounsfield Unit, HRP: High-risk plaque, kVp: kilovoltage peak, mAs: milliampere-second, PCAT: pericoronary adipose tissue, RCA: right coronary artery, SD: standard deviation, SIS: segment involvement score, SNR: signal to noise ratio, SSS: segment stenosis score.

3.3.1. Univariable analysis

All CAD characteristics were significantly associated with PCAT gradient: presence of NCP (−2% p < .001), presence of obstructive stenosis (8% p = .01), SSS (1% p < .001), SIS (1% p < .001), high-risk plaque (5% p < .001). Detailed results are presented in Table 3.

3.3.2. Multivariable analysis

In multivariable analysis, age (0.1% p < .001), male sex (3% p < .001), non-sinus rhythm (6% p = .01), 120 kVp (4% p < .001), signal to noise ratio (1% p < .001) and pixel spacing (37% p < .001) were all independently associated with higher PCAT gradient values. Also, each beat per minute increase in heart rate (−0.1% p = .02), each increase in mAs (−0.02% p = .003) and contrast to noise ratio (−1% p < .001) was independently associated with lower PCAT gradient values. Furthermore, none of the CAD characteristics showed evidence of an association with PCAT gradient: presence of NCP (0% p = .79), presence of obstructive stenosis (4% p = .28), SSS (0% p = .94), SIS (0% p = .65) and presence of high-risk plaque (2% p = .25). Detailed regression results are presented in Table 3.

3.3.3. Sensitivity analysis

In the individuals with calcium score of zero and no CAD (n = 1003), in univariable analyses we found the same parameters to have a significant association with PCAT gradient as in the whole patient group with zero calcium score, except for poor image quality and heart rate which were non-significant. In multivariable analysis, the same patient characteristics and imaging characteristics were significant, except for heart rate. Results are presented in Supplementary table 3.

3.4. Validation group: zero calcium score group – different scanner

Using a different scanner, PCAT attenuation values were higher compared to the main zero calcium score group (−77 ± 12 vs −92 ± 9, p < .001). The attenuation values ranged between −105 HU and −49 HU, while gradient values ranged between −21% and 90%.

3.4.1. Univariable analysis

In contrast to our main study group, none of the plaque markers were associated with PCAT attenuation (Table 2), while only the presence of plaque was associated with higher PCAT gradient values (5% p = .02; Table 3). However, several patient and imaging characteristics were associated with PCAT HU and gradient similar to our findings in the main zero calcium score group (Tables 2–3).

3.4.2. Multivariable analysis

Similar to our findings in the main study group with zero calcium score, none of the plaque markers were associated with PCAT attenuation or gradient in multivariable analyses. However similarly, several patient and imaging characteristics remained significantly associated with PCAT markers (Tables 2–3).

DOI:10.14753/SE.2024.2997

Table 2
The relationship between clinical characteristics, CCTA acquisition parameters, coronary artery disease characteristics and PCAT attenuation in the different study groups.

Predictors	Zero calcium score group (n = 1652)						Zero calcium score group – different scanner (n = 330)						Moderate to severe CAD group (n = 330)					
	Univariable model			Multivariable model			Univariable model			Multivariable model			Univariable model			Multivariable model		
	HU	95% CI	p	HU	95% CI	p	HU	95% CI	p	HU	95% CI	p	HU	95% CI	p	HU	95% CI	p
Clinical characteristics																		
Age [y]	0.1	[0.0; 0.1]	**.001**	0.0	[-0.1; 0.0]	.23	0.1	[-0.04; 0.2]	.27	0.1	[-0.02; 0.2]	.09	0.01	[-0.1; 0.2]	.84	−0.1	[-0.2; 0.1]	.44
Male sex	2.6	[1.7; 3.5]	**<.001**	1.4	[0.5; 2.3]	**.003**	0.9	[-1.6; 3.5]	.47	2.6	[-0.1; 5.3]	.06	3.0	[0.001; 6.0]	.05	1.1	[-1.6; 3.9]	.41
BMI [kg/m^2]	0.1	[0.0; 0.2]	.14	−0.4	[-0.5; −0.3]	**<.001**	−0.4	[-0.6; −0.1]	**.01**	−0.4	[-0.7; −0.1]	**.01**	−0.3	[-0.6; 0.05]	.09	−0.4	[-0.7; −0.1]	**.02**
Hypertension [mmHg]	1.1	[0.2; 2.0]	**.01**	0.3	[-0.6; 1.1]	.53	0.1	[-2.4; 2.7]	.93	0.6	[-2.1; 3.3]	.67	−0.1	[-3.4; 3.2]	.94	−0.9	[-3.7; 1.9]	.53
Diabetes	0.7	[-1.1; 2.4]	.46	0.7	[-1.0; 2.3]	.42	−1.3	[-13.0; 10.3]	.82	2.4	[-8.8; 13.7]	.67	0.3	[-4.0; 4.5]	.90	−1.4	[-4.9; 2.1]	.42
Dyslipidemia	0.5	[-0.5; 1.5]	.30	0.1	[-0.8; 1.0]	.88	−1.0	[-3.8; 1.8]	.48	−0.7	[-3.5; 2.0]	.61	1.3	[-1.7; 4.2]	.41	2.1	[-0.5; 4.6]	.11
Smoking	0.3	[-0.9; 1.6]	.62	0.1	[-1.0; 1.2]	.92	0.8	[-2.8; 4.4]	.66	1.5	[-1.9; 4.9]	.39	0.1	[-3.9; 4.2]	.95	−0.03	[-3.4; 3.3]	.99
CCTA acquisition parameters																		
Non-sinus rhythm	1.3	[-1.9; 4.4]	.44	2.6	[-0.3; 5.5]	.08	−4.5	[-13.4; 4.3]	.31	4.9	[-4.7; 14.4]	.32	−8.9	[-18.4; 0.6]	.07	0.8	[-8.5; 10.0]	.87
Heart rate [beats/ minute]	−0.2	[-0.3; −0.2]	**<.001**	−0.2	[-0.2; −0.1]	**<.001**	−0.2	[-0.3; −0.1]	**<.001**	−0.2	[-0.3; −0.1]	**<.001**	−0.1	[-0.2; 0.03]	.12	−0.1	[-0.2; 0.1]	.32
Poor image quality	−3.6	[-5.4; −1.8]	**<.001**	−1.3	[-3.0; 0.5]	.15	−7.4	[-11.7; −3.1]	**<.001**	−5.2	[-9.5; −0.9]	**.02**	−5.7	[-11.6; 0.1]	.05	−0.6	[-5.4; 4.2]	.80
Tube voltage 120 kVp	6.2	[5.4; 7.1]	**<.001**	7.7	[6.7; 8.7]	**<.001**	0.2	[-0.1; 0.4]	.14	0.2	[-0.1; 0.4]	.17	0.5	[0.3; 0.7]	**<.001**	0.5	[0.3; 0.7]	**<.001**
Tube current [mAs]	−0.02	[-0.03; −0.004]	**.01**	−0.02	[-0.03; −0.01]	**<.001**	−0.01	[-0.02; −0.0002]	**.04**	−0.01	[-0.02; 0.002]	.12	−0.1	[-0.1; −0.05]	**<.001**	−0.04	[-0.1; −0.02]	**<.001**
CNR	0.0	[-0.1; 0.1]	.94	−1.3	[-1.7; −1.0]	**<.001**	0.4	[0.2; 0.6]	**<.001**	0.3	[-0.8; 1.4]	.59	−0.1	[-0.3; 0.1]	.23	−1.5	[-2.5; −0.5]	**.002**
SNR	0.0	[0.0; 0.1]	.48	1.4	[1.0; 1.7]	**<.001**	0.4	[0.2; 0.6]	**<.001**	0.1	[-1.1; 1.3]	.90	−0.1	[-0.3; 0.2]	.56	1.6	[0.5; 2.7]	**.004**
Pixel Spacing [mm^3]	30.5	[22.5; 38.6]	**<.001**	32.4	[24.9; 39.9]	**<.001**	49.3	[-20.4; 119.1]	.16	80.9	[13.2; 148.5]	**.02**	129.6	[103.5; 155.7]	**<.001**	100.0	[73.9; 126.1]	**<.001**
Coronary artery disease characteristics																		
Presence of plaque	2.3	[1.4; 3.3]	**<.001**	0.1	[-1.2; 1.4]	.93	2	[-0.6; 4.5]	.13	3.6	[-0.2; 7.3]	.06	–	–	–	–	–	–
Presence of obstructive stenosis	1.3	[-3.4; 6.1]	.58	1.1	[-4.5; 6.6]	.71	9.9	[-3.5; 23.3]	.15	13.1	[-2.0; 28.2]	.09	3.5	[-0.2; 7.2]	.06	2.3	[-1.5; 6.2]	.24
SSS [n]	0.6	[0.3; 0.8]	**<.001**	−0.4	[-1.1; 0.4]	.39	−0.1	[-0.7; 0.6]	.88	−0.5	[-2.8; 1.8]	.66	0.5	[0.2; 0.7]	**<.001**	−0.2	[-0.8; 0.3]	.46
SIS [n]	1.0	[0.6; 1.4]	**<.001**	0.8	[-0.4; 2.0]	.18	−0.1	[-0.9; 0.8]	.84	−0.4	[-3.3; 2.4]	.77	1.1	[0.6; 1.6]	**<.001**	0.9	[-0.2; 1.9]	.09
Presence of HRP	5.6	[3.2; 8.1]	**<.001**	1.9	[-0.3; 4.2]	.10	−3.3	[-16.7; 10.1]	.62	−0.2	[-14.0; 13,7]	.98	2.9	[-1.5; 7.2]	.19	3.7	[0.1; 7.2]	**.04**

Univariable and multivariable linear regression models demonstrating the effects of clinical characteristics, CTA acquisition setting and CAD characteristics on PCAT attenuation. Significant predictors are marked in bold. All variables were entered into the multivariable models.

Abbreviations: BMI: body mass index, CNR: contrast to noise ratio, CTA: coronary CT angiography, HRP: High-risk plaque, kVp: kilovoltage peak, mAs: milliampere-second, PCAT: pericoronary adipose tissue, SIS: Segment involvement score, SNR: Signal to noise ratio, SSS: Segment Stenosis Score.

DOI:10.14753/SE.2024.2997

Table 3
The relationship between clinical characteristics, CCTA acquisition parameters, coronary artery disease characteristics and PCAT gradient in the different study groups.

Predictors	Zero calcium score group (n = 1652)						Zero calcium score group – different scanner (n = 330)						Moderate to severe CAD group (n = 330)					
	Univariable model			Multivariable model			Univariable model			Multivariable model			Univariable model			Multivariable model		
	%	95% CI	p	%	95% CI	p	%	95% CI	p	%	95% CI	p	%	95% CI	p	%	95% CI	p
Clinical characteristics																		
Age [y]	0.1	[0.1; 0.2]	**<.001**	0.1	[0.1; 0.2]	**<.001**	0.1	[-0.04; 0.3]	.12	0.2	[0.03; 0.4]	**.03**	0.2	[-0.1; 0.4]	.14	0.1	[-0.2; 0.3]	.47
Male sex	3.1	[2.0; 4.2]	**<.001**	3.1	[1.8; 4.3]	**<.001**	6.8	[2.6; 11.0]	**.002**	9.1	[4.5; 13.7]	**<.001**	5.6	[0.3; 10.9]	**.04**	4.0	[-1.2; 9.1]	.13
BMI [kg/m^2]	0.4	[0.3; 0.5]	**<.001**	−0.1	[-0.2; 0.1]	.38	−0.2	[-0.7; 0.2]	.32	−0.4	[-0.9; 0.03]	.06	−0.1	[-0.7; 0.4]	.63	−0.2	[-0.7; 0.4]	.55
Hypertension [mmHg]	2.2	[1.1; 3.4]	**<.001**	0.2	[-1.0; 1.3]	.78	1.5	[-2.8; 5.7]	.49	−0.1	[-4.7; 4.4]	.96	3.2	[-2.6; 9.1]	.28	0.5	[-4.8; 5.8]	.84
Diabetes	1.6	[-0.6; 3.9]	.16	0.1	[-2.1; 2.2]	.97	−7.6	[-27.0; 11.8]	.44	−4.4	[-23.5; 14.7]	.65	1.2	[-6.3; 8.7]	.76	−3.4	[-9.9; 3.2]	.31
Dyslipidemia	1.8	[0.6; 3.1]	**.004**	0.8	[-0.5; 2.0]	.22	−1.2	[-5.9; 3.5]	.63	−0.4	[-5.1; 4.3]	.85	3.5	[-1.7; 8.8]	.19	3.8	[-0.9; 8.5]	.12
Smoking	0.8	[-0.8; 2.3]	.35	0.9	[-0.6; 2.4]	.25	−1.8	[-7.8; 4.2]	.55	−0.2	[-6.1; 5.6]	.93	−0.1	[-7.3; 7.0]	.97	0.03	[-6.2; 6.2]	.99
CCTA acquisition parameters																		
Non-sinus rhythm	4.8	[0.7; 8.8]	**.02**	5.6	[1.7; 9.5]	**.01**	−5.2	[-19.9; 9.6]	.49	7.7	[-8.5; 23.9]	.35	−17.6	[-34.4; −0.9]	**.04**	−0.8	[-18.1; 16.5]	.93
Heart rate [beats/ minute]	−0.1	[-0.2; −0.1]	**<.001**	−0.1	[-0.15; −0.01]	**.02**	−0.3	[-0.4; −0.1]	**.002**	−0.3	[-0.5; −0.1]	.005	−0.2	[-0.4; −0.012]	**.04**	−0.1	[-0.3; 0.1]	.21
Poor image quality	−3.2	[-5.5; −0.8]	**.008**	−2.2	[-4.5; 0.1]	.07	−10.1	[-17.3; −2.9]	**.01**	−7.8	[-15.1; −0.5]	**.04**	−11.0	[-21.4; −0.7]	**.04**	−2.8	[-11.9; 6.2]	.54
Tube voltage 120 kVp	5.4	[4.3; 6.6]	**<.001**	4.0	[2.7; 5.3]	**<.001**	0.4	[0.02; 0.7]	**.04**	0.3	[-0.1; 0.6]	.19	0.7	[0.2; 1.1]	**.002**	0.4	[0.1; 0.8]	**.02**
Tube current [mAs]	0.0	[0.0; 0.0]	.82	−0.02	[-0.04; −0.01]	**.003**	−0.01	[-0.03; 0.01]	.36	−0.01	[-0.03; 0.01]	.38	−0.1	[-0.1; −0.1]	**<.001**	−0.1	[-0.1; −0.03]	**<.001**
CNR	−0.2	[-0.3; −0.1]	**<.001**	−1.4	[-1.8; −0.9]	**<.001**	0.5	[0.1; 0.8]	**.004**	0.4	[-1.4; 2.2]	.64	−0.2	[-0.5; 0.1]	.26	−2.3	[-4.2; −0.5]	**.01**
SNR	−0.2	[-0.3; −0.1]	**<.001**	1.3	[0.8; 1.8]	**<.001**	0.5	[0.2; 0.9]	**.003**	0.03	[-2.0; 2.0]	.98	−0.1	[-0.5; 0.3]	.57	2.6	[0.5; 4.6]	**.02**
Pixel Spacing [mm^3]	41.1	[30.9; 51.4]	**<.001**	36.5	[26.4; 46.6]	**<.001**	16.1	[-100.6; 132.7]	.79	63.3	[-51.7; 178.2]	.28	211.9	[164.8; 259.0]	**<.001**	157.4	[108.6; 206.1]	**<.001**
Coronary artery disease characteristics																		
Presence of plaque	−2.2	[2.0; 4.4]	**<.001**	0.2	[-1.5; 2.0]	.79	5.3	[1.0; 9.6]	**.02**	5.1	[-1.2; 11.5]	.11	–	–	–	–	–	–
Presence of obstructive stenosis	7.5	[1.5; 13.5]	**.01**	4.0	[-3.4; 11.5]	.28	14.0	[-8.3; 36.4]	.22	8.2	[-17.5; 33.9]	.53	6.4	[-0.1; 13.0]	.05	2.0	[-5.2; 9.2]	.58
SSS [n]	0.9	[0.6; 1.2]	**<.001**	0.0	[-1.0; 1.1]	.94	0.7	[-0.4; 1.8]	.21	0.3	[-3.6; 4.1]	.88	1.0	[0.6; 1.4]	**<.001**	−0.1	[-1.1; 1.0]	.92
SIS [n]	1.4	[0.9; 1.8]	**<.001**	0.4	[-1.2; 2.0]	.65	0.8	[-0.6; 2.2]	.25	−1.5	[-6.3; 3.4]	.56	2.3	[1.5; 3.2]	**<.001**	1.4	[-0.6; 3.3]	.17
Presence of HRP	5.3	[2.2; 8.4]	**<.001**	1.8	[-1.3; 4.9]	.25	10.2	[-12.1; 32.6]	.37	10.0	[-13.5; 33.5]	.40	2.7	[-5.0; 10.4]	.49	3.5	[-3.1; 10.2]	.30

Univariable and multivariable linear regression models demonstrating the effects of clinical characteristics, CTA acquisition setting and CAD characteristics on PCAT gradient. Significant predictors are marked in bold. All variables were entered into the multivariable models.

Abbreviations: BMI: body mass index, CNR: contrast to noise ratio, CTA: coronary CT angiography, HRP: High-risk plaque, kVp: kilovoltage peak, mAs: milliampere-second, PCAT: pericoronary adipose tissue, SIS: Segment involvement score, SNR: signal to noise ratio, SSS: segment stenosis score.

3.5. Validation group: moderate to severe CAD group

PCAT values ranged between −82 HU and −50 HU, while the gradient values ranged between −22% and 116%.

3.5.1. Univariable analysis

Among plaque markers, SSS and SIS were associated with PCAT attenuation (1 HU $p < .001$; 1 HU $p < .001$, respectively). In case of PCAT gradient, similarly only SSS and SIS were significantly associated (1% $p < .001$, 2% $p < .001$, respectively). However, several patient and image acquisition characteristics also showed a significant association with PCAT HU (Table 2) and gradient (Table 3).

3.5.2. Multivariable analysis

After correcting for all patient and image acquisition parameters, only the presence of high risk plaque showed borderline association with PCAT attenuation (4 HU $p = .04$; Table 2), while similar to the main cohort of patients with zero calcium score, none of the plaque markers were associated with PCAT gradient (Table 3). Nevertheless, similarly to the initial cohort, BMI and several image acquisition parameters were associated with PCAT HU (Table 2), while only image acquisition settings showed a significant association with PCAT gradient (Table 3).

Representative images from all three groups showing how different heart rates influence PCAT attenuation and PCAT gradient values are shown in Fig. 2.

3.6. Cardiovascular outcomes

During the average follow-up time of 3.0 years in the zero calcium score group, two individuals suffered acute myocardial infarction, their PCAT attenuation and gradient values were: −93 HU and −79 HU and −1% and 19% respectively. In the validation cohort with zero calcium score scanned on a different scanner, there were no events within the average follow-up time of 0.7 years, while there were 7 events in the moderate to severe CAD group over the average of 2.2 years. Their PCAT attenuation ranged between: −88 HU and −64 HU, while the gradient values were between 7% and 51%.

4. Discussion

PCAT attenuation and gradient are considered markers of perivascular inflammation and have been shown to be associated with several cardiovascular conditions. However, being based on HU values, they are potentially confounded by patient and image acquisition characteristics. In our primary study group of individuals with zero calcium score, we show in 1652 patients that PCAT attenuation and gradient can have a wide range of values. Nevertheless, in our univariable results CAD markers showed associations with PCAT markers. However, many of the patient and imaging parameters such as: male sex, heart rate, tube voltage and current and pixel spacing were also significantly associated with PCAT attenuation. While our univariable results confirm previous associations of PCAT attenuation and gradient with NCP characteristics, these associations did not persist after correcting for patient and image acquisitions parameters, of which many were independently associated with PCAT markers in multivariable analysis. Similar results were observed in individuals imaged on a different CT scanner and also in individuals with moderate to severe CAD.

In a study with in vivo and ex vivo models, Antonopoulos et al. demonstrated phenotypic changes in PCAT, hence in PCAT attenuation values, as a response to vascular inflammation and inflamed vulnerable plaques at the time of a major adverse cardiac event. Strengthening the association between PCAT and inflammation, Goeller et al. found a positive correlation between pro-inflammatory serum markers (MCP-1 and IL-7) and PCAT attenuation and a negative correlation between anti-inflammatory cytokines (IL-4, IL-10, IL-13) and PCAT attenuation,[23] although these correlations were weak (Pearson correlation coefficient range: −0.12 to 0.23). Similarly, PCAT attenuation showed an association with 18F-sodium fluoride uptake on PET-CT imaging in stable patients with high-risk plaque features on CCTA, providing another link with established markers of inflammation.[8] Regarding the association of PCAT attenuation with coronary plaques, Goeller et al. found higher PCAT attenuation values around the culprit lesions as compared with non-culprit lesions in patients with acute coronary syndrome.[16] However, our results indicate that there are certain factors that must be considered before drawing conclusions using PCAT markers.

First, in our study, the patients with a low cardiovascular risk referred for a CCTA demonstrated a large variability of PCAT attenuation and gradient values. A wealth of evidence demonstrates that patients with zero calcium score are at low risk for adverse events.[10,24,25] Therefore, one would expect that the PCAT values would be universally low and exhibit low variability, especially in individuals with zero calcium scores and no plaque. However, PCAT attenuation and PCAT gradient had a wide range of values. This may be mainly due to our second finding that PCAT markers are significantly associated with imaging and patient characteristics. Most prior studies use the original definition of PCAT attenuation (originally called fat attenuation index) based on the study by Antonopoulos et al.,[5] meaning there were no correction factors applied for possible confounding.[9,19] Some studies include only a couple of factors, but the number of variables included in the models varies largely (supplementary table 1).[26–28]

To overcome the aforementioned limitations, instead of adjusting for possible confounders in the statistical models of specific studies, Oikonomou et al. used a modified PCAT attenuation parameter to predict later outcomes in the CRISP CT-study.[17] This corrected differences in HU values between 100 and 120 kVp using a correction factor derived from 17 individuals scanned on a dual-source system by simply dividing the average attenuation of free-hand regions of interest drawn in the pericardial fat on 100 and 120 kVp images (−96.1/-86.2 = 1.11485).[29,30] However, several of the factors that our study found to independently influence PCAT attenuation values were not corrected for, such as heart rate. Furthermore, as such characteristics as heart rate significantly influence PCAT attenuation values beyond image quality parameters (eg. contrast to noise ratio, signal to noise ratio), it seems challenging to establish robust estimates of PCAT attenuation and to determine normal PCAT attenuation and gradient values. Chatterjee et al. proposed correcting PCAT attenuation with adjacent lumen attenuation values to account for variations in image and patient characteristics.[30] Following correction, they did not find any association between PCAT and major adverse cardiovascular events in the CORE320 trial participants. Also, simply using a different CT scanner the average PCAT attenuation was 15 HU higher, while both the main study group and the validation group consisted of individuals with zero calcium score. These results show the need for normalization of images prior to PCAT measurements. Further multi-center efforts are needed using a wide range of patients and imaging machinery to create a diverse database on which the optimal normalization protocols are developed. Conventional statistical and artificial intelligence techniques may help to correct for the possible confounding of these parameters to achieve standardized comparable PCAT measurements that are independent of patient and imaging characteristics. Until then, researchers should use as similar as possible scan characteristics and correct their statistical models for all possible confounders. In case of longitudinal analyses, same scanners and acquisition protocols should be used to minimize bias.

Our study has some limitations. First, our main study group consisted of patients with low cardiovascular risk with zero coronary calcium scores from a single center study scanned using the same CT and similar imaging protocols, which might have resulted in a selection bias. However, we found very similar results in our validation cohorts strengthening our results. Second, only two readers segmented PCAT volumes with a single software, which artificially reduced variation, therefore the results are only generalizable with caution. Third, only one CCTA reconstruction algorithm was used in each group. However,

DOI:10.14753/SE.2024.2997 Journal of Cardiovascular Computed Tomography 17 (2023) 34–42

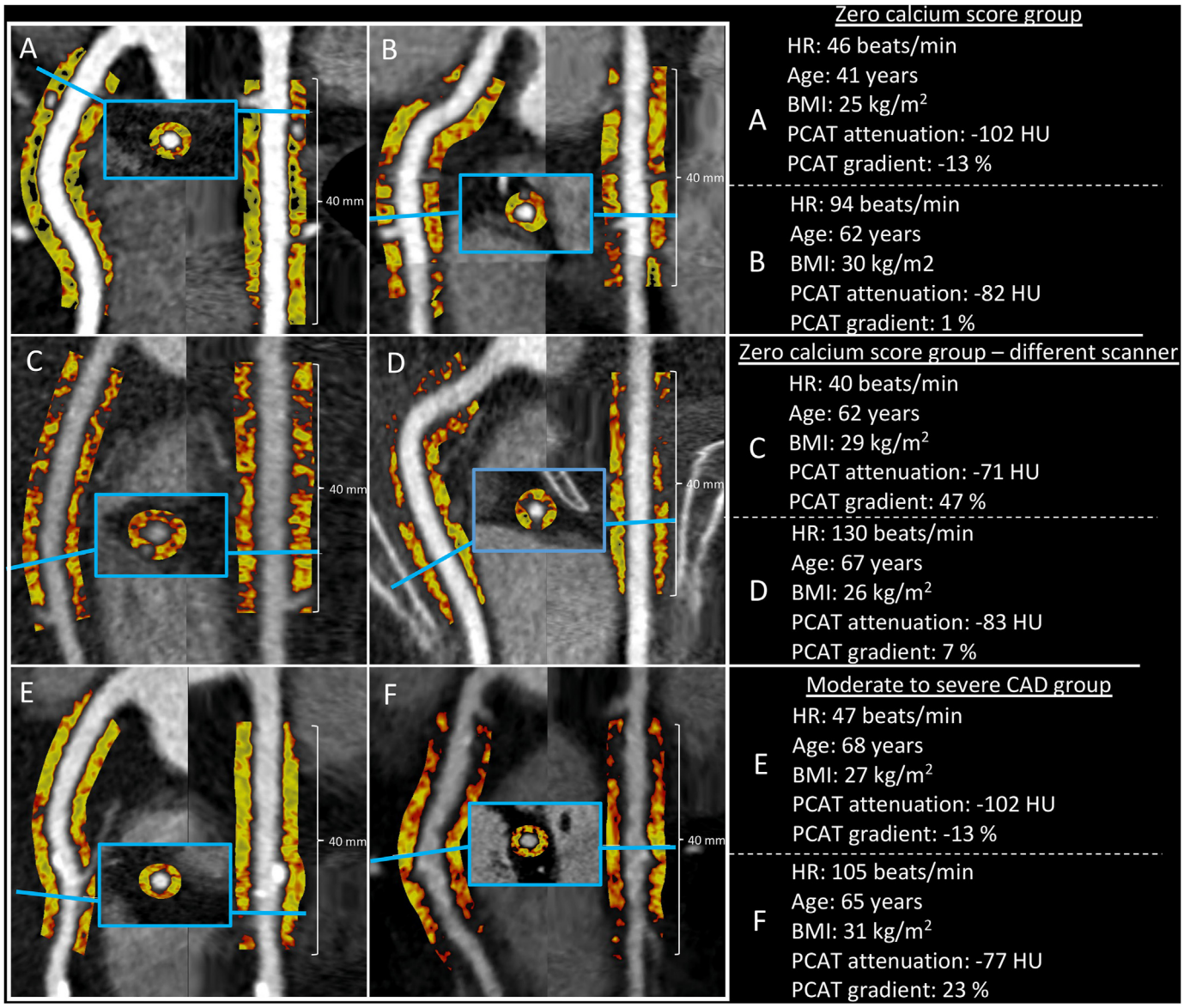

Fig. 2. Representative images showing PCAT attenuation and PCAT gradient differences in patients with different heart rates. Panel A, B show two representative images from the zero calcium score group. Patients were scanned on a Philips - Brilliance iCT 256 and had a calcium score of zero. Panel C, D show two representative cases from the zero calcium score group - different scanner group. Patients were scanned on a GE - CardioGraphe and had a calcium score of zero. Panel E, F show two representative images from the moderate to severe CAD group. Patients were scanned on a Philips - Brilliance iCT 256 and had obstructive CAD. Patients within all three cohorts had a wide range of PCAT attenuation and gradient values. Abbreviations: BMI: body mass index, CAD: coronary artery disease, HR: heart rate, HU: Hounsfield unit, PCAT: pericoronary adipose tissue.

reconstruction algorithms are known to affect HU values thus representing an additional factor which may need to be considered when correcting for confounders when analyzing PCAT. Fourth, our outcome analyses may be underpowered. Nevertheless, in the individuals who experience myocardial infarction, we found a wide range of values. Moreover, other studies have found other factors also to be associated with PCAT markers, therefore our list of potential confounders may not be complete.[31,32]

5. Conclusions

Based on our results, PCAT attenuation and gradient show a wide range of values in individuals with low cardiovascular risk (calcium score = 0). These markers are significantly influenced by different image acquisition and patient characteristics. After correcting for these metrics, associations between PCAT and CAD markers do not persist, highlighting the importance of correcting for all possible confounders before evaluating the additive value of PCAT markers. Future studies extensively correcting for possible confounders are needed to validate the additive value of PCAT measurements.

Funding

Project no. RRF-2.3.1-21-2022-00003 has been implemented with the support provided by the European Union. Project no. NVKP_16-1–2016-0017 ('National Heart Program') has been implemented with the support provided from the National Research, Development and Innovation Fund of Hungary, financed under the NVKP_16 funding scheme. Melinda Boussoussou MD was supported by the ÚNKP-22-3-II-SE (ÚNKP-22-3-II-SE-51), New National Excellence Program of the Ministry for Innovation

and Technology from the source of the National research, Development and Innovation fund and by the EFOP-3.6.3-VEKOP-16-2017-00009 project fund.

Conflicts of interest

None.

Appendix A. Supplementary data

Supplementary data to this article can be found online at https://doi.org/10.1016/j.jcct.2022.09.006.

References

1. Lechner K, von Schacky C, McKenzie AL, et al. Lifestyle factors and high-risk atherosclerosis: pathways and mechanisms beyond traditional risk factors. *Eur J Prev Cardiol*. 2020;27:394–406.
2. Khera AV, Emdin CA, Drake I, et al. Genetic risk, adherence to a healthy lifestyle, and coronary disease. *N Engl J Med*. 2016;375:2349–2358.
3. Hoffmann U, Truong QA. Computed tomography coronary plaque imaging as a secondary end point for randomized pharmaceutical trials. *Circulation: Cardiovascular Imaging*. 2010;3:225–227.
4. deSouza NM, Achten E, Alberich-Bayarri A, et al. Validated imaging biomarkers as decision-making tools in clinical trials and routine practice: current status and recommendations from the EIBALL* subcommittee of the European Society of Radiology (ESR). *Insights into Imaging*. 2019;10:87.
5. Antonopoulos AS, Sanna F, Sabharwal N, et al. Detecting human coronary inflammation by imaging perivascular fat. *Sci Transl Med*. 2017;9.
6. Patel NH, Dey AK, Sorokin AV, et al. Chronic inflammatory diseases and coronary heart disease: insights from cardiovascular CT. *J Cardiovasc Comput Tomogr*. 2022;16:7–18.
7. Goeller M, Tamarappoo BK, Kwan AC, et al. Relationship between changes in pericoronary adipose tissue attenuation and coronary plaque burden quantified from coronary computed tomography angiography. *Eur Heart J Cardiovasc Imaging*. 2019;20:636–643.
8. Kwiecinski J, Dey D, Cadet S, et al. Peri-coronary adipose tissue density is associated with (18)F-sodium fluoride coronary uptake in stable patients with high-risk plaques. *JACC Cardiovasc Imaging*. 2019;12:2000–2010.
9. Goeller M, Rahman Ihdayhid A, Cadet S, et al. Pericoronary adipose tissue and quantitative global non-calcified plaque characteristics from CT angiography do not differ in matched South Asian, East Asian and European-origin Caucasian patients with stable chest pain. *Eur J Radiol*. 2020;125, 108874.
10. Budoff MJ, Shaw LJ, Liu ST, et al. Long-term prognosis associated with coronary calcification: observations from a registry of 25,253 patients. *J Am Coll Cardiol*. 2007;49:1860–1870.
11. Bergström G, Persson M, Adiels M, et al. Prevalence of subclinical coronary artery atherosclerosis in the general population. *Circulation*. 2021;144:916–929.
12. Hollenberg EJ, Lin F, Blaha MJ, et al. Relationship between coronary artery calcium and atherosclerosis progression among patients with suspected coronary artery disease. *JACC Cardiovasc Imaging*. 2022;15:1063–1074.
13. Maurovich-Horvat P, Ferencik M, Voros S, Merkely B, Hoffmann U. Comprehensive plaque assessment by coronary CT angiography. *Nat Rev Cardiol*. 2014;11:390–402.
14. Simon J, Száraz L, Szilveszter B, et al. Calcium scoring: a personalized probability assessment predicts the need for additional or alternative testing to coronary CT angiography. *Eur Radiol*. 2020;30:5499–5506.
15. Shaw LJ, Blankstein R, Bax JJ, et al. Society of cardiovascular computed tomography/north American society of cardiovascular imaging - expert consensus document on coronary CT imaging of atherosclerotic plaque. *J Cardiovasc Comput Tomogr*. 2021;15:93–109.
16. Goeller M, Achenbach S, Cadet S, et al. Pericoronary adipose tissue computed tomography attenuation and high-risk plaque characteristics in acute coronary syndrome compared with stable coronary artery disease. *JAMA Cardiol*. 2018;3:858–863.
17. Oikonomou EK, Marwan M, Desai MY, et al. Non-invasive detection of coronary inflammation using computed tomography and prediction of residual cardiovascular risk (the CRISP CT study): a post-hoc analysis of prospective outcome data. *Lancet*. 2018;392:929–939.
18. Lin A, Kolossvary M, Yuvaraj J, et al. Myocardial infarction associates with a distinct pericoronary adipose tissue radiomic phenotype: a prospective case-control study. *JACC Cardiovasc Imaging*. 2020;13:2371–2383.
19. Tzolos E, McElhinney P, Williams MC, et al. Repeatability of quantitative pericoronary adipose tissue attenuation and coronary plaque burden from coronary CT angiography. *J Cardiovasc Comput Tomogr*. 2021;15:81–84.
20. Janosi A, Ofner P. [National myocardial infarction registry of Hungary]. *Orv Hetil*. 2014;155:740–744.
21. Sinka Laszlone Adamik E, Hari P, Poth A, et al. Quality assurance of national internet-based patient register data: experiences during the operation of the Hungarian Myocardial Infarction Registry, 2010-2020. *Orv Hetil*. 2021;162:61–68.
22. Blondal M, Ainla T, Eha J, et al. Comparison of management and outcomes of ST-segment elevation myocardial infarction patients in Estonia, Hungary, Norway, and Sweden according to national ongoing registries. *Eur Heart J Qual Care Clin Outcomes*. 2022;8:307–314.
23. Goeller M, Achenbach S, Herrmann N, et al. Pericoronary adipose tissue CT attenuation and its association with serum levels of atherosclerosis-relevant inflammatory mediators, coronary calcification and major adverse cardiac events. *J Cardiovasc Comput Tomogr*. 2021;15:449–454.
24. Blaha MJ, Blumenthal RS, Budoff MJ, Nasir K. Understanding the utility of zero coronary calcium as a prognostic test: a Bayesian approach. *Circ Cardiovasc Qual Outcomes*. 2011;4:253–256.
25. Blaha M, Budoff MJ, Shaw LJ, et al. Absence of coronary artery calcification and all-cause mortality. *JACC Cardiovasc Imaging*. 2009;2:692–700.
26. Kanaji Y, Hirano H, Sugiyama T, et al. Pre-percutaneous coronary intervention pericoronary adipose tissue attenuation evaluated by computed tomography predicts global coronary flow reserve after urgent revascularization in patients with non-ST-segment-elevation acute coronary syndrome. *J Am Heart Assoc*. 2020;9, e016504.
27. Hoshino M, Yang S, Sugiyama T, et al. Peri-coronary inflammation is associated with findings on coronary computed tomography angiography and fractional flow reserve. *J Cardiovasc Comput Tomogr*. 2020;14:483–489.
28. Honold S, Wildauer M, Beyer C, et al. Reciprocal communication of pericoronary adipose tissue and coronary atherogenesis. *Eur J Radiol*. 2021;136, 109531.
29. Okayama S, Soeda T, Takami Y, et al. The influence of effective energy on computed tomography number depends on tissue characteristics in monoenergetic cardiac imaging. *Radiol Res Pract*. 2012;2012, 150980.
30. Chatterjee D, Shou BL, Matheson MB, et al. Perivascular fat attenuation for predicting adverse cardiac events in stable patients undergoing invasive coronary angiography. *J Cardiovasc Comput Tomogr*. 2022. online ahead of print.
31. Sugiyama T, Kanaji Y, Hoshino M, et al. Determinants of pericoronary adipose tissue attenuation on computed tomography angiography in coronary artery disease. *J Am Heart Assoc*. 2020;9, e016202.
32. Raggi P, Gadiyaram V, Zhang C, Chen Z, Lopaschuk G, Stillman AE. Statins reduce epicardial adipose tissue attenuation independent of lipid lowering: a potential pleiotropic effect. *J Am Heart Assoc*. 2019;8, e013104.

The International Journal of Cardiovascular Imaging (2022) 38:1601–1611
https://doi.org/10.1007/s10554-022-02533-y

ORIGINAL PAPER

The effect of left atrial wall thickness and pulmonary vein sizes on the acute procedural success of atrial fibrillation ablation

Melinda Boussoussou[1] · Bálint Szilveszter[1] · Borbála Vattay[1] · Márton Kolossváry[1] · Milán Vecsey-Nagy[1] · Zoltán Salló[1] · Gábor Orbán[1] · Perge Péter[1] · Piros Katalin[1] · Nagy Klaudia Vivien[1] · Osztheimer István[1] · Pál Maurovich-Horvat[2] · Béla Merkely[1] · László Gellér[1] · Nándor Szegedi[1]

Received: 27 October 2021 / Accepted: 20 January 2022 / Published online: 9 February 2022

Abstract

Nowadays, a novel contact-force guided ablation technique is used for enclosing pulmonary veins in patients with atrial fibrillation (AF). We sought to determine whether left atrial (LA) wall thickness (LAWT) and pulmonary vein (PV) dimensions, as assessed by cardiac CT, could influence the success rate of first-pass pulmonary vein isolation (PVI). In a single-center, prospective study, we enrolled consecutive patients with symptomatic, drug-refractory AF who underwent initial radiofrequency catheter ablation using a modified CLOSE protocol. Pre-procedural CT was performed in all cases. Additionally, the diameter and area of the PV orifices were obtained. A total of 1034 LAWT measurements and 376 PV area measurements were performed in 94 patients (mean CHA_2DS_2-VASc score 2.1 ± 1.5, mean age 62.4 ± 12.6 years, 39.5% female, 38.3% persistent AF). Mean procedure time was 81.2 ± 19.3 min. Complete isolation of all PVs was achieved in 100% of patients. First-pass isolation rate was 76% and 71% for the right-sided PVs and the left-sided PVs, respectively. No difference was found regarding comorbidities and imaging parameters between those with and without first-pass isolation. LAWT (mean of 11 regions or separately) had no effect on the acute procedural outcome on logistic regression analysis (all $p \geq 0.05$). Out of all assessed parameters, only RSPV diameter was associated with a higher rate of successful right-sided first pass isolation (OR 1.01, $p = 0.04$). Left atrial wall thickness does not have an influence on the acute procedural success of PVI using ablation index and a standardized ablation protocol. RSPV diameter could influence the probability of right sided first-pass isolation.

Keywords Radiofrequency ablation · Pulmonary vein isolation · Atrial fibrillation · Computed tomography · CLOSE protocol · Left atrial wall thickness

Abbreviations

AF	Atrial fibrillation
BMI	Body mass index
CI	Confidence interval
CT	Computed tomography
ICC	Intraclass correlation coefficient
LA	Left atrium
LA-PV	Left atrium-pulmonary vein
LAWT	Left atrial wall thickness
LIPV	Left inferior pulmonary vein
LSPV	Left superior pulmonary vein
PV	Pulmonary vein
PVI	Pulmonary vein isolation
RIPV	Right inferior pulmonary vein
RSPV	Right superior pulmonary vein
SD	Standard deviation
OR	Odds ratio
TIA	Transient ischemic attack

✉ Melinda Boussoussou
melinda.b.md@gmail.com

[1] Semmelweis University Heart and Vascular Center, Városmajor utca 68., Budapest 1122, Hungary

[2] Medical Imaging Centre, Korányi Sándor u. 2., Budapest 1082, Hungary

Introduction

Atrial fibrillation (AF) is the most common sustained cardiac arrhythmia [1], with globally increasing prevalence and incidence. Since triggers of AF originate from the pulmonary veins (PVs), pulmonary vein isolation (PVI) became the backbone of the treatment of AF [2, 3]. The durable isolation of the PVs remains challenging; however, new technologies might facilitate achieving better results [4]. One of

DOI:10.14753/SE.2024.2997

the most recent catheter ablation strategies is the CLOSE protocol, a contact-force-guided approach using contiguous and optimized radiofrequency lesions to enclose pulmonary veins [5–7]. The CLOSE protocol and modified CLOSE protocols [8] were shown to provide excellent procedural outcomes in recent studies evaluating the safety and 1-year single-procedural freedom from AF. Lesion contiguity and consistency are substantial factors of acute procedural success in such procedures. Moreover, the contiguous and durable lesion set might be associated with a higher chance of long-term arrhythmia-free survival [9].

The importance of cardiac CT before AF ablation is unquestionable, as it helps both to the plan of the procedure and to the selection of optimal patients for ablation [10–12]. Left atrial (LA) wall thickness (LAWT) and PV anatomy, assessed by cardiac CT, might influence the efficacy of radiofrequency catheter ablation [9, 13, 14]. It has been suggested that greater local atrial wall thickness could lead to reconnected PVs and thus the CLOSE protocol might need further modifications to create proper LA lesions. However, less advanced ablation strategies were used in those studies, therefore former results may not apply for the latest ablation techniques.

We hypothesised that using a novel, modified CLOSE protocol proper isolation of the PVs is achievable even in patients with larger LAWT. First-pass isolation is a valuable marker of PVI's acute procedural success [15, 16]. The effects of PV anatomy and LAWT on successful first-pass isolation has not yet been investigated. Therefore, our current study aimed to determine the relationship between the acute procedural success assessed by the presence of first-pass isolation and LAWT, measured by cardiac CT. Moreover, we assessed the potential role of PV anatomy in the rate of first-pass isolation.

Methods

Patient population

In our single-center, prospective, observational cohort study, 186 consecutive patients with symptomatic drug-refractory AF were screened who underwent radiofrequency ablation between January of 2019 and September of 2020. Exclusion criteria were previous catheter ablation procedure, absence of pre-procedural LA cardiac CT or poor cardiac CT image quality (Consort diagram: Fig. 1). Overall, we analyzed a total of 94 patients who met all inclusion and exclusion criteria.

All patients agreed to the pre-procedural imaging and the ablation procedure and provided written consent to data retrieval and analysis. The study protocol was reviewed and approved by the institutional review board and was in accordance with the declarations of Helsinki.

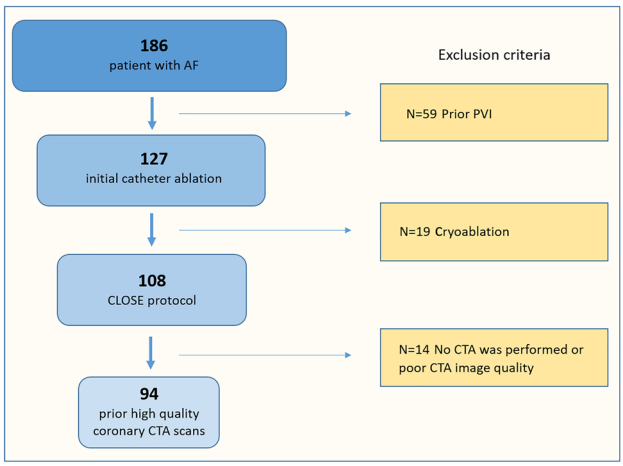

Fig. 1 Patients with atrial fibrillation were enrolled in the study population, between the time interval of 2019 January to 2020 December who underwent PVI using the CLOSE protocol. After excluding cases with cryoablation, prior PVI and suboptimal CT image quality a total of 94 patients were analysed. *AF* atrial fibrillation, *PVI* pulmonary vein isolation

CT imaging of the left atrium and the pulmonary veins

All patients underwent contrast-enhanced multi-detector CT imaging before the catheter ablation procedure to determine the PV and LA anatomy. Cardiac CT scans were performed on a 256-slice scanner (Brilliance iCT 256, Philips Healthcare, Best, The Netherlands) with prospective ECG-triggered axial acquisition mode during inspiratory breath hold and arm raised position. For proper heart-rate control, oral or intravenous beta-blocker was administered before the CT scans in patients with a heart rate above 65 beats per minute. In patients with a heart rate of less than 75 beats per minute, mid-diastolic triggering was applied with 3–5% padding (73–83% of the R–R interval), and in those with ≥ 75 beats per minute, systolic triggering was chosen (35–45% of the R–R interval). Depending on body mass index, 100–120 kV tube voltage and 200–300 mAs tube current were used. Image acquisition was performed with 270-ms gantry rotation time and 128 × 0.625-mm detector collimation. Intravenous iodinated contrast agent (80–100 ml Iomeron 400, Bracco Imaging Ltd.) was administered at a flow rate of 4.5–5.5 ml/s via 18-gauge catheter from antecubital vein access using a four-phasic contrast protocol as described elsewhere [17]. XCC convolution kernel, and iDose level 5 iterative reconstruction were used. CT data sets were reconstructed with 0.8-mm slice thickness and 0.4-mm increment [18].

DOI:10.14753/SE.2024.2997

Image analysis

The measurements of the LAWT and the PVs were carried out by utilizing a commercially available software (Philips IntelliSpace Portal v.6.2, Philips Healthcare). The maximum wall thickness areas were assessed in 11 separate LA locations, including the right, middle and left part of the roof, mid-posterior and infero-posterior regions. Representative images of each location are depicted on Fig. 2. These areas of interest were considered the most commonly targeted locations during catheter ablation procedures of AF [19–25]. In addition, the wall thickness at the left lateral ridge and mitral isthmus were evaluated based on Hayashietal et al. [24]. To measure the roof thickness of the LA, an oblique coronal plane was acquired parallel to the superior PV or posterior wall (Number 1, 4, 7 in Figs. 2 and 3), whereas to measure the mid-posterior and infero-posterior wall (Number 2, 5, 8, 3, 6, 9 in Figs. 2 and 3) an oblique axial plane perpendicular to the posterior LA wall was acquired. The LAWT at the right and left roof and right and left infero-posterior areas were assessed 10 mm away from the LA–PV connection. The wall thickness at the mitral isthmus was measured by obtaining an axial plane that corresponds to Number 10 in Figs. 2 and 3. The LA ridge wall thickness was measured 5 mm inside the center of the left superior PV with an oblique perpendicular plane view to the superior left lateral ridge (Number 11 in Figs. 2 and 3). We calculated mean and maximal LAWT for the left (Number 7–9) and right side (Number 1–3) at the thickest portion of the given segment and for all measured segments.

The PV anatomy and diameter were also analyzed for all patients on the contrast-enhanced cardiac CT images. A normal PV anatomy was defined as the presence of four distinct PVs (e.g. left superior, left inferior, right superior and right inferior pulmonary veins) (Fig. 4). Left or right common trunk was defined when the superior and inferior PVs were connected/fused into one common ostium. First, we selected a given PV orifice and adjusted centerlines manually. The orifices were defined at the angle where the veins departed from the curvature of the LA [26] then we measured the areas and effective diameters perpendicular to the vessel wall based on the maximum and minimum diameter of the orifices [13]. In case of a left or right common trunk the measurements were carried out in the common ostium.

Ablation procedure

Indications for AF ablation procedures and periprocedural anticoagulation were in accordance with the current guideline [27]. PVI was performed with radiofrequency energy, using the point-by-point technique, with the support of the CARTO3 (Biosense Webster, Inc., Baldwin Park, CA, USA) electroanatomical mapping system. The goal of each procedure was the complete electrical isolation of all PVs from the LA with circumferential, contiguous ablation lines. First, a fast anatomical map of the LA was created with a multipolar mapping catheter (Lasso® NAV Eco, Biosense Webster, Inc., Baldwin Park, CA, USA). Then, radiofrequency ablations were applied in a point-by-point manner with ThermoCool SmartTouch® (Biosense Webster, Inc., Baldwin Park, CA, USA) ablation catheter

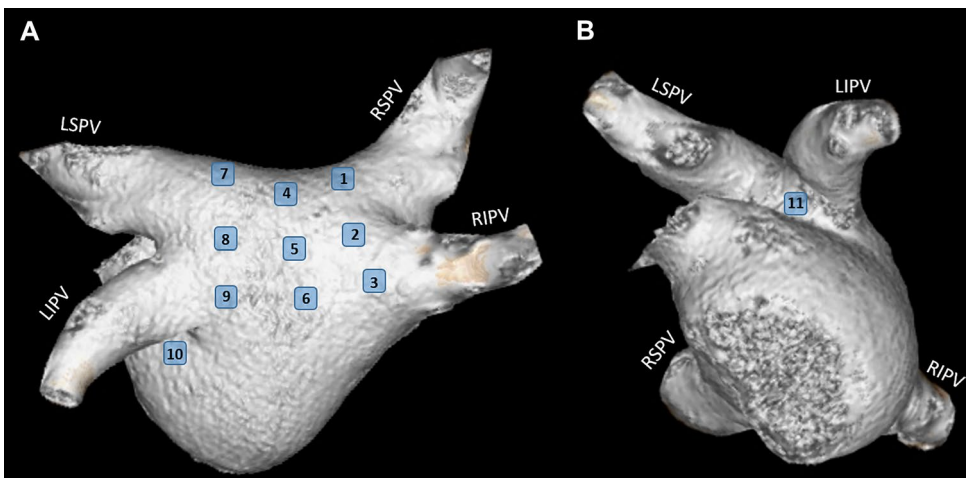

Fig. 2 Volume rendered 3D CT images demonstrate the 11 locations where the wall thickness was measured in the left atrium (modified after Hayashi et al. [24]). On **A** the LA is in a posterior view whereas **B** represents the left lateral view of the LA. The numbers show the following left atrial areas: 1: right roof. 2: right mid-posterior, 3: right infero-posterior, 4: middle part of the roof, 5: middle part of the mid-posterior, 6: middle part of the infero-posterior, 7: left of the roof, 8: left of the mid-posterior, 9: left of the infero-posterior, 10: mitral isthmus, 11: left lateral ridge. *LA* left atrium, *LIPV* left inferior pulmonary vein, *LSPV* left superior pulmonary vein, *RIPV* right inferior pulmonary vein, *RSPV* right superior pulmonary vein

DOI:10.14753/SE.2024.2997

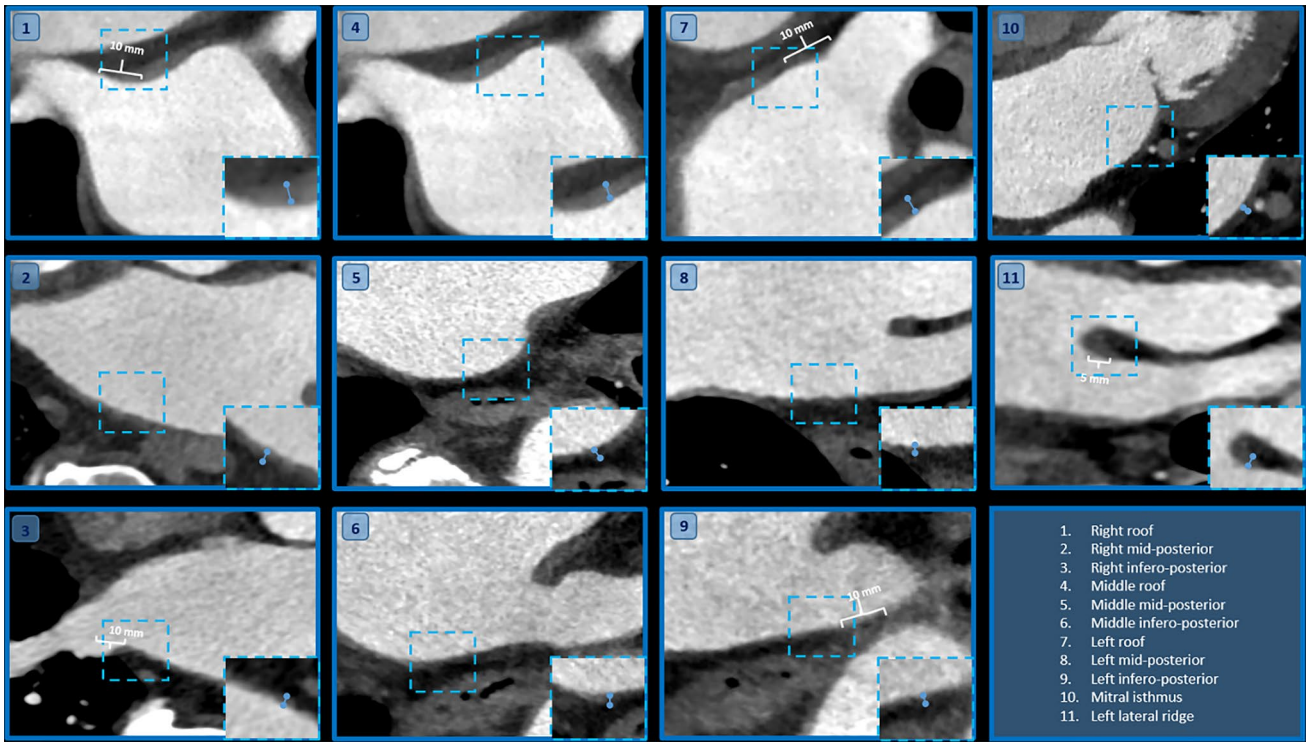

Fig. 3 Left atrial wall thickness (LAWT) was measured at 11 sites based on Hayashi et al. as demonstrated on the CT images. The numbers indicate the same locations for LAWT assessment as illustrated in Fig. 2. The dashed squares show the area of interest which are enlarged in the right-hand corner of every image. The blue line between the two dots represents the size of the measured LAWT. The roof and the infero-posterior wall thickness (Number 1, 3, 7 and 9) were assessed at 10 mm distance from the junction of the left atrium and pulmonary vein. LAWT at the ridge was measured at the center of the left superior PV (5 mm from the LA wall). *LA* left atrium, *LAWT* left atrial wall thickness, *PV* pulmonary vein

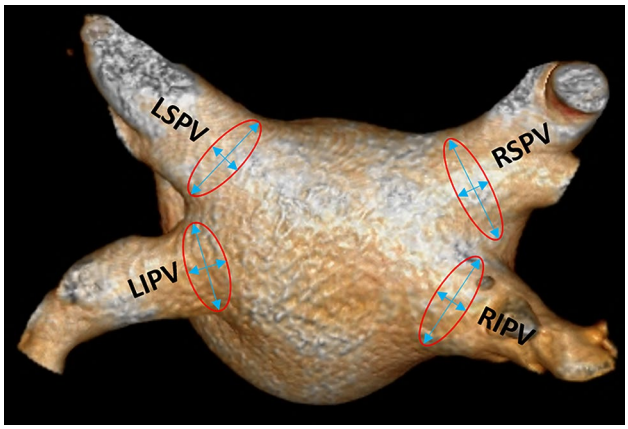

Fig. 4 Volume-rendered images show a typical pulmonary vein anatomy with left inferior and superior pulmonary veins and right inferior and superior pulmonary veins. The red circles represent the area of the ostium of each PVs while the blue arrows the maximum and minimum diameters of the orifices. *LIPV* left inferior pulmonary vein, *LSPV* left superior pulmonary vein, *RIPV* right inferior pulmonary vein, *RSPV* right superior pulmonary vein

through a steerable sheath (Agilis, Abbott). The ablations were guided by the modified CLOSE protocol: inter-lesion distance < 6 mm at all sites, ablation index target value 400 on the posterior wall and 500 on the anterior wall, target contact force 10–40 g (Fig. 5). During ablation, the mapping catheter was placed in the contralateral PVs to blind the operator for the presence or absence of first-pass isolation. After completing the circumferential ablation line around the ipsilateral PVs, the mapping catheter was placed in the ablated PVs and both entrance and exit block were evaluated. Entrance block was defined by the absence of local PV potentials on the mapping catheter placed in the PVs, while exit block was assessed by pacing at multiple sites inside the PVs. First-pass isolation was defined as the presence of both entrance and exit block after finishing the first-pass ablation circle. If PV conduction was still present after finishing the first-pass ablation circle, it was defined as first-pass isolation absent. Of course, in these cases, ablation was continued until bidirectional PV disconnection was achieved. After finishing the ablation on one side, the mapping catheter was left in those PVs and ablation was performed at the other side as well. Again, after finishing the ablation circle at the other side,

DOI:10.14753/SE.2024.2997

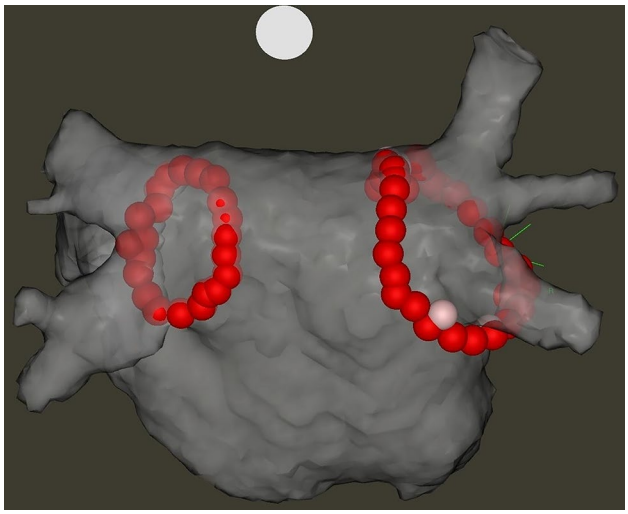

Fig. 5 Electroanatomical map of the left atrium after pulmonary vein isolation performed with the modified CLOSE protocol (postero-anterior view). All red ablation tags indicate an ablation index value > 400 on the posterior wall and > 500 on the anterior wall. The inter-tag distance is < 6 mm between all points

the mapping catheter was moved to these PVs to assess the entrance and exit block and the presence or absence of first-pass isolation. All PVs were repeatedly evaluated after a 20 min waiting period to assess acute PV reconnection. All patients without complications were discharged the day after the procedure.

Statistical analysis

Continuous variables are presented as mean and standard deviation, whereas categorical parameters are presented as frequency with percentages. Independent sample t-test was used to compare LAWT between different LA wall territories or for assessing the differences between PVs with or without first pass isolation.

Thereafter logistic regression analysis was used to identify predictors of procedural success regarding the left or the right pulmonary veins. Univariate logistic regression models included anthropometrical parameters, comorbidities, periprocedural data, LA appendage flow as assessed by transeosophagial echocardiography, left atrial volume (LAV), mean and maximum LAWT, PV diameters according to sidedness (left sided LAWT and PV diameters for the ablation of the left side and right sided LAWT and PV diameters for the right side).

Reproducibility of measurements (intra- and inter-observer agreement) was carried out using intraclass correlation coefficient (ICC) in 20 patients by a single reader. All analyses were conducted using STATA v13.0. A two-sided p-value smaller than 0.05 was considered statistically significant.

Results

Overall, 94 patients were included in the analysis (mean age 62.4 ± 12.6 years, mean body mass index (BMI) 28.1 ± 3.5 kg/m^2, 39.4% female). The total number of LAWT measurements were 1034. Moreover, 376 pulmonary vein ostium diameters and areas were measured. The baseline characteristics of the study population are summarized in Table 1.

Left atrial measurements

The mean LAWT was 1.35 ± 0.46 mm with a range of 0.2–2.6 mm. Results of CT-based assessment of LAWT are shown in Table 2. The left infero-posterior mean thickness was the lowest with a mean value of 0.83 ± 0.49 mm, and was significantly smaller compared to the right roof, right mid-posterior, right infero-posterior, middle roof, middle mid-posterior and the mitral isthmus and left lateral ridge LA locations ($p < 0.01$). The left lateral ridge had the largest LAWT, with a mean value of 1.95 ± 0.77 mm and was significantly larger than other LA locations ($p < 0.01$).

Regional differences were assessed by combining several measurement points. We found that LAWT on the right side (roof, mid-posterior, infero-posterior) was significantly larger as compared to the middle (roof, mid-posterior, infero-posterior) and left side (roof, mid-posterior, infero-posterior) (all $p < 0.01$). The infero-posterior region (right infero-posterior, middle infero-posterior, left infero-posterior) was substantially thinner than the mean middle (right mid-posterior, middle mid-posterior, left mid-posterior) and mean roof total (right roof, middle roof, left roof ($p = 0.01$ and $p = 0.08$, respectively). Table 3 summarizes PV diameters and areas.

The effect of clinical and CT-derived parameters on the first-pass isolation rate

Complete electrical isolation of all PVs was achieved in 100% of the PVs. No peri-procedural complications occurred. Successful first-pass isolation was achieved in 71 cases on the left side and 67 cases on the right side. Successful first-pass isolation of all PVs was achieved in 51 patients. There were no acute reconnections during the 20 min waiting period after the ablation. Regarding anthropometrics and clinical risk factors, we detected no association with the first-pass isolation success rate, based on univariate regression analysis, regardless of left, right or both sided first-pass isolation. Shorter procedural time was found in

DOI:10.14753/SE.2024.2997

Table 1 Patient characteristics

Parameters	Total N = 94	Successful first-pass isolation in all PVs N = 51	Absence of first-pass isolation in at least one PV N = 43	p value
Antropometric data and comoribities				
Age (years), (mean ± SD)	62.4 ± 12.6	62.8 ± 10.3	62.0 ± 15.0	0.06
Female sex, n (%)	37 (39.40)	23 (45.10)	14 (32.60)	0.21
Body mass index (kg/m^2), (mean ± SD)	28.14 ± 3.49	27.91 ± 3.56	28.44 ± 3.43	0.81
Body surface area (m^2), (mean ± SD)	2.04 ± 0.19	2.04 ± 0.20	2.06 ± 0.20	0.14
Diabetes, n (%)	14(14.90)	5 (9.80)	0 (0.0)	0.06
Hypertension, n (%)	61(64.90)	36 (70.60)	25 (58.10)	0.20
Hyperlipidaemia, n (%)	26 (27.70)	19 (37.30)	7 (16.30)	**0.03**
Prior Stroke/TIA, n (%)	4 (4.30)	2 (3.90)	2 (4.70)	0.86
Persistent AF, n (%)	36 (38.30)	17 (33.30)	19 (44.20)	0.28
CHA_2DS_2-VASc score, (mean ± SD)	2.11 ± 1.46	2.03 ± 1.36	2.10 ± 1.57	0.71
Procedural parameters				
LAT (min), (mean ± SD)	61.87 ± 15.63	62.08 ± 17.29	61.62 ± 13.57	0.89
Procedure time (min), (mean ± SD)	81.16 ± 19.29	75.31 ± 14.21	88.44 ± 22.27	**0.01**
Fluoroscopy time (min), (mean ± SD)	214.15 ± 177.28	192.69 ± 172.03	239.18 ± 182.17	0.61
Fluoroscopy dose (mGym2), (mean ± SD)	0.34 ± 1.13	0.22 ± 0.443	0.49 ± 1.61	0.06
Echocardiographic parameters				
Ejection fraction (%), (mean ± SD)	57.90 ± 8.00	58.28 ± 7,57	57.38 ± 8.51	0.63
LAA flow, cm/s	57.08 ± 24.24	57.58 ± 24.19	56.37 ± 24.71	0.40
CT derived parameter				
LAV (ml), (mean ± SD)	101.61 ± 39.82	99.67 ± 35.43	104.02 ± 45.03	0.08

Significant values are marked in bold

AF atrial fibrillation, *CI* confidence interval, *LAA flow* left atrial appendage flow, *LAT* left atrial time, *LAV* left atrial volume, *LAWT* left atrial wall thickness, *LIPV* left inferior pulmonary vein, *LSPV* left superior pulmonary vein, *PV diameter* pulmonary vein diameter, *RIPV* right inferior pulmonary vein, *RSPV* right superior pulmonary vein, *SD* standard deviation, *OR* odds ratio, *TIA* transient ischemic attack

Table 2 The left atrial wall thickness values in 11 locations

LA locations	Mean	SD	Standard error	95% CI for mean		Minimum	Maximum
				Lower bound	Upper bound		
1	1.79	0.81	0.08	1.63	1.96	0.20	4.20
2	1.93	0.79	0.08	1.77	2.09	0.10	4.00
3	1.56	0.75	0.07	1.41	1.72	0.10	3.10
4	1.21	0.60	0.06	1.09	1.33	0.10	2.80
5	1.29	0.66	0.06	1.16	1.43	0.20	3.20
6	0.97	0.54	0.05	0.86	1.08	0.10	2.50
7	1.01	0.52	0.05	0.89	1.11	0.10	2.40
8	1.01	0.59	0.06	0.89	1.13	0.20	2.80
9	0.83	0.49	0.05	0.73	0.94	0.10	2.30
10	1.24	0.67	0.06	1.10	1.38	0.10	2.70
11	1.95	0.77	0.08	1.79	2.11	0.20	4.00
Total	1.35	0.76	0.02	1.30	1.39	0.10	4.20

1: right roof, 2: right mid-posterior, 3: right infero-posterior, 4: middle roof, 5: middle mid-posterior, 6: middle infero-posterior, 7: left roof, 8: left mid-posterior, 9: left infero-posterior, 10: mitral isthmus, 11: left lateral ridge

CI confidence interval, *LA* left atrium, *SD* standard deviation

DOI:10.14753/SE.2024.2997

Table 3 CT based assessment of LA-PV parameters

	First-pass on left side	Unsuccessful first-pass on left side	p value	First-pass on right side	Unsuccessful first-pass on right side	p value
PV diameter (mm), (mean ± SD)						
LIPV	17.6 ± 6.0	16.4 ± 4.0	0.31	NA	NA	NA
LSPV	18.6 ± 3.1	17.2 ± 3.9	0.19	NA	NA	NA
RSPV	NA	NA	NA	21.3 ± 3.2	19.9 ± 3.7	**0.04**
RIPV	NA	NA	NA	18.0 ± 3.1	17.3 ± 2.6	0.23
PV area (mm^2), (mean ± SD)						
LIPV	269.6 ± 220.2	224.1 ± 116.9	0.33	NA	NA	NA
LSPV	281.0 ± 98.4	250.0 ± 94.6	0.08	NA	NA	NA
RSPV	NA	NA	NA	371.6 ± 111.3	312.5 ± 122.7	0.09
RIPV	NA	NA	NA	266.9 ± 88.4	241.8 ± 62.2	0.31
LAWT (mm), (mean ± SD)						
Mean total	1.35 ± 0.46	1.32 ± 0.51	0.78	1.34 ± 0.46	1.32 ± 0.54	0.83
Mean roof	1.39 ± 0.59	1.21 ± 0.53	0.18	1.36 ± 0.56	1.27 ± 0.66	0.52
Mean mid-posterior	1.39 ± 0.60	1.41 ± 0.74	0.91	1.37 ± 0.65	1.45 ± 0.62	0.64
Mean infero-posterior	1.12 ± 0.52	1.09 ± 0.62	0.89	1.09 ± 0.55	1.18 ± 0.57	0.51
Mean left	1.21 ± 0.44	1.18 ± 0.49	0.74	NA	NA	NA
Mean right	NA	NA	NA	1.74 ± 0.66	1.79 ± 0.68	0.74

Significant values are marked in bold

CT computer tomography, *LAA flow* left atrial appendage flow, *LA-PV* left atrial-pulmonary veins, *LAWT* left atrial wall thickness, *LIPV* left inferior pulmonary vein, *LSPV* left superior pulmonary vein, *NA* not applicable, *PV diameter* pulmonary vein diameter, *RIPV* right inferior pulmonary vein, *RSPV* right superior pulmonary vein, *SD* standard deviation

those cases, where first-pass isolation was achieved on both sides (p = 0.03).

We also found that LAWT did not influence first-pass isolation rate during PVI guided by our standardized ablation strategy. Among all assessed parameters, only the diameter of the RSPV was associated with the success rate of right-sided first pass isolation, as a wider RSPV diameter led to an easier first-pass isolation (OR 1.01, p = 0.04). Other cardiac CT and echocardiography-derived parameters did not influence the success rate of first-pass isolation (p > 0.05, see Table 4).

Reproducibility was assessed in 20 patients at 11 regions of interest (20 × 11 measurements) in terms of wall thickness, moreover the area and diameter of each pulmonary veins were also assessed. The intra- and inter-reader ICC for the assessment of LAWT were 0.98 (CI 0.97–0.98) and 0.92 (CI 0.79–0.97), respectively. The intra-reader area and diameter ICC's minimum and maximum range were between 0.94 and 0.99 and 0.98–0.99 respectively while the inteR–Reader area and diameter ICC's minimum and maximum range were between 0.78–0.92 and 0.80–0.94, respectively.

Discussion

Our main findings indicate that using ablation index with a standardized ablation protocol in drug-refractory AF patients results in a high acute procedural success rate independently from CT-derived LAWT. Regarding the PV anatomy, RSPV diameter might influence the rate of first-pass isolation. The assessment of PV diameters and LAWT were highly reproducible.

Recent advancements in ablation techniques, catheter types and pre-ablation imaging have paved the way for effective and safe therapies in treating AF [10]. A novel ablation quality marker was first introduced by Nakagawa et al., based on a canine study [28]. Ablation index is a quality marker and a surrogate measure for the quality of the ablation lesions [29]. Several studies have reported that it is a useful tool for a durable PVI as it incorporates contact force, power and time in a weighted non-linear formula [29, 30]. In an in vitro study, the reliability of AI was validated with a good correlation with lesion width and lesion depth and volume using different contact angle, RF power and contact force settings [31]. Furthermore, in an in vivo study by El Haddad et al. a substantial difference was found in the minimum value of AI for durable segments between the anterior and posterior parts of the circle, which indicates the role of wall thickness in different regions of the atrium. It has been

DOI:10.14753/SE.2024.2997

Table 4 Univariate logistic regression analysis for the detection of predictors of achieving first-pass isolation

Parameters	First-pass isolation in all PVs				First-pass isolation in case of right-sided PVs				First-pass isolation in case of left-sided PVs			
	p value	OR	95% CI		p value	OR	95% CI		p value	OR	95% CI	
Age	0.75	1.00	0.97	1.03	0.18	1.02	0.98	1.06	0.76	1.00	0.97	1.04
Female sex	0.21	0.58	0.25	1.36	0.21	0.51	0.17	1.46	0.77	0.87	0.34	2.18
Body mass index	0.13	1.10	0.97	1.24	0.38	1.06	0.92	1.23	0.49	1.04	0.91	1.20
Diabetes	0.07	0.32	0.09	1.13	0.51	0.65	0.18	2.37	0.14	0.40	0.12	1.35
Hypertension	0.21	1.72	0.73	4.06	0.82	1.11	0.41	3.0	0.23	1.75	0.70	4.38
Hyperlipidaemia	0.02	3.05	1.13	8.20	0.09	3.03	0.81	11.30	0.45	1.48	0.52	4.24
Prior stroke/TIA	0.86	0.83	0.11	6.20	0.94	0.92	0.09	9.38	0.86	1.21	0.12	12.26
Paroxysmal/persistent AF	0.28	1.58	0.68	3.65	0.80	1.12	0.42	2.99	0.75	1.15	0.46	2.87
CHA2DS2-VASc	0.65	0.92	0.66	1.29	0.69	1.08	0.72	1.60	0.28	0.82	0.57	1.17
Ablation parameters												
LAT	0.88	1.00	0.98	1.03	0.99	1.00	0.97	1.03	0.91	1.00	0.97	1.03
Procedure time	0.00	0.95	0.93	0.98	0.16	0.98	0.96	1.00	0.031	0.97	0.94	0.99
Fluoroscopy time	0.21	0.99	0.99	1.00	0.29	0.99	0.99	1.00	0.756	1.00	0.99	1.00
Echocardiographic parameters												
Ejection fraction, (mean ± SD)	0.62	1.01	0.95	1.07	0.21	1.0	0.97	1.10	0.71	0.98	0.92	1.05
LAA flow	0.83	1.00	0.98	1.02	0.20	0.98	0.96	1.00	0.29	1.01	0.98	1.03
CT derived parameters												
LAV, (mean ± SD)	0.60	0.99	0.98	1.00	0.47	0.99	0.98	1.00	0.62	1.00	0.99	1.01
PV diameter, (mean ± SD)												
LIPV	0.29	1.00	0.99	1.00	NA	NA	NA	NA	0.32	1.00	0.99	1.00
LSPV	0.10	1.00	0.99	1.00	NA	NA	NA	NA	0.19	1.00	0.99	1.00
RSPV	0.16	1.00	0.99	1.00	**0.04**	1.00	1.00	1.01	NA	NA	NA	NA
RIPV	0.06	1.00	1.00	1.01	0.22	1.00	0.99	1.01	NA	NA	NA	NA
PV area												
LIPV	0.33	1.04	0.96	1.12	NA	NA	NA	NA	0.33	1.04	0.95	1.15
LSPV	0.12	1.11	0.97	1.27	NA	NA	NA	NA	0.09	1.13	0.98	1.32
RSPV	0.07	1.13	0.99	1.29	0.08	1.15	0.97	1.35	NA	NA	NA	NA
RIPV	0.05	1.15	0.99	1.33	0.30	1.09	0.92	1.29	NA	NA	NA	NA
LAWT, (mean ± SD)												
Mean total	0.35	0.66	0.27	1.59	0.82	1.12	0.40	3.10	0.77	1.15	0.44	2.99
Mean roof	0.56	1.22	0.60	2.49	0.51	1.31	0.56	3.05	0.17	1.74	0.77	3.93
Mean mid-posterior	0.09	0.56	0.28	1.09	0.63	0.83	0.39	1.76	0.90	0.95	0.47	1.93
Mean infero-posterior	0.16	0.58	0.27	1.25	0.50	0.74	0.31	1.78	0.89	1.05	0.46	2.41
Mean left	0.53	1.18	0.68	2.05	NA	NA	NA	NA	0.73	1.18	0.43	3.19
Mean right	0.64	0.88	0.52	1.48	0.73	0.88	0.42	1.83	NA	NA	NA	NA
Mitral isthmus	0.34	0.74	0.40	1.37	0.84	1.07	0.52	2.21	0.67	0.86	0.44	1.70
Left lateral ridge	0.32	1.31	0.76	2.24	0.05	2.01	0.99	4.05	0.93	1.02	0.57	1.84

Significant values are marked in bold

AF atrial fibrillation, *CI* confidence interval, *CT* computer tomography, *LAA flow* left atrial appendage flow, *LAT* left atrial time, *LAV* left atrial volume, *LAWT* left atrial wall thickness, *LIPV* left inferior pulmonary vein, *LSPV* left superior pulmonary vein, *PV diameter* pulmonary vein diameter, *RIPV* right inferior pulmonary vein, *RSPV* right superior pulmonary vein, *SD* standard deviation, *OR* odds ratio, *TIA* transient ischemic attack

shown that a higher ablation index value is necessary in the anterior segments to avoid the reconnections [32]. However, data on the optimal ablation index target values on the anterior and posterior wall are controversial [5, 8, 30, 33].

At present, no gold standard measurement for atrial wall thickness is available, however cardiac CT can reliably assess LAWT due to its high spatial and temporal resolution [34–36]. It has been demonstrated that there is an inter-and intra-patient variability in LAWT across paroxysmal versus

DOI:10.14753/SE.2024.2997

persistent AF patients [23, 37]. Moreover, several studies investigated the role of LAWT in PVI in light of AF recurrence [38–41]. However, these results are controversial in terms of the locations of the thickest region in LA and the role of LAWT on procedural efficacy [19, 40]. Of note, less advanced ablation techniques were used in these studies.

Mulder et al. first analysed the association between LAWT and acute PV reconnection in those patients who underwent AI-guided AF ablation. Based on their study results, local wall thickness had an impact on the occurrence of acute PV reconnections both in the anterior and posterior segments [14].

These findings are in contrast with our study results as we did not find a connection between LAWT (mean wall thickness of all 11 region) and the acute procedural outcome despite substantial differences across different regions of the LA in our patient population. This discrepancy might be explained by the difference in the procedural endpoints, as we investigated the effect of LAWT on the first pass isolation rate. We could not even use the acute PV reconnection as an endpoint as there was a total absence of acute PV reconnection in our current study using our highly effective, standardized ablation protocol, (e.g. the modified CLOSE protocol) with slightly higher minimal target contact force values than in the study by Mulder et al. (e.g. 10 g vs 5 g) [14], and with the use of a steerable sheath for ablation that might enable more stable catheter-tissue contact during ablations.

Based on the findings of El Haddad et al. this novel approach was introduced for enclosing the PV with optimized and contiguous RF lesions to achieve optimal lesion continuity and depth [5]. The use of these criteria in 130 patients showed a high rate of first-pass isolation [5]. In addition, it proved to be more effective than PVI using only AI with also higher first-pass isolation incidence [7]. Our AI target values (400 on the posterior wall and 500 on the anterior wall) were associated with an acceptably high rate of first-pass PVI isolation and the absence of acute reconnection. Using these AI target values, sufficiently large lesions were created even in case of a thicker atrial wall, indicated by the similar first-pass isolation rates in case of different LAWT values [42]. Thus, our standardized approach seems to be an appropriate choice to create a good quality ablation line that is independent from LAWT. Of note, a recent study showed that LAWT-tailored, individualized AI values might result in similarly good results, even with somewhat lower AI targets. On the other hand, this approach is time consuming, but does not seem to be better in efficacy or safety [43].

Out of all assessed parameters, only RSPV diameter was associated with a higher right-sided successful PVI on first-pass isolation. Despite the fact that the right pulmonary vein region is challenging in terms of PVI, due to its epicardial connection with the carina and the right atrium [44, 45], RSPV diameter size could positively influence the outcome of PVI. In the current study, we demonstrated that wider RSPV diameter could possibly lead to a successful first-pass isolation. This might be explained by the higher freedom in catheter navigation in those cases where the RSPV was not very narrow and thus, the angle between the RSPV and the LA is less pronounced.

Although the results of our study showed that LAWT measured by cardiac CT does not influence the acute success rate of AF ablation using the modified CLOSE protocol, the role of pre-ablation cardiac CT is well established and provides invaluable information for procedural planning, LAA assessment and patient selection. At last, we would like to mention that the procedural safety was excellent with the current standardized ablation protocol, compared to previous results [46].

Limitations

We acknowledge the limitations of our study. Firstly, this was a single-center study with a relatively low number of patients, however our study provides the first insight into the association of LAWT thickness on the procedural success of first pass ablation using a standardized ablation protocol. On the other hand, LAWT was measured in 11 LA segments in each patient, resulting in a detailed evaluation of the LA identifying its role in contemporary AF management using RF ablation. Although the main focus of the study was the evaluation of the acute procedural success of the modified CLOSE protocol in light of LAWT measurements by cardiac CT, further evaluation of the long-term procedural success (AF recurrence) of the modified CLOSE protocol is warranted. LAV was mostly derived from diastolic phases (due to the clinical CT protocol) and therefore it does not reflect the maximal LA volume for a given patient and limits our conclusions regarding this parameter.

Conclusion

Using standardized ablation protocol in paroxysmal and persistent AF patients leads to a high first pass isolation rate and high acute procedural success independently from the LAWT. Larger RSPV diameter showed an association with right-sided successful first pass isolation.

Acknowledgements The current article has been previously presented at scientific conferences such as The Hungarian PhD Scientific Days 2021, European Society of Cardiology Congress 2021, Society of Cardiovascular Computed Tomography Congress 2021.

Author contributions All authors contributed to the study conception and design. All authors read and approved the final manuscript.

DOI:10.14753/SE.2024.2997

Funding Open access funding provided by Semmelweis University. Project no. NVKP_16-1–2016-0017 ('National Heart Program') has been implemented with the support provided from the National Research, Development and Innovation Fund of Hungary, financed under the NVKP_16 funding scheme. The research was financed by the Thematic Excellence Programme (2020-4.1.1.-TKP2020) of the Ministry for Innovation and Technology in Hungary, within the framework of the Therapeutic Development and Bioimaging thematic programmes of the Semmelweis University. Melinda Boussoussou MD was supported by the ÚNKP-21-3-II-SE, New National Excellence Program of the Ministry for Innovation and Technology from the source of the National research, Development and Innovation fund. M. Boussoussou and B. Vattay were supported by the "NTP-NFTÖ" (Nemzeti Tehetség Program, Nemzet Fiatal Tehetségeiért Ösztöndíj) program of the Ministry of Human Capacities in Hungary (EMMI) and by the EFOP-3.6.3-VEKOP-16-2017-00009.

References

1. Haïssaguerre M et al (1998) Spontaneous initiation of atrial fibrillation by ectopic beats originating in the pulmonary veins. N Engl J Med 339(10):659–666
2. Jaïs P et al (2002) Distinctive electrophysiological properties of pulmonary veins in patients with atrial fibrillation. Circulation 106(19):2479–2485
3. Calkins H et al (2017) 2017 HRS/EHRA/ECAS/APHRS/SOLAECE expert consensus statement on catheter and surgical ablation of atrial fibrillation: executive summary. J Interv Card Electrophysiol 50(1):1–55
4. Szegedi N et al (2021) The role of local impedance drop in the acute lesion efficacy during pulmonary vein isolation performed with a new contact force sensing catheter-a pilot study. PLoS ONE 16(9):e0257050
5. Taghji P et al (2018) Evaluation of a strategy aiming to enclose the pulmonary veins with contiguous and optimized radiofrequency lesions in paroxysmal atrial fibrillation: a pilot study. JACC Clin Electrophysiol 4(1):99–108
6. Phlips T et al (2018) Improving procedural and one-year outcome after contact force-guided pulmonary vein isolation: the role of interlesion distance, ablation index, and contact force variability in the 'CLOSE'-protocol. Europace 20:f419–f427
7. Berte B et al (2020) Pulmonary vein isolation using ablation index vs. CLOSE protocol with a surround flow ablation catheter. Europace 22(1):84–89
8. Lee SR et al (2019) Efficacy of the optimal ablation index-targeted strategy for pulmonary vein isolation in patients with atrial fibrillation: the OPTIMUM study results. J Interv Card Electrophysiol 55(2):171–181
9. Osorio J et al (2020) First pass isolation predicts clinical success after contact force guided paroxysmal atrial fibrillation ablation. Eur Heart J 41(22):ehaa946-0421
10. Szegedi N et al (2021) Orientation of the right superior pulmonary vein affects outcome after pulmonary vein isolation. Eur Heart J. https://doi.org/10.1093/ehjci/jeab041
11. Wei W et al (2014) Anatomical characteristics of pulmonary veins for the prediction of postoperative recurrence after radiofrequency catheter ablation of atrial fibrillation. PLoS ONE 9(4):e93817
12. Hauser TH et al (2015) Prognostic value of pulmonary vein size in prediction of atrial fibrillation recurrence after pulmonary vein isolation: a cardiovascular magnetic resonance study. J Cardiovasc Magn Reson 17(1):49
13. Chen J et al (2017) Assessments of pulmonary vein and left atrial anatomical variants in atrial fibrillation patients for catheter ablation with cardiac CT. Eur Radiol 27(2):660–670
14. Mulder MJ et al (2020) Impact of local left atrial wall thickness on the incidence of acute pulmonary vein reconnection after Ablation Index-guided atrial fibrillation ablation. Int J Cardiol Heart Vasc 29:100574
15. Ninomiya Y et al (2021) Absence of first-pass isolation is associated with poor pulmonary vein isolation durability and atrial fibrillation ablation outcomes. J Arrhythm 37(6):1468–1476
16. Osorio J et al (2021) Predictors of clinical success after paroxysmal atrial fibrillation catheter ablation. J Cardiovasc Electrophysiol 32(7):1814–1821
17. Karady J et al (2017) The effect of four-phasic versus three-phasic contrast media injection protocols on extravasation rate in coronary CT angiography: a randomized controlled trial. Eur Radiol 27(11):4538–4543
18. Karády J et al (2017) The effect of four-phasic versus three-phasic contrast media injection protocols on extravasation rate in coronary CT angiography: a randomized controlled trial. Eur Radiol 27(11):4538–4543
19. Suenari K et al (2013) Left atrial thickness under the catheter ablation lines in patients with paroxysmal atrial fibrillation: insights from 64-slice multidetector computed tomography. Heart Vessels 28(3):360–368
20. Imada M et al (2007) Anatomical remodeling of left atria in subjects with chronic and paroxysmal atrial fibrillation evaluated by multislice computed tomography. Int J Cardiol 119(3):384–388
21. Hoffmeister PS et al (2007) Evaluation of left atrial and posterior mediastinal anatomy by multidetector helical computed tomography imaging: relevance to ablation. J Interv Card Electrophysiol 18(3):217–223
22. Pan NH et al (2008) Aging dilates atrium and pulmonary veins: implications for the genesis of atrial fibrillation. Chest 133(1):190–196
23. Nakamura K et al (2011) Left atrial wall thickness in paroxysmal atrial fibrillation by multislice-CT is initial marker of structural remodeling and predictor of transition from paroxysmal to chronic form. Int J Cardiol 148(2):139–147
24. Hayashi H et al (2014) Left atrial wall thickness and outcomes of catheter ablation for atrial fibrillation in patients with hypertrophic cardiomyopathy. J Interv Card Electrophysiol 40(2):153–160
25. Takahashi K et al (2015) Relation between left atrial wall thickness in patients with atrial fibrillation and intracardiac electrogram characteristics and ATP-provoked dormant pulmonary vein conduction. J Cardiovasc Electrophysiol 26(6):597–605
26. Jazayeri MA et al (2017) Impact of radiofrequency ablation of atrial fibrillation on pulmonary vein cross sectional area: implications for the diagnosis of pulmonary vein stenosis. J Atr Fibrillation 10(1):1531
27. Kirchhof P et al (2017) 2016 ESC guidelines for the management of atrial fibrillation developed in collaboration with EACTS. Rev Esp Cardiol (Engl Ed) 70(1):50

DOI:10.14753/SE.2024.2997

28. Nakagawa H et al (2013) Abstract 12104: Prospective study using a new formula incorporating contact force, radiofrequency power and application time (force-power-time index) for quantifying lesion formation to guide long continuous atrial lesions in the Beating Canine Heart. Circulation 128:A12104–A12104
29. Das M et al (2017) Ablation index, a novel marker of ablation lesion quality: prediction of pulmonary vein reconnection at repeat electrophysiology study and regional differences in target values. Europace 19(5):775–783
30. Solimene F et al (2019) Safety and efficacy of atrial fibrillation ablation guided by Ablation Index module. J Interv Card Electrophysiol 54(1):9–15
31. Kawaji T et al (2019) Limitations of lesion quality estimated by ablation index: an in vitro study. J Cardiovasc Electrophysiol 30(6):926–933
32. El Haddad M et al (2017) Determinants of acute and late pulmonary vein reconnection in contact force-guided pulmonary vein isolation: identifying the weakest link in the ablation chain. Circ Arrhythm Electrophysiol 10(4):e004867
33. Hussein A et al (2018) Use of ablation index-guided ablation results in high rates of durable pulmonary vein isolation and freedom from arrhythmia in persistent atrial fibrillation patients: the PRAISE study results. Circ Arrhythm Electrophysiol 11(9):e006576
34. Budoff MJ et al (2008) Diagnostic performance of 64-multidetector row coronary computed tomographic angiography for evaluation of coronary artery stenosis in individuals without known coronary artery disease: results from the prospective multicenter ACCURACY (Assessment by Coronary Computed Tomographic Angiography of Individuals Undergoing Invasive Coronary Angiography) trial. J Am Coll Cardiol 52(21):1724–1732
35. Meijboom WB et al (2008) Diagnostic accuracy of 64-slice computed tomography coronary angiography: a prospective, multicenter, multivendor study. J Am Coll Cardiol 52(25):2135–2144
36. Paech DC, Weston AR (2011) A systematic review of the clinical effectiveness of 64-slice or higher computed tomography angiography as an alternative to invasive coronary angiography in the investigation of suspected coronary artery disease. BMC Cardiovasc Disord 11:32
37. Beinart R et al (2011) Left atrial wall thickness variability measured by CT scans in patients undergoing pulmonary vein isolation. J Cardiovasc Electrophysiol 22(11):1232–1236
38. Zuo K et al (2019) Correlation of left atrial wall thickness and atrial remodeling in atrial fibrillation: Study based on low-dose-ibutilide-facilitated catheter ablation. Medicine (Baltimore) 98(15):e15170
39. Nakatani Y et al (2019) Impacts of the body size on the left atrial wall thickness and atrial fibrillation recurrence after catheter ablation. Heart Vessels 34(8):1351–1359
40. Nakatani Y et al (2018) Heterogeneity in the left atrial wall thickness contributes to atrial fibrillation recurrence after catheter ablation. Heart Vessels 33(12):1549–1558
41. Inoue J et al (2016) Effect of left atrial wall thickness on radiofrequency ablation success. J Cardiovasc Electrophysiol 27(11):1298–1303
42. Okamatsu H et al (2019) High-power application is associated with shorter procedure time and higher rate of first-pass pulmonary vein isolation in ablation index-guided atrial fibrillation ablation. J Cardiovasc Electrophysiol 30(12):2751–2758
43. Teres C et al (2021) Personalized paroxysmal atrial fibrillation ablation by tailoring ablation index to the left atrial wall thickness: the "Ablate by-LAW" single-centre study-a pilot study. Europace. https://doi.org/10.1093/europace/euab216
44. Garg L et al (2020) Impact of left atrial bipolar electrogram voltage on first pass pulmonary vein isolation during radiofrequency catheter ablation. Front Physiol 11:594654
45. Yoshida K et al (2019) Epicardial connection between the right-sided pulmonary venous carina and the right atrium in patients with atrial fibrillation: a possible mechanism for preclusion of pulmonary vein isolation without carina ablation. Heart Rhythm 16(5):671–678
46. Szegedi N et al (2019) Repeat procedure is a new independent predictor of complications of atrial fibrillation ablation. Europace 21(5):732–737